



PROGRAMME OF
THE EUROPEAN UNION



Validation Report

SERVICES SUPPORTING THE EUROPEAN
ENVIRONMENT AGENCY'S (EEA)
IMPLEMENTATION OF THE COPERNICUS
EUROPEAN GROUND MOTION SERVICE –
PRODUCT VALIDATION.



Date: 19/12/2023

Doc. Version: **2.0**

Content ID: **SPECIFIC CONTRACT No 3506/RO-COPERNCA/EEA.58973**
Implementing Framework service contract No EEA/DIS/RO/21/009

**Document Control Information**

Document Title	EGMS Validation Report
Project Title	Services supporting the European Environment Agency's (EEA) implementation of the Copernicus European Ground Motion Service – product validation.
Document Authors	Joan Sala Calero, Malte Vöge, Joana Esteves Martins, Daniel Raucoules, Marcello de Michelle, Amalia Vradi, Filippo Vecchiotti
Project Owner	Lorenzo Solari
Project Manager	Joan Sala Calero
Document Code	D7.1_Validation_Report.docx
Document Version	3.0
Distribution	Public
Date	19/12/2023

Document Approver(s) and Reviewer(s):

Name	Role	Action	Date
Lorenzo Solari	Project owner	Approved	12/12/2023

Document history

Revision	Date	Created by	Short description of changes
Draft	18/09/2023	Joan Sala Calero	Initial draft version
Draft v2	07/11/2023	Joan Sala Calero	modified reporting structure
Final	12/12/2023	Joan Sala Calero	Final report version



Contents

EXECUTIVE SUMMARY	4
1 INTRODUCTION	5
1.1 The European Ground Motion Service.....	5
1.2 Validation concept	5
2 VALIDATION HIGHLIGHTS.....	7
2.1 Service validation objectives	7
2.2 Service compliance checks.....	9
2.3 Thematic areas (applications)	11
Landslides	11
Mining and post-mining	12
Urban.....	13
Groundwater exploitation.....	14
Volcanism	15
3 VALIDATION RESULTS	17
3.1 Applicability and Usability	17
3.1.1 Methodology overview	19
3.1.2 Index of Agreement (IoA) overview	19
3.1.3 Validation results per thematic area.....	22
Landslides	22
Mining and post-mining	27
Urban.....	40
Groundwater exploitation.....	49
Volcanism	51
3.2 Consistency/Accuracy	53
3.2.1 Methodology overview	54
3.2.2 Index of Agreement overview	56
3.2.3 Validation results per thematic area.....	59
Landslides	59
Mining and post-mining	70
Urban.....	75
Groundwater exploitation.....	84
REFERENCES	90
GLOSSARY	92
ANNEX: InSAR concepts summary	93

EXECUTIVE SUMMARY

- The validation exercise has been performed in 38 areas distributed across Europe and rooted on the comparison or **agreement** between site datasets and EGMS products.
- EGMS provides valuable information to study **landslide** phenomena. The EGMS's L2 products (Line-of-Sight) can be potentially used to delimitate ground motion polygons considering the slope orientation and satellite acquisition geometry. These moving areas could be used to complement the manually maintained national and regional inventories as demonstrated in this document by the Spanish and French examples, where the national ground motion databases were used.
- EGMS is not only able to detect landslides but also **accurately follow** their deformation trend as seen in the comparison with Automatic Total Stations in Tyrol, Austria. It is important to note that local **north-south** movements cannot be estimated (or are greatly underestimated) due to the geometry of the satellite acquisitions. This is an unsolvable problem, linked to the geometry of acquisition of the satellite, and not to the EGMS processing technique.
- The EGMS portfolio can be used to detect large scale active **mining** and **post-mining** induced ground motion. One of the best examples that proves this is the comparison with piezometric in-situ data in the Turow mine area, located in Poland, at the border with Czech Republic, and Germany. EGMS matches in-situ-derived **linear** deformation rates; however, the EGMS struggles to follow deformations when they become **non-linear**. This is a known limiting factor of the technique applied.
- EGMS products have been tested against in-situ measurements in one of the most iconic **groundwater** over exploitation areas in Europe: Lorca, in Spain. Both validation against GNSS and piezometric data provided high quality results, also highlighting a strong correlation between subsidence rates and the increase of the soft-soil layer's thickness.
- EGMS products have been tested in complex environments such as the Etna active **volcano** in Sicily. Despite the dynamism of the area, EGMS is able to map reliably the displacements.
- EGMS offers very high MP density in **urban areas** complying with its technical specifications. Moreover, it is able to capture significant settlements as it is demonstrated by the test site in Norway, in the area of the Oslo central station. There, ground motion is primarily caused by the reduction of pore pressure, mainly resulting from groundwater pumping for engineering works.
- Active Deformation Areas (**ADAs**) is a clustering technique used to aggregate Measurement Points (MPs) into polygons that show the same deformation pattern. They have been widely used in comparison with different types of site datasets.



1 INTRODUCTION

1.1 The European Ground Motion Service

The Earth's surface is in constant motion, whether driven by natural phenomena such as tectonic activity or volcanism or influenced by human activities such as groundwater extraction or mining. This dynamic nature can have significant impacts on both infrastructure and natural ecosystems. The European Ground Motion Service (EGMS) was created in response to clear user needs raised from different perspectives of the ground motion community. Representing the forefront of space-based remote sensing technology, the EGMS uses Synthetic Aperture Radar Interferometry (InSAR) data derived from Sentinel-1 to detect and precisely measure ground movements across Europe with millimetre precision. The EGMS provides three levels of products updated annually:

- **Basic/L2a:** Line-of-sight (LOS) velocity maps in ascending and descending orbits with annotated geolocalisation and quality measures per measurement point. Basic products are referred to a local reference point.
- **Calibrated/L2b:** LOS velocity maps in ascending and descending orbits referenced to a model derived from global navigation satellite systems time-series data. Calibrated products are absolute, being no longer relative to a local reference point.
- **Ortho/L3:** Components of motion (horizontal and vertical) anchored to the reference geodetic model. Ortho products are based on the Calibrated/L2b product resampled to a 100m grid.

More information about the product levels is available [here](#).

1.2 Validation concept

According to Congalton and Russell (2001), validation is an integral component of mapping projects incorporating Earth Observation data. In this sense, the validation exercise synthetized in this report is understood as a measure of agreement between reference (ground and Earth Observation) data and the EGMS.

This report concerns the EGMS first update, with reference period **2015-2021**. Future versions of the report will release validation outcomes after each annual product update.

The validation of the EGMS has the following goals and it is built upon the following concepts:

- It verifies the **usability** of the data for different applications according to *initial user requirements* and with respect to the *fields of application* foreseen by the [EGMS Product Specifications](#) and the [EGMS End User Requirements](#) documents.
- It determines if the **quality** of the products is consistent with the technical specifications for different areas and applications, and if the quality level is sufficient for supporting

such applications. In parallel, it is used to confirm the conclusions of the [EGMS Quality Assurance and Control Report](#).

It addresses the **completeness** and **consistency** of the data products together with their **accuracy**.

- The validation exercise has been designed to be **transparent** and **reproducible**, therefore the code and datasets used (depending on license agreements) will be published in the form of editable Jupyter **notebooks**. The expected time of publication is Q2 2024.
- The validation of EGMS products is based on the comparison of data of different nature. Therefore, a complete **agreement** is most likely impossible, and differences may not be related to a quality issue.
- It is performed by the validation consortium composed by Sixense, NGI, TNO, BRGM, GeoSphere, and Terrasigna with the following data providers: CNR-IREA, CSIC-IGME, CNIG, IGN, Geopartner, DTU, CGS, and LNEG.

The validation exercise is performed on 38 areas distributed across Europe. The datasets used in the validation exercise are described in [D3.1-Validation Data Collection](#) together with the environmental and geological site characteristics reported in [D5-Validation Areas](#).

Seven different validation activities were designed to establish the agreement between different local and regional data sources and the EGMS portfolio. The chosen high-level procedures and validation criteria are documented in [D6.1-Validation Methodologies](#). To be able to intercompare and guarantee reproducibility the normalized IoA (Index of Agreement) will be referenced throughout the validation documentation whenever a quantitative comparison can be performed (0=disagreement, 1=agreement). The activities that assess the usability of the EGMS product may contain expert based thresholds and qualitative assessment based on the ancillary data available.

This report is structured into two main sections, each targeting different types of readers. Section 2 “Validation Highlights” is intended for those readers seeking general and concise conclusions from the validation exercise. For readers new to InSAR, appendix sections are provided at the end of the document, offering a list of abbreviations, and describing fundamental concepts related to radar (interferometric) ground motion products.

Section 3 “Validation results” is intended for readers familiar with InSAR products, providing expert conclusions for each of the sites selected for the different thematic areas of application. Within this section, the analysis of results is divided into two groups: applicability/usability and accuracy/precision.

2 VALIDATION HIGHLIGHTS

In this section, the insights derived from Section 3 "Validation results" are summarized and simplified with a focus on applicability. The goal is to capture the significance of EGMS for potential applications within the defined thematic areas. This summary is targeted to users who may be relatively new to InSAR.

2.1 Service validation objectives

Validation is the confirmation, through the provision of evidence, that the requirements for a specific intended use or application have been fulfilled. A set of validation activities were conducted to ensure and provide confidence that EGMS products are able to accomplish its intended use, goals, and objectives (i.e., to meet stakeholder requirements).

Figure 1 on the next page summarizes the validation components and the processes involved:

- **Methodology:** Different procedures were implemented taking as inputs the EGMS product levels and the independent data available on selected sites. The methods enable the comparison of site data with EGMS subsets. Their descriptions can be consulted on [D6.1-Validation Methodologies](#).
- **Data:** Site datasets are key to provide validation of EGMS product levels. Datasets were collected with a relevant temporal overlap with the EGMS time series (targeting >85%) and their properties (license, format, coverage) were documented in [D3.1-Validation Data Collection](#) and [D5-Validation Areas](#).
- **Criteria checked:** Different criteria were used to compare validation site datasets with the EGMS portfolio. For example, some methods focus their analyses on velocity and displacement rates whereas others analyze the XYZ positioning of the EGMS Measurement Points (MP) or their density.
- **Index of Agreement (IoA):** the concept is documented in section 2 of [D6.1-Validation Methodologies](#) and referenced across the EGMS validation documentation. A set of normalized IoAs are used to compare EGMS products and independent site datasets.
- **Thematic areas:** The main application areas or use cases of the EGMS were identified in order to evaluate the strengths and limitations of the products when dealing with specific problems related to natural or anthropogenic ground deformation phenomena.

The **reproducibility** of the validation workflows is ensured by the Jupyter Notebook environment and scripts that allow for translating methodologies into code taking the validation site data as inputs. The outputs are normalized **IoA** that combined with expert knowledge and literature enable a better understanding of applicability of EGMS ground motion portfolio to certain **Thematic Areas**.

The compliance with the service specifications has also been considered in the validation processes with a special focus on the MP density as described in section 2.2.



PROGRAMME OF
THE EUROPEAN UNION

Copernicus
Europe's eyes on Earth

 Land
Monitoring Service

 European
Environment
Agency

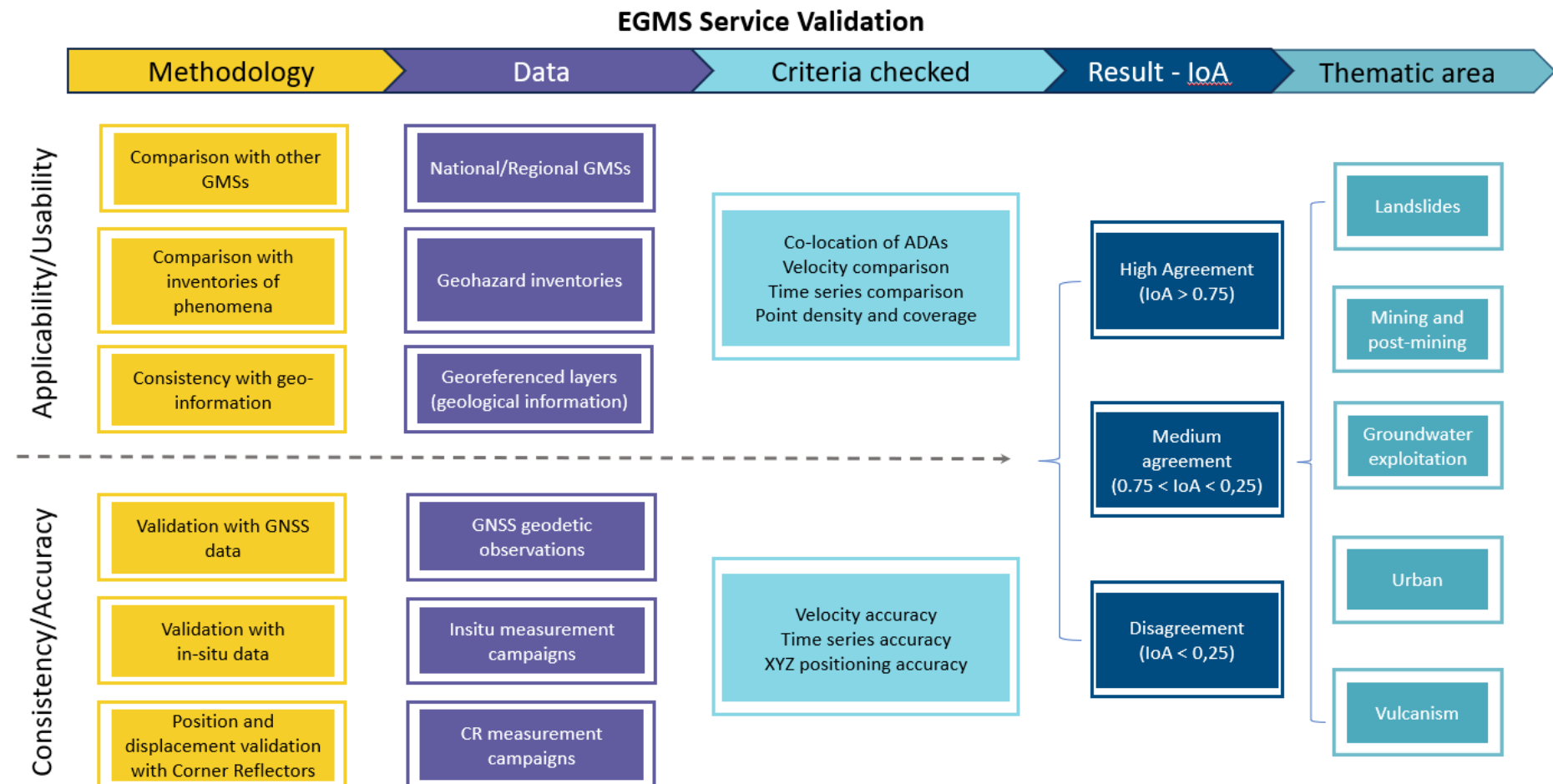


Figure 1: Graphical abstract for EGMS validation. CR, corner reflector. ADA, active deformation area. GNSS, global navigation satellite system. GMs, ground motion services. IoA, Index of Agreement.

2.2 Service compliance checks

An important aspect of the validation exercise involves assessing the compliance of EGMS product levels with their technical specifications based on the user requirements. When dealing with a point-based dataset with associated coordinates, one of the most straightforward aspects to verify is the Measurement Point (MP) density.

The land cover data consists of quality-controlled polygons from Urban Atlas, spanning over 12 urban areas and their surroundings at different latitudes. Figure 2 shows 8 major urban areas and 4 mountainous sites, which were included to enhance statistical representation. The compiled and averaged statistics cover an area comparable to the size of Switzerland, making it a substantial and representative subset of the EGMS. In Figure 3, it can be observed how the EGMS Basic and Calibrated products meet the established minimum requirements outlined in the [EGMS Product Specifications](#) document (e.g., >5,000 MP/km² for the continuous urban fabric land cover class). It was not meaningful to test the density of the Ortho product because it is a resampled version of the Calibrated one.

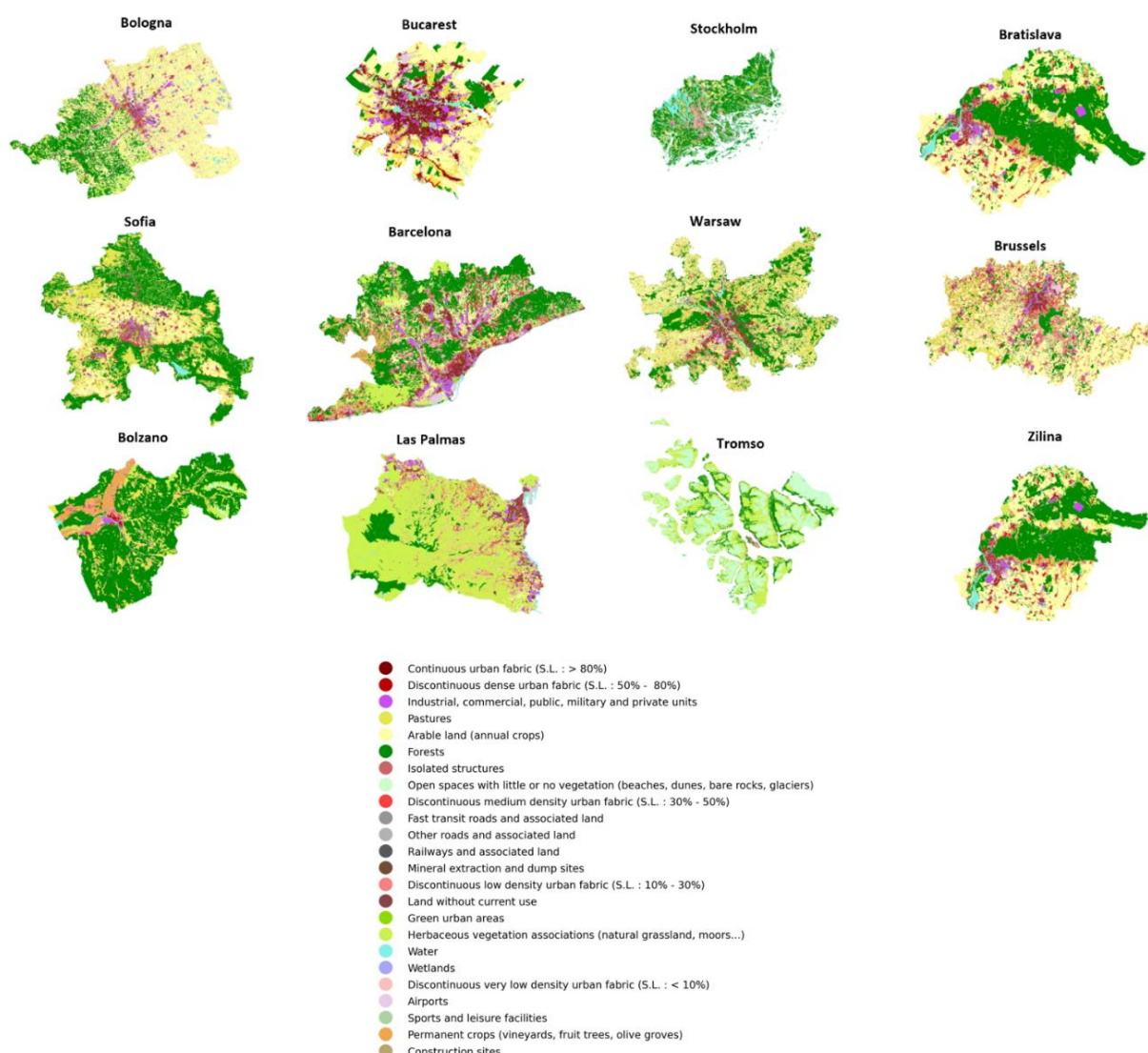


Figure 2: Land cover and land use classes for Urban Atlas 2018 in the selected sites

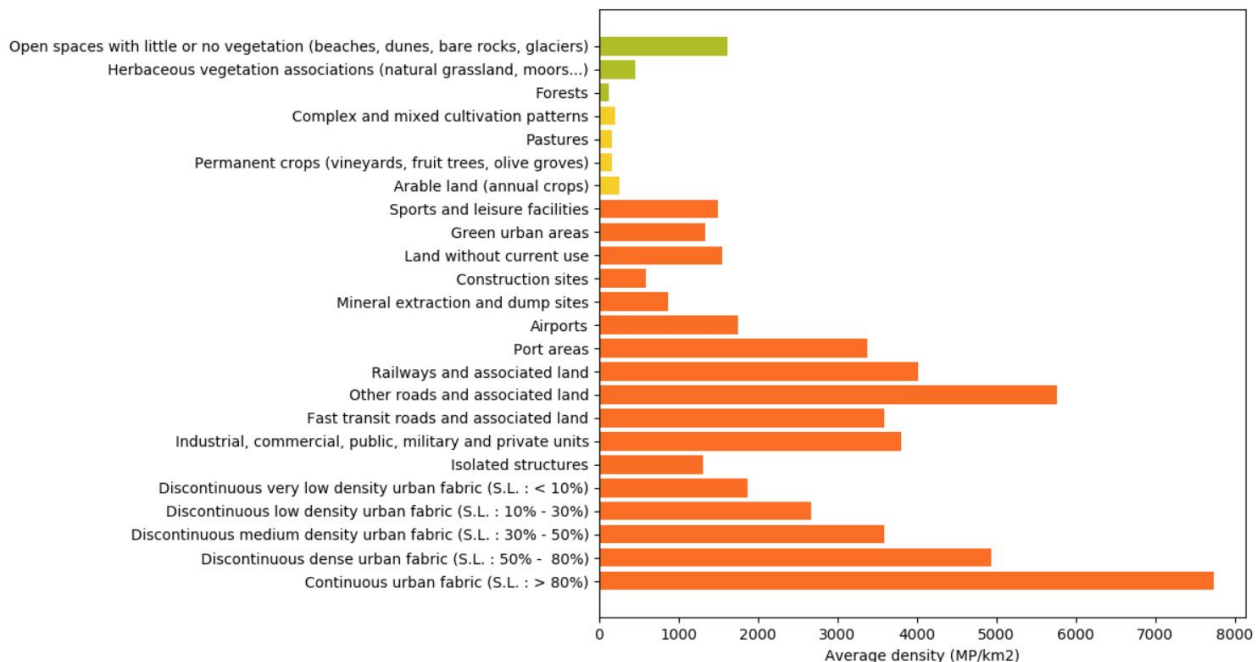


Figure 3: EGMS measurement point (MP) density for Basic and Calibrated products across 12 Urban Atlas sites

The outcome of this statistical analysis enables users to understand how the MP density clearly adapts to the surface properties (Figure 4: roughness and variability/changes). In this context, Figure 3 clearly illustrates how artificial surfaces, such as the urban built-up environment, exhibit the highest densities, whereas surfaces characterized by consistent changes, such as agricultural areas, construction sites, and forests, yield lower MP densities.



Figure 4: Land cover and reflectance (left: surfaces where InSAR offers higher density of measurements, right: surfaces where InSAR obtains lower density)

2.3 Thematic areas (applications)

In this section the expert validation results and IoA reported in Section 3 are summarized for each of the thematic areas.

Landslides

Landslides encompass a wide range of phenomena involving downhill ground movement. EGMS products can measure surface deformation at the millimetre level over extended periods, making them well-suited for detecting landslides characterized by cyclical and widespread movements. A key challenge in dealing with slope movements lies in the acquisition geometry (see Annex for details). Figure 5 illustrates how the MPs measured in the ascending and descending orbits (L2 products, Basic and Calibrated) cover different sides of a north oriented valley, as a consequence of the non-perpendicular satellite acquisition geometry (see Annex for geometrical constraints).

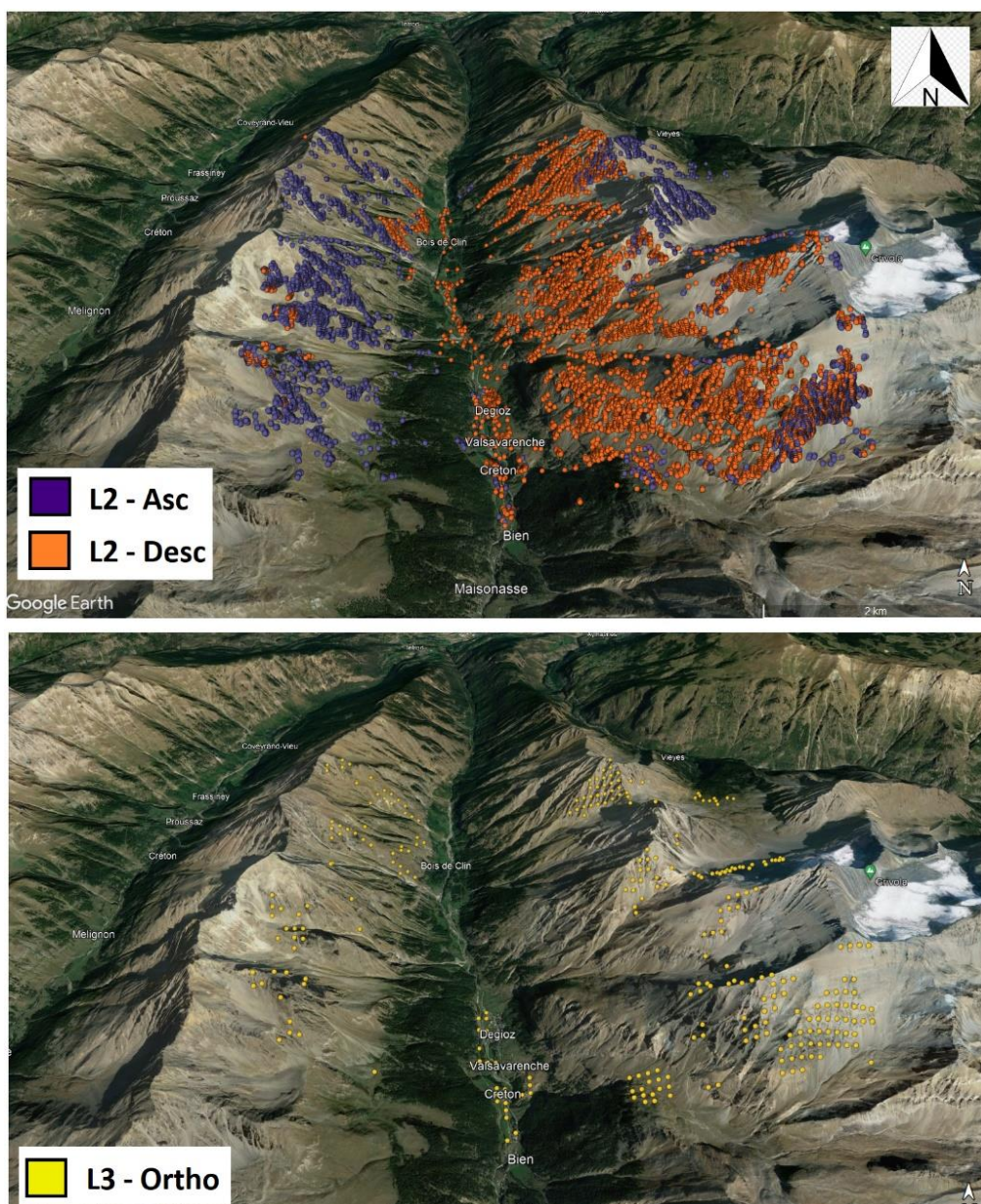


Figure 5: Different Measurement Point densities for L2 Ascending/Descending products (top) versus the Ortho product (bottom);
(basemap: google)



Figure 5 also shows the limitations of the Ortho/L3 product in very steep valleys where the absence of overlapping ascending and descending MPs prevents the decomposition into East-West (horizontal) and Up-Down (vertical) movements.

EGMS (Basic/L2a, Calibrated/L2b) LOS products in combination with clustering algorithms that group MPs into Active Deformation Areas (ADAs) (Appendix-1 of [D6.1-Validation Methodologies](#)) provide valuable inputs for enhancing existing field landslide inventories. The national landslide inventories of France and Spain were used in specific areas of the **Alps** and **Pyrenees** to assess the overlap of the EGMS products with manually maintained databases and confirming the potential of enriching them using the EGMS information. An essential consideration in landslide analyses involves slope orientation and the magnitude of displacement leading to surface changes. EGMS Basic and Calibrated products have proven effective for studying slow-moving and medium/large landslides spanning several hectares. In terms of accuracy, the comparison with in-situ Automatic Total Stations (ATS) in **Tyrol** (Austria) yielded satisfactory results, except for those landslides moving in the North/South direction (see Annex for measurement limitations of InSAR). In conclusion, LOS products (Basic and Calibrated) prove to be more suitable for landslide detection setting thresholds on velocity, particularly in highly mountainous areas where the MP density is intrinsically linked to both the acquisition geometry and the orientation of topographic slopes.

Mining and post-mining

The EGMS has proven to be an effective tool for characterizing ground motion induced by mining activity, including both open pit and underground mines. It is important to note that in some cases it faces limitations in monitoring active dumping/excavation areas and measuring fast motion or surface changes but that is a limitation of the technique and not of the EGMS itself (consult Annex for a list of some known limitations of InSAR).

Turow was selected as a validation site, providing in-situ data for this purpose. Turow is the second largest **active coal mine** in Poland. The mining operations not only deplete water supplies but also trigger subsidence in the border areas of Germany and Czech Republic. To validate the effectiveness of the EGMS, an extensive network of water boreholes (Figure 6) has been employed to monitor the impacts of Turow mining in the vicinity of the open-pit lignite mine near the Czech-Polish border. All product levels scored IoAs above 0.8 when compared to piezometric data indicating that the EGMS results correlate well with the ground information and, thus, the EGMS is able to capture the ground motion phenomena.

Freyming-Merlebach, situated in the **Lorraine** region of France near the border with Germany, faced growing concerns as the city experienced uplifts attributed to natural water filling in formerly exploited underground coal mines (**post-mining**). To address this, over 850 annual levelling measurements were used to validate the EGMS data. The goal was not to evaluate the different known accuracy of two measurement techniques (InSAR versus in situ) but rather to confirm their general agreement to characterize the deformation phenomena. The result of the comparison highlighted that the EGMS Basic and Calibrated products are well suited for monitoring this type of ground motion phenomena.

Similar post-mining effects were studied in **Limburg** (Netherlands), where the location of ADAs of both the Dutch GMS and the EGMS exhibit clear overlap. Additionally, assessment of other mining sites such as **La Unión** (Spain) focus on the storage of mine waste and the motion of these waste materials (commonly known as 'tailings'), revealing a clear correlation between the

presence of a tailing and motion. General agreement has been found in all mining sites making the EGMS a valuable tool for this application.

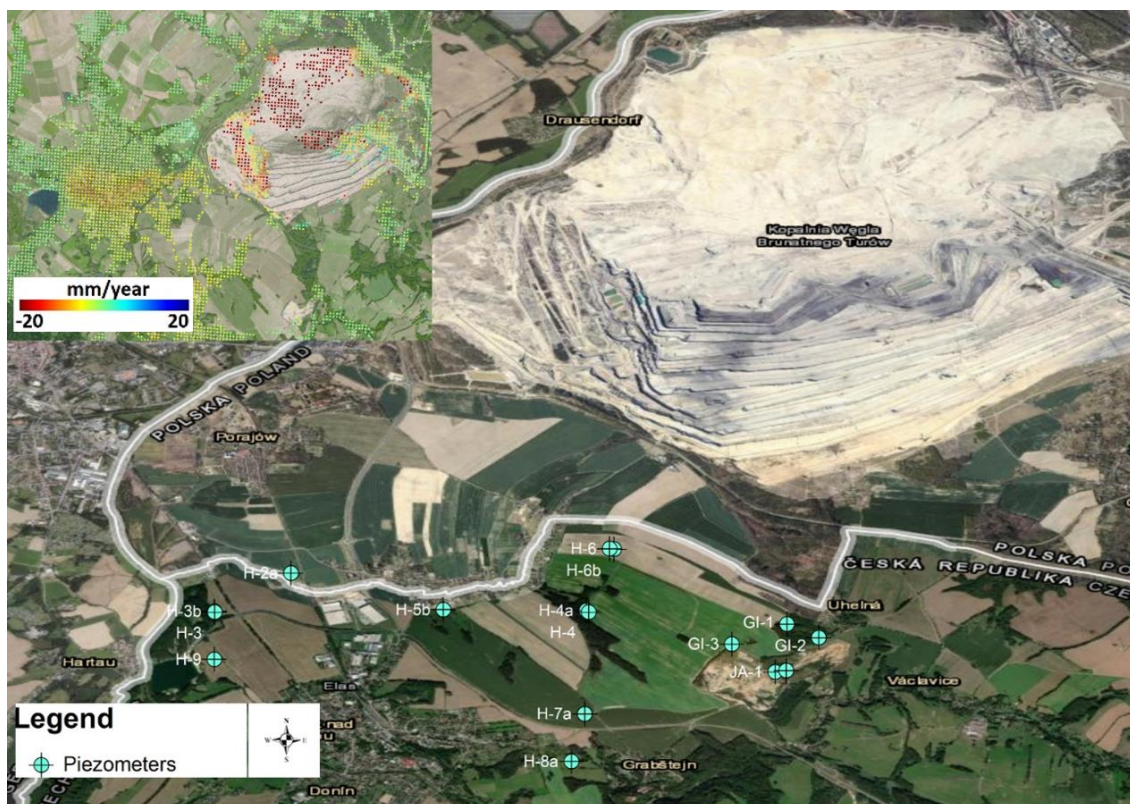


Figure 6: EGMS L3/Ortho up-down displacements (top-left) and location of in-situ measurements at the Turow mine site.
(basemap: google)

Urban

Oslo (Norway) was selected as a validation site for assessing urban subsidence and the impact of engineering works/construction. Over the past 10-15 years, the vicinity of the Oslo central station has undergone extensive building and infrastructure development. Construction activities have led to significant settlements in the area, primarily caused by the reduction of pore pressure, mainly resulting from leakage associated with drilling activities. A clear correlation between subsidence and anthropogenic activity was found in the EGMS products. In parallel, depth-to-bedrock and soil thickness maps exhibit a strong spatial correlation with EGMS deformation areas.

Thyborøn (Denmark) is located on a sandy barrier facing the North Sea and is vulnerable to flooding from the adjacent Linford due to its low elevation (1.0 – 2.5m). Coastal subsidence is believed to be a consequence of the overall sedimentary structure of the barriers and landfills, including the compression of certain layers. In Thyborøn, the ADAs coming from a ground motion map produced by DTU and the ones obtained from EGMS show similarities in the harbour area. Corner Reflectors (CR) were used to determine congruence between time series, location, and height measurements of CRs and EGMS MPs at and around the CRs' vicinity, with accuracies meeting predefined specifications and allowing the correct detection of the ground motion.

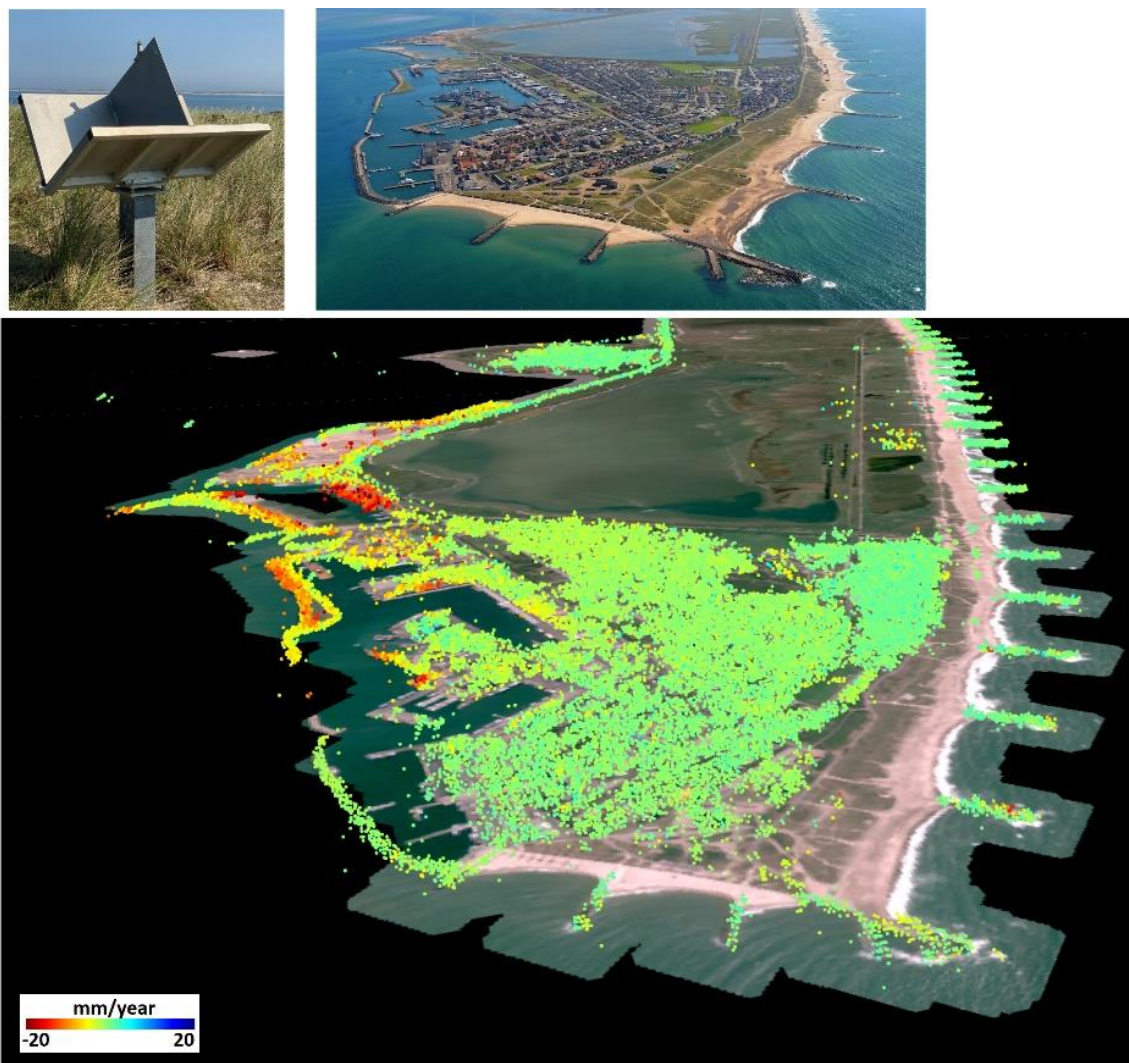


Figure 7: EGMS Calibrated/L2b velocities showing coastal subsidence at the Thyborøn validation site (basemap: google)

Groundwater exploitation

The **Guadalentín basin** in south-eastern Spain is one of the driest regions in Europe (Figure 8). The aquifer is located between the cities of Lorca and Puerto Lumbreras. The continuous extraction of groundwater, mainly for agricultural use, led to subsidence. EGMS products effectively capture this phenomenon, allowing for a comparison with GNSS and in-situ measurements (including levelling campaigns and piezometers) to estimate accuracy/precision and assess soil characteristics.

The non-linearity of the subsidence induced by the water table fluctuations poses a challenge for any InSAR result and the EGMS is no exception (see section 3.2). However, the spatial patterns of this deformation are successfully captured, as evidenced by comparisons with ancillary geodata such as soft soil thickness. Unfortunately, validation data is not available at the same weekly frequency as the EGMS, making direct comparisons for accuracy challenging. Despite that, a general sense of agreement between EGMS and in situ measures was found.

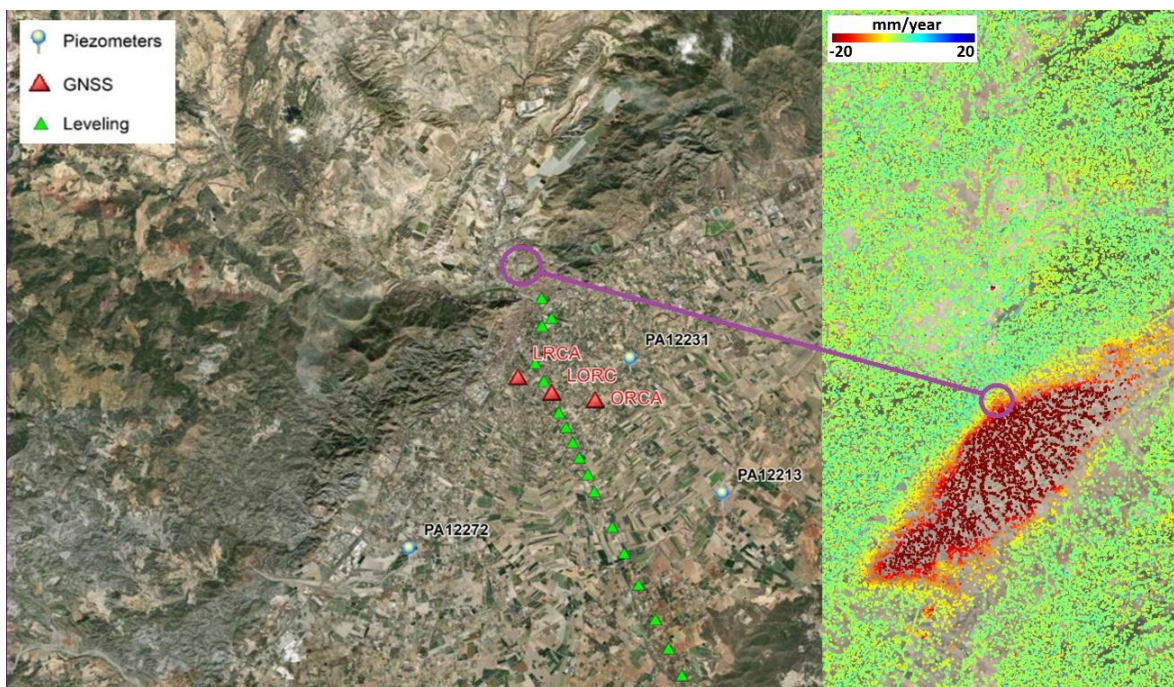


Figure 8: Ground water over exploitation induced subsidence in Lorca (Spain) is captured by the EGMS Calibrated/L2b ascending product. Locations of in-situ measurements and GNSS stations inserted.

Volcanism

The validation site at **Mount Etna** was selected due to its active volcanism, making it the largest active volcano in Europe. In December 2018, an eruption occurred from fissures located on the volcano's eastern flank.

An ad-hoc InSAR processing conducted by CNR-IREA provided all product levels for comparison with the EGMS products. The comparison revealed a general agreement between the two InSAR datasets (see Section 3 for details). ADA polygons from L2 products overlap and slight differences were observed for the Ortho/L3 products. Both datasets captured the general motion associated with volcanic activity and an atypically large earthquake event (Figure 9). Additionally, discernible fault lineaments showed differences. However, along the flanks of the volcano, the vertical velocity component is generally smaller than the horizontal component, potentially making it more sensitive to differences in the Calibrated product, from which the Ortho is derived.

For those new to InSAR, it is important to note that LOS ascending and descending orbits produce different maps (Figure 9) due to the acquisition geometry, viewing Etna from different sides (refer to Annex for more details). In a few words, the volcanic edifice is recording a sort of lateral spreading process with the east flank moving to the east and the western flank to the west. Moreover, a rather strong earthquake event (December 2018) can be observed in the time series in Figure 9 on top of the volcanic activity.

In conclusion, the comparison with the IREA products resulted in an IoA of 0.9, reflecting that the datasets match very well despite the dynamic character of the volcanic system and the very non-linear time series, demonstrating that the EGMS is capable of reliably mapping displacements under such difficult conditions.

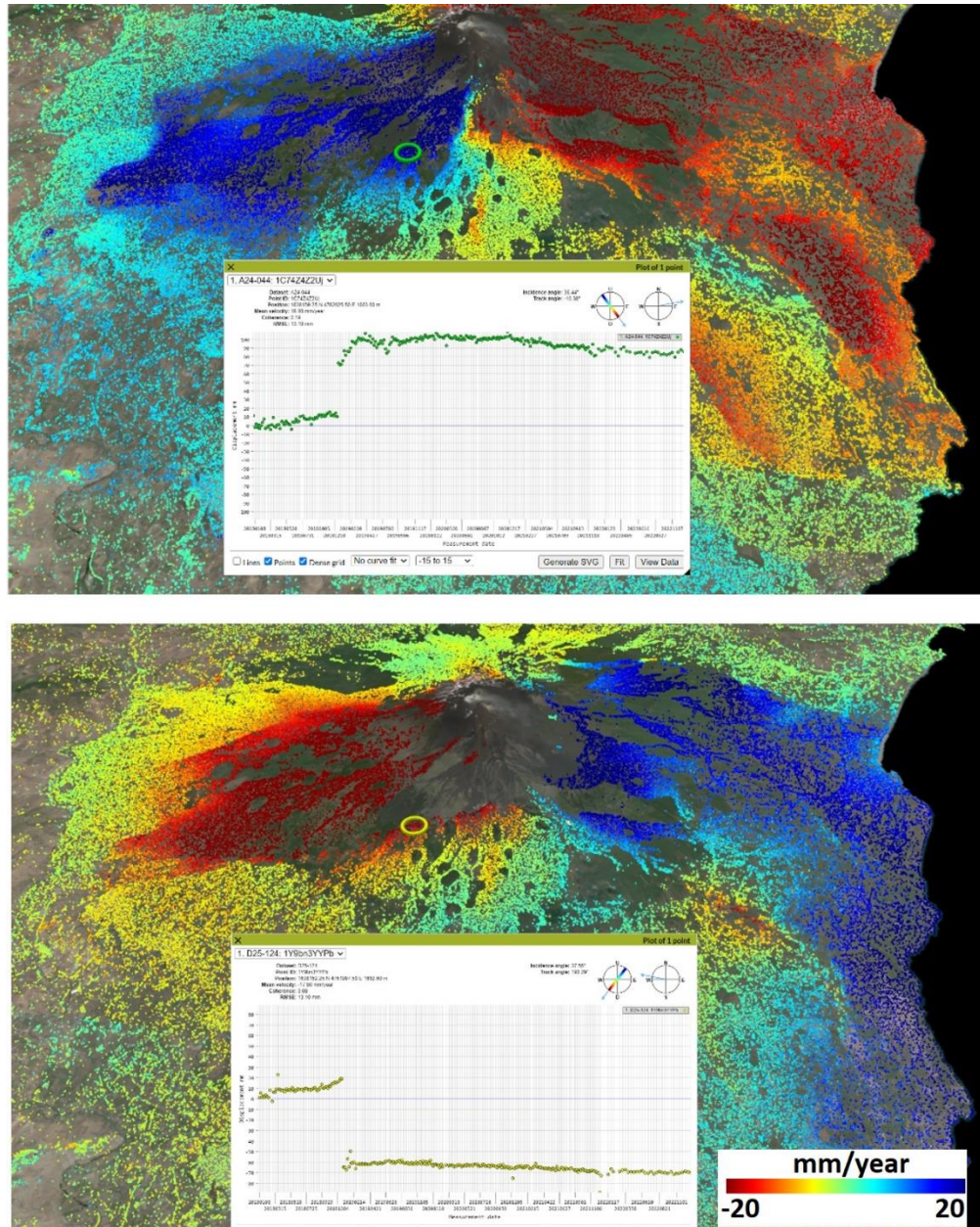


Figure 9: Ascending (top) and Descending (bottom) EGMS Calibrated/L2b products and selected time series over Etna Volcano, Italy. The jump in the time series is related to a strong earthquake.



3 VALIDATION RESULTS

This section presents the validation results organized per thematic area, structured as a technical report tailored for readers already familiar with InSAR processing results and seeking a comprehensive understanding of the usability, quality, consistency, and accuracy of the EGMS.

The results are categorized into two groups based on the nature of the site data, aiming to separate qualitative and quantitative analyses. The **IoA**, described in Section 3.1.2, have been considered to facilitate the intercomparison of results across different sites. The first section evaluates **applicability and usability** by thematic area, while the second assesses overall **consistency and accuracy** in comparison with other ground motion field measurement techniques.

3.1 Applicability and Usability

This section is designed to assess the applicability of the EGMS portfolio in characterizing specific phenomena within the defined thematic areas of the Service, adhering to the specifications. The EGMS portfolio in these sites is compared to other high-resolution and geo-localised data sources such as:

- Other operational and quality-controlled Ground Motion Services (GMS) or InSAR results, to study and compare EGMS's ability to capture known deformation trends and phenomena.
- High-resolution land cover layers, aimed at exploring the correlation between surface characteristics versus measurement point density and time series attributes quality.
- National inventories of geo-localised phenomena or geohazards, aiding in the identification of the kind of phenomena most suitable for representation in the EGMS products.
- Geological, lithological, hydrogeological, geomorphological, and geotechnical maps to correlate observed deformation trends with soil characteristics.
- Aerial photography and high-resolution land cover layers, providing insights into MP density and sensitivity to changes.
- Digital elevation models and derived slope data, enhancing the interpretation of geometrical constraints in the 3D plane.
- Inventories of anthropic activities that can trigger surface motion including mining, quarrying, geothermal fluids extraction, oil and gas extraction, and water pumping. Matching these with observed EGMS deformation areas presents an opportunity to discover which phenomena are captured.

The following Table 1 and Figure 10 provide a summary of the validation sites, with descriptions available in the documents [D3.1-Validation Data Collection](#) and [D5-Validation Areas](#):

Table 1: Overview of validation sites (Usability)

	Consistency with other GMS	Consistency with inventories of phenomena	Consistency with geo-information
Landslides	Aosta valley (IT)	Spanish national inventory (ES) French national inventory (FR)	Not evaluated
Mining and post-mining	Limburg (NL)	Lorraine region (FR)	Silesia (CZ) La Unión (ES)
Urban / Anthropogenic	Thyborøn (DK) Po delta (IT)	Not evaluated	Oslo (NO) Tagus valley (PT)
Groundwater exploitation	Not evaluated	Not evaluated	Lorca (ES)
Extra (Volcanism)	Etna (IT)	Not evaluated	Not evaluated

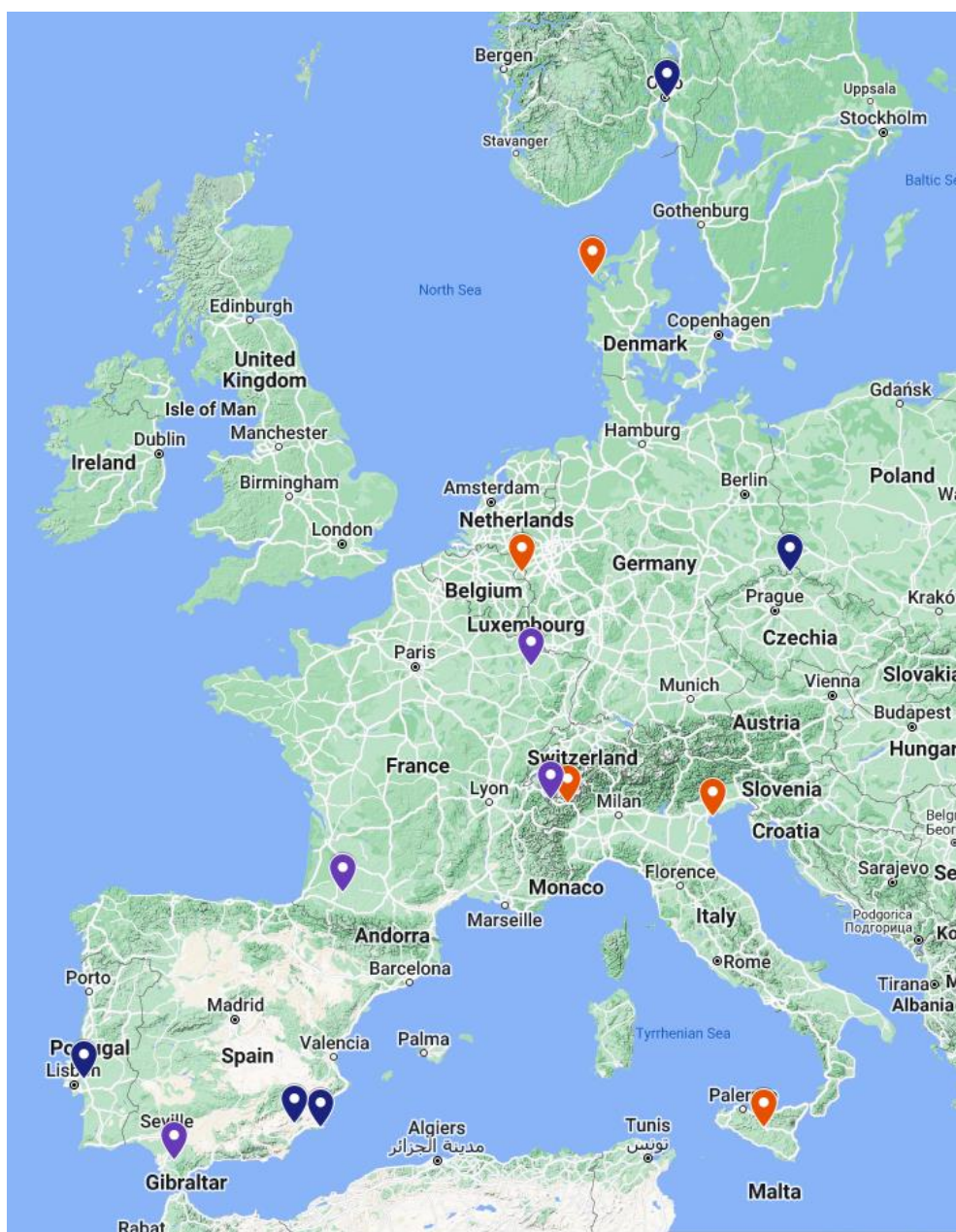


Figure 10: Validation objectives and thematic areas versus validation sites (Applicability/Usability). The colours refer to the different activities reported in the previous table. (basemap: google)

3.1.1 Methodology overview

Three validation activities were conducted across various validation sites (Figure 10). Detailed methodologies for each activity can be found in document:

- **Comparison with other GMS:** The EGMS results are compared with quality-controlled and validated datasets from existing operational national/regional GMSs. The validation is conducted separately for each product level and acquisition geometry. Due to varying availability of product levels in the respective public national/regional GMSs, the validation is limited to comparable datasets. Additionally, two independently quality-controlled and validated ad-hoc processing results (Etna/Italy and Thyborøn/Denmark) are included in the analysis. Spatial resampling to 30x30m and automated detection of ADAs are performed to facilitate intercomparison of different GMSs. The datasets are not re-referenced to a common reference point or to a common GNSS model.
- **Comparison with inventories of phenomena:** The main goal is to compare the EGMS data with information provided by inventories such as points or polygons representing the geometry, expected velocity or qualitative characteristics of the phenomena, dates of events or recorded damage. This activity aims to test EGMS's detection capabilities, particularly in geohazards management, exploring the potential of EGMS data to complement or build inventories where they are lacking. The main focus is on the capability to detect known phenomena, and when available, the similarity between polygons, derived both from inventories and EGMS, serves as a key validation indicator for mapping geohazards. The characteristics of the addressed phenomena (size and velocity of movement) are considered to have an impact on the validation analysis.
- **Consistency checks with ancillary data:** This activity employs national inventories of geomorphological, geotechnical, and geological data, alongside expert judgement, and automated procedures to identify ADAs in the EGMS time series datasets. An ADA is a cluster of MPs exhibiting the same deformation pattern represented with a polygon (the concept and algorithms are explained in Appendix 1 of [D6.1-Validation Methodologies](#)). This validation activity aims to assess the consistency of EGMS results with geological, geomorphological, and geotechnical data, employing the concept of radar-interpretation. Ancillary data is used as support for the interpretation, e.g., in case of landslides, active faults or mining activity. While there are no derived quantitative statistics or metrics directly translated to IoA values, this approach provides valuable insights into the alignment of EGMS products with geological and geotechnical considerations.

3.1.2 Index of Agreement (IoA) overview

For those cases where quantitative comparisons between EGMS products and site data can be performed, summarized validation activities and methodologies mentioned above, reproducible IoA have been conceived. Each index corresponds to a validation methodology applied to the different sites presented in Figure 10 (colour coded by methodology). The following Table 2 provides a summary of each IoA, specifying the EGMS product levels under evaluation:



Table 2: Index of Agreement (IoA) for Applicability/Usability

IoA	Methodology	Short description of how the index is calculated	Approach	EGMS product
Spatial overlap between moving areas (EGMS vs GMS)	Comparison with other GMSs	Maximum of: (Number ADAs with > 30% overlap) * 100 / Number ADAs OR (Total overlap area all ADAs * 100) / (Total area joined ADAs)	ADA Surface overlap	L2a/L2b/L3 (*)
Relative velocity difference (EGMS vs GMS)	Comparison with other GMSs	(abs(dVel) * 100) / maximum (absolute (Vel _{EGMS} + Vel _{validation})/2, 3.0)	Difference between measures	L2a/L2b/L3 (*)
Velocity correlation coefficient (EGMS vs GMS)	Comparison with other GMSs	Spatial correlation of velocity values on common grid using Pearson ¹ Correlation coefficient (linear correlation)	Correlation	L2a/L2b/L3 (*)
Displacement correlation coefficient (EGMS vs GMS)	Comparison with other GMSs	Mean of Temporal correlation of time series using Pearson ¹ Correlation coefficient (linear correlation)	Correlation	L2a/L2b/L3 (*)
Phenomena captured (yes/no)	Comparison with inventories of phenomena	This parameter is positive if the motion detected by EGMS inside the inventory polygons is significantly different (2 mm/y) from all the EGMS points outside the inventoried phenomenon.	Binary detection based on velocity threshold	L2a/L2b
EGMS ADA and phenomena area intersection	Comparison with inventories of phenomena	Polygons intersection between EGMS active deformation areas (ADA) polygons and polygons representing phenomena/events.	Polygon intersection	L2a/L2b
EGMS ADA and phenomena location/point	Comparison with inventories of phenomena	EGMS active deformation areas (ADA) polygons contain match the inventories of phenomena represented with points.	Point within polygon	L2a/L2b

1- Pearson correlation coefficient: <https://www.sciencedirect.com/topics/social-sciences/pearson-correlation-coefficient>



ADA detection vs land cover maps	Consistency with geo-information	Correlation between anthropogenic land cover classes and deformation areas obtained from EGMS.	Expert based assessment	L2a/L2b/L3
ADA detection vs geological maps	Consistency with geo-information	Correlation between depth to bedrock and deformation patterns coming from EGMS.	Expert based assessment	L2a/L2b/L3
ADA detection vs soil thickness maps	Consistency with geo-information	Correlation between soil thickness maps and deformation patterns coming from EGMS.	Expert based assessment	L2a/L2b/L3
ADA Comparison with fault lines positions	Consistency with geo-information	Delineation between EGMS-ADA polygons and fault lines.	Expert based assessment	L2a/L2b/L3

(*) Product selection depending on availability in other GMS:

- Aosta Valley: Basic/L2a
- Limburg: Calibrated/L2b
- Thyborøn: Basic/L2a
- Po River Delta: Basic/L2a
- Etna Basic/L2a + Calibrated/L2b + Ortho/L3

3.1.3 Validation results per thematic area

In this section, site descriptions and results are collectively presented, providing an overview per thematic area and validation strategy or objective. For a complete description of the sites, including metadata, please refer to [D3.1-Validation Data Collection](#) and [D5-Validation Areas](#).

Landslides

Aosta Valley (Italy)

This region, located in the Italian Alps, experiences a variety of gravitational phenomena including shallow landslides (e.g., debris flows, planar and rotational slides), rockfalls, large slope instabilities and deep-seated gravitational slope deformations. Figure 11 shows a comparison of displacement velocities between the EGMS and the regional GMS of the Region Aosta Valley (RVDA) for the Basic (Level 2a) product in ascending orbit, track 88. Both datasets have been resampled to cover the same period from February 2015 to December 2021. The comparison reveals good agreement between the detected ADAs, with the RVDA dataset detecting 44 ADAs, compared to 29 ADAs in the EGMS dataset. This difference is primarily attributed to the higher MP density in the RVDA dataset, most likely due to differences in the applied processing algorithms (EGMS: PSP-IFSAR; RVDA GMS: SqueeSAR).

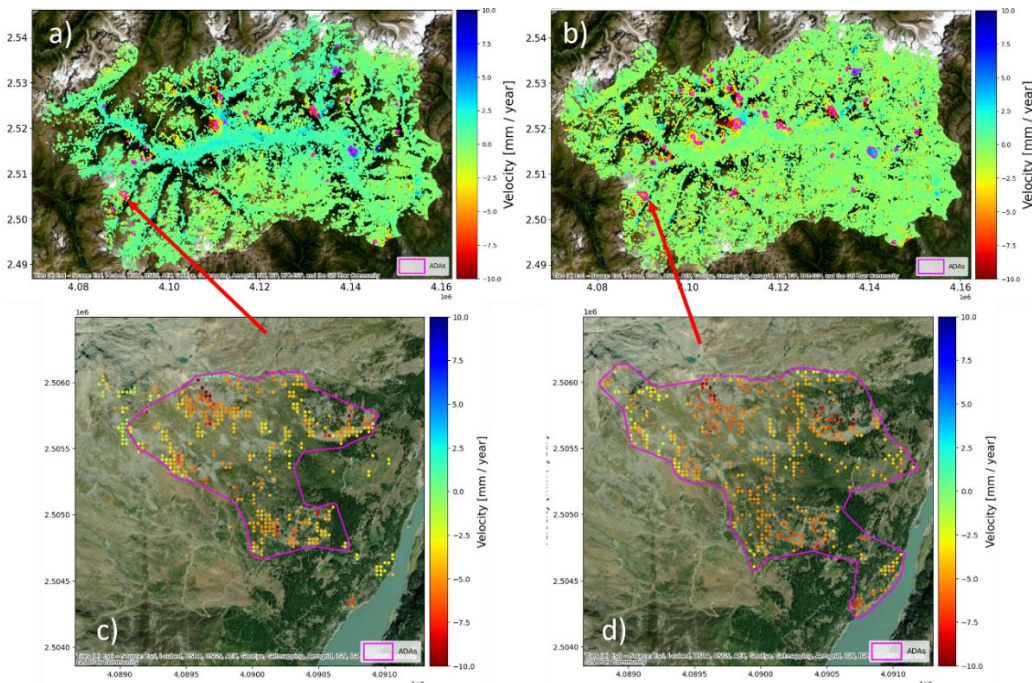


Figure 11: Displacement comparison for Aosta Valley (Italy): (a) Basic/L2a displacement velocities (EGMS, track 88/ASC); (b) RVDA displacement velocities. For the ADA marked by red arrows: (c) and (d) close-ups of corresponding velocity maps.

Another notable difference is the presence of slightly positive velocity values in the main valley, crossed by the region's largest river Dora Baltea, visible in the EGMS data in ascending orbit (track 88) but not in the RVDA dataset. It is important to note that the descending dataset (track 66) for the same area does not exhibit the same difference. As only one of the EGMS tracks shows these positive values, and because of the correlation with the topography, this could be due to a residual atmospheric signal, that was not completely filtered out during the data processing. This signal does not prevent the detection of landslides along the valley flanks. Despite this difference in the valley, the velocity distribution for the ADA maps shown in Figure

11 c) and d), along with the time-series in Figure 11, still demonstrate a very good agreement between the EGMS and the regional dataset.

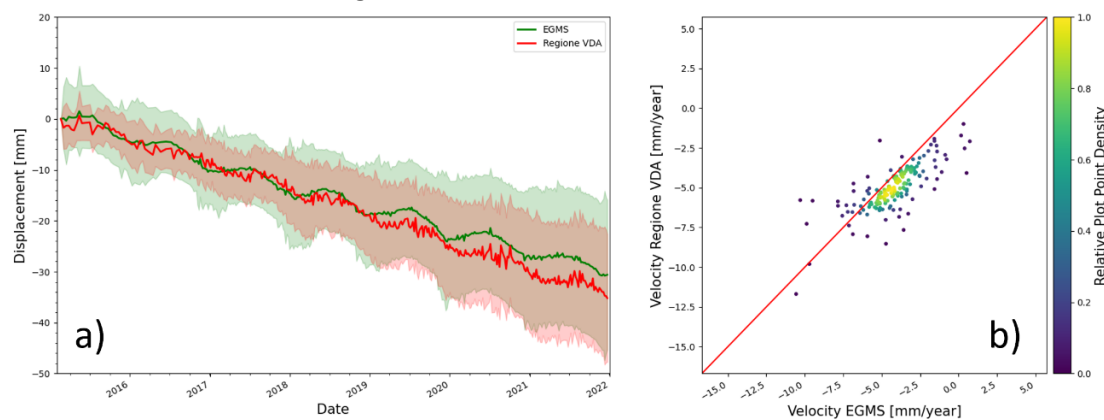


Figure 12: a) Average and standard deviation of ADA time-series for EGMS Basic and RVDA; (b) velocity correlation for ADA area.

Table 3 presents the averaged validation measures for all Basic/L2a products that have been compared, along with the resulting IoAs.

Table 3: Aosta valley IoA

Vale d'Aosta	Validation Measure	IoA
Spatial overlap [%]	60.36	0.62
Relative Velocity Difference [%]	34.33	1.00
Velocity Correlation	0.72	0.80
Displacement Time Series Correlation	0.78	1.00
Total		0.85

Conclusion for the Aosta Valley area:

The most significant difference can be observed in the ascending product, where the bottom of the central valley appears to experience an uplift of a few mm/year, this is most likely due to unfiltered atmosphere contributions.

The difference in the number of ADAs detected in the two datasets can be attributed to differences in MP density and coverage, rather than disparities in velocity values. Despite this difference, the detection identifies the same major landslide areas, as reflected in the resulting IoA of 0.85, which underlines the good agreement of the two datasets. This indicates the usability of the EGMS for regional-level landslide mapping activities.

French national landslide inventory

National inventories are typically compiled through field investigations, sometimes supplemented with aerial photos or optical satellite imagery. When ground motion is identified in the field, a georeferenced point is archived in the inventory.

The national French inventory in the Alpes Maritimes (bordering Italy and facing the Mediterranean Sea) contains over 500 landslides. Given the mountainous nature of these areas,

the density of MPs is expected to correlate with slope, aspect, and land cover. Additionally, the density is also expected to vary based on the ascending/descending orbits.

The selected site has experienced numerous episodes of intense rainfall over the past two decades, with some particularly notable in year 2000, February and November 2014, October 2015, and more recently in October 2020, with events happening in the Vésubie, Roya and Tinée valleys during the Alex storm triggering damaging landslide events. This area also encompasses deep-seated landslides that are rooted in bedrock and are often slow moving.

To compare EGMS with the inventories, a geometrical match between ADA polygons and inventory points is performed, considering the total number of inventory points and ADA polygons (as exemplified in Figure 13).

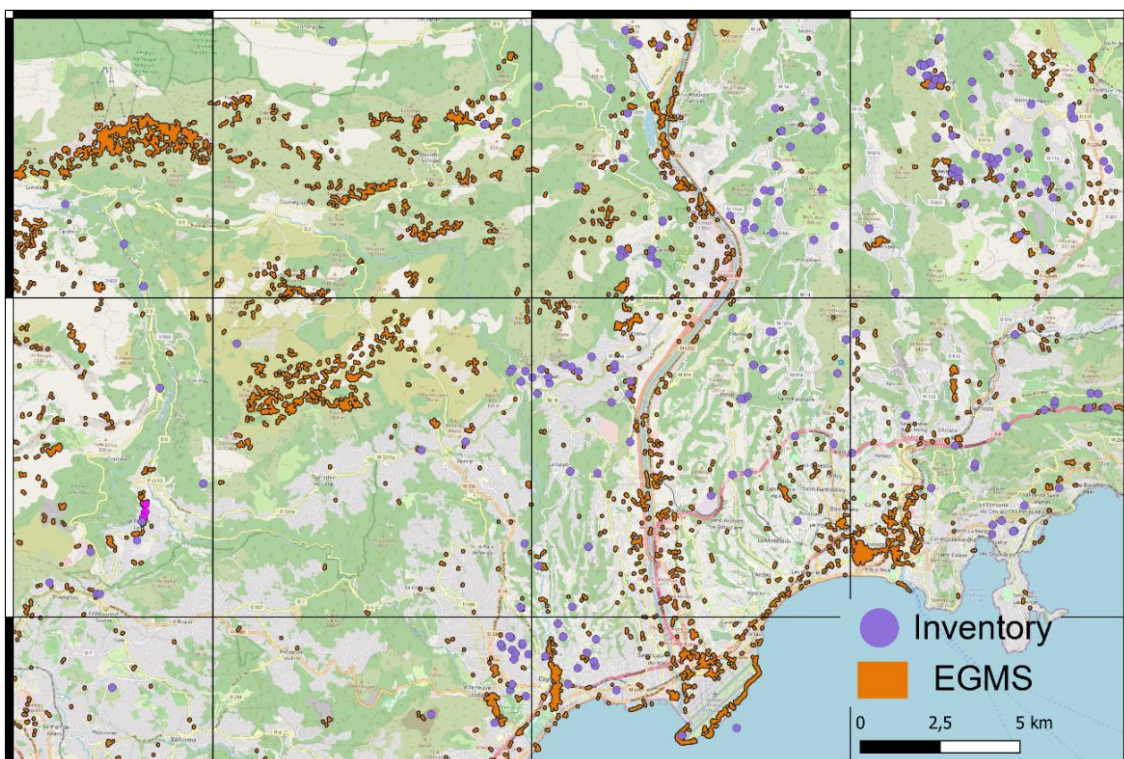


Figure 13: ADA polygons from EGMS L2a products (track 161/ASC / track 139/DESC) compared with inventory points in the Alpes Maritimes site.

In the ascending orbit, 54% of inventory points fall inside an ADA polygon, while 7% of ADA polygons include an inventory point. In the descending orbit, 25% of inventory points fall inside an ADA polygon, and 3% of ADA polygons host an inventory point. This result demonstrates how EGMS might be able to detect slow moving landslides that may not be visible on the ground. The MP density in the EGMS is primarily influenced by the type of land cover type, with MPs located even in remote areas. In contrast, national inventories are based on field observations, surveys, and damage reports, typically concentrated near built environments. This result should not be understood as a negative outcome, instead it highlights that over half of the landslides identified by the EGMS are not recorded in the national inventory, presenting opportunities for enhancements in national inventories.



This result underscores the significant influence of ascending and descending L2 geometries of acquisition on the number of MPs. As the Ortho/L3 products combine ascending and descending geometries into a 100m grid, they inherently contain fewer EGMS points.

L2 products prove to be more suitable for detecting landslides motion detection – particularly in highly mountainous areas where the MP density is intricately linked to both the acquisition geometry and the orientation of topographic slopes (Figure 13).

L2 products consist of 1D measurements in the LOS direction and are particularly valuable for detecting slow motions ranging from 1mm/year to approximately 20 cm/year. While L2 has the limitation of not providing 2D/3D motion components, for landslide detection, the sense/direction of motion is less restrictive than in other thematic areas.

The results from Basic/L2a are sufficient for landslide detection within the detectable ground motion regime, including instances of acceleration/deceleration.

It is worth noting that North/South oriented landslides might either go unnoticed or be inaccurately characterized in terms of maximum velocity and time series. InSAR cannot measure horizontal movements in the North/South direction, and it can only measure the vertical component of such movement. Sensitivity to the horizontal component increases in the East-West oriented landslides. In conclusion, this is not a limitation of the EGMS products but rather an InSAR limitation.

IoA: Do EGMS polygons contain points from national inventories?

In the ascending orbit, 54% of inventory points fall within EGMS polygons, while 7% of EGMS polygons host an inventory point. In descending mode, 25% of inventory points fall inside an EGMS polygon, with 3% of EGMS polygons hosting an inventory point.

When interpreting these numbers, it is crucial to consider that the EGMS may have the capability to map unstable areas that have not been previously recognized on the ground, and thus are not yet included in the inventory. Therefore, in several instances, even though the IOA appears low, the EGMS may significantly contribute to improving national inventories.

Spanish national landslide inventory

The Spanish national risk inventory was also considered for validation purposes, primarily focusing on landslides, with thousands of related phenomena included in the inventory for the selected study areas. The example presented here is focused on the Arcos de la Frontera landslide, Spain. To identify landslide phenomena in the EGMS products, detection is considered positive/match if the velocities detected by the EGMS within the inventory polygons are

significantly different from the surrounding areas. The criterion for detection is the mean velocity difference between “inside the polygon” and “outside the polygon”, with a velocity difference threshold set at >2 mm/year.

In **Arcos de la Frontera**, the average EGMS velocity (depicted by green points in Figure 14) within the national archive polygons (represented by red polygons in Figure 14) is 8.6 mm/yr. In contrast, the average velocity recorded by the EGMS in the stable buffer area around the inventory polygons is 1.3 mm/yr. The land use in the Arcos de la Frontera landslide area includes both vegetated and built-up sections. As expected, MPs on the Arcos de la Frontera landslide are visible on the built area only.

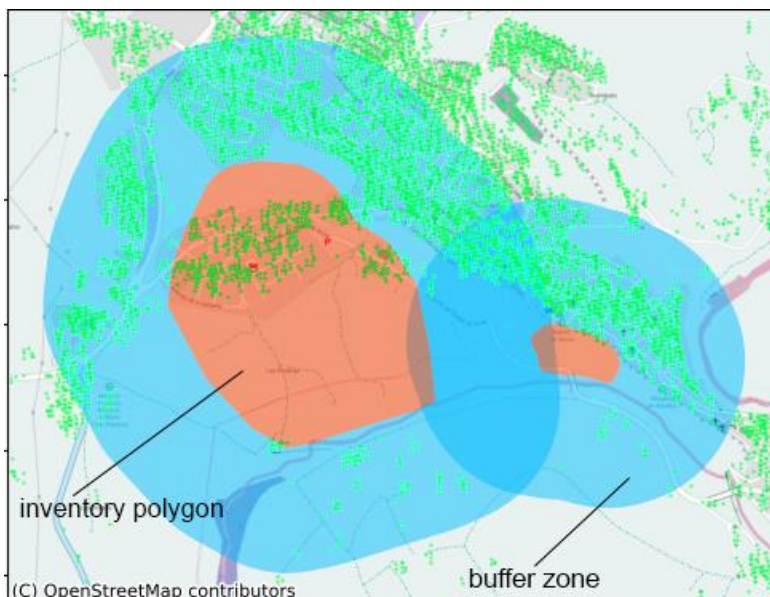


Figure 14: Arcos de la Frontera test site, Spain. EGMS velocities (L2a/Basic track 147/ASC) within the inventory polygons (depicted in red) are compared with velocities outside the inventory polygons (buffer area depicted in blue).

IoA: Does the EGMS detect motion within the polygons from the national inventories?

The detection is considered successful because the average difference in EGMS values between inside and outside the inventory polygons exceeds 2 mm/yr.

Another example involves the **Rules reservoir**, located on the river Guadaleo, downstream from its confluence with the Izbor river, in the municipality of Vélez de Benaudalla. The reservoir collects the water from the southern slopes of Sierra Nevada Mountain range, from Sierra de Lújar and from La Contraviesa. The 30 km² basin surrounding the reservoir is affected by several landslides, most of them reported in the national inventory. In this validation site, the comparison of geometry and surface of inventory polygons with Ortho/L3 (vertical) EGMS derived polygons is tested. The inventory polygons are based on field mapping and a previous InSAR survey (Reyes-Carmona et al., 2020) (Figure 15).

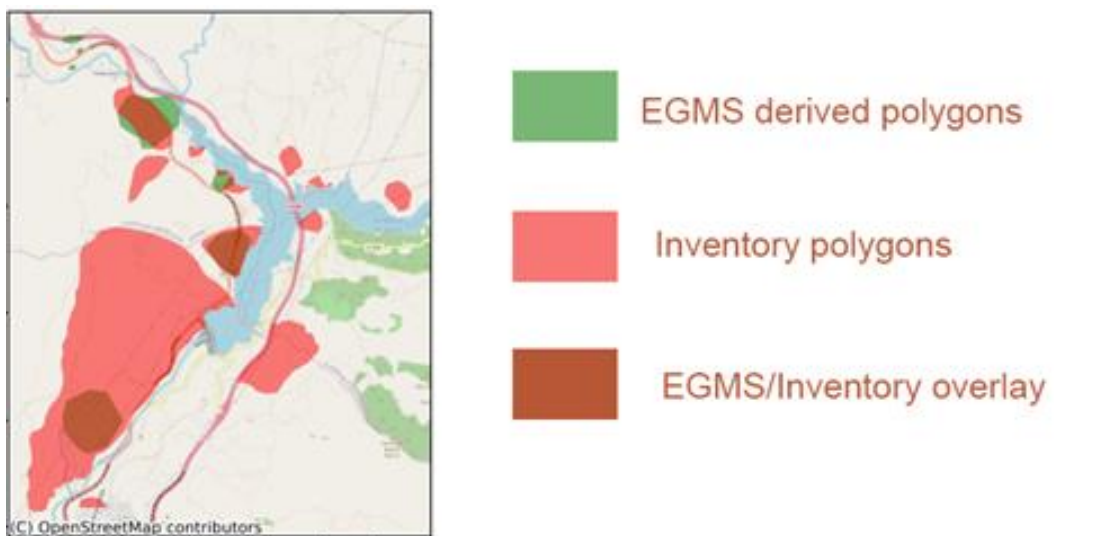


Figure 15: Rules reservoir area, Spain. Overlapping area between inventory polygons and EGMS ADAs (L2a/Basic 147/ASC).

The cross-comparison criterion applied in this context involves computing the surface areas of both the inventory polygons and the EGMS derived polygons. To facilitate the comparison, a simple indicator is proposed: the surface area of the intersection between the corresponding polygons (both inventory and EGMS) is divided by their average surface area. The EGMS polygon is considered as a positive match for mapping if this value is higher than 0.5.

IoA: Are EGMS polygons similar to polygons from national inventories?

In the Rules reservoir area, the proportion of EGMS-derived polygons considered consistent with the inventory equals to 26% of the affected areas. As depicted in Figure 15, the inventoried polygons are only partially covered due to locally insufficient MP density. Nevertheless, similar to previous sites, the EGMS data might enable the detection of new active landslide areas.

Mining and post-mining

Limburg (Netherlands)

The **Limburg** area, situated in the southeast of the Netherlands, is a former coal mining region characterized by predominantly urban landscapes with gentle topography, reaching a maximum elevation of approximately 322 m. Coal mining activities in the Limburg area were abandoned in the 1970s. In 1994, the hydrologically connected, neighbouring German mining operations were also terminated, leading to the cessation of all mining-related ground water pumping (Cuenca et al, 2012). The subsequent rise of the water table resulted in uplift across areas in the Netherlands, Germany, and Belgium.

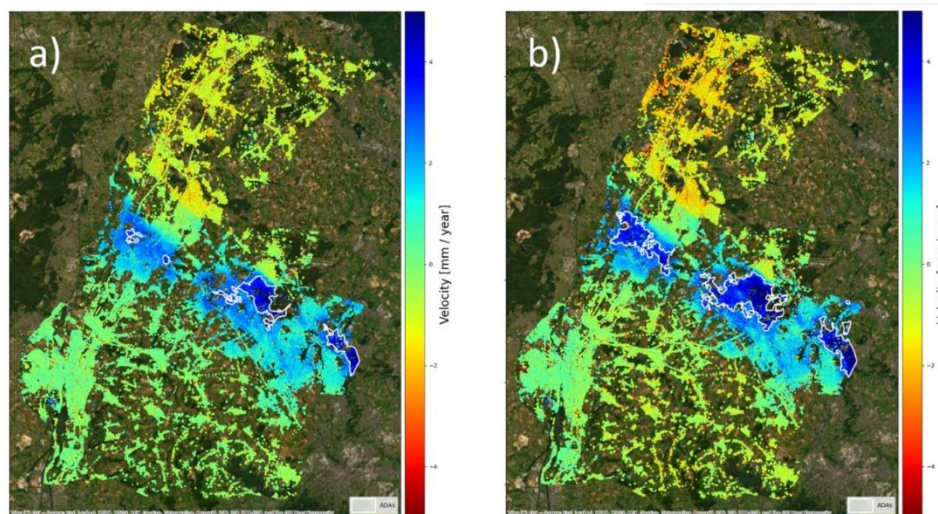


Figure 16: Comparison of velocities between the EGMS Calibrated/ L2b product of track 88/ASC (a) and the Dutch GMS (b). Detected ADAs are depicted by the white polygons.

Figures 16 and 17 show a comparison of the velocities between the EGMS and the Dutch GMS for the Calibrated/L2b product of ascending track 88. The white polygons indicate the detected ADAs. Given the relatively minor deformations detected, velocity thresholds for points and clusters in ADAs detection have been set to >3 mm/year.

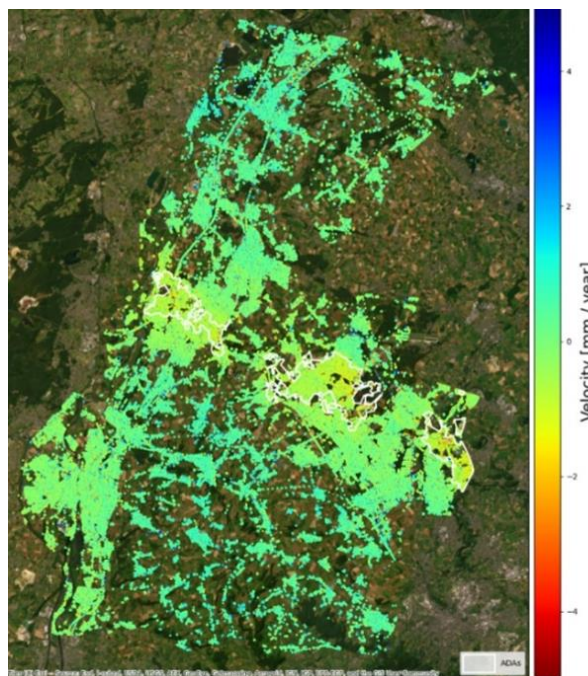


Figure 17: Velocity difference ($dvel = vel_{EGMS} - vel_{Dutch GMS}$) between the EGMS and the Dutch GMS. Detected ADAs are depicted by the white polygons.

The overall patterns in the velocity maps appear consistent between the two datasets. The amplitude of the velocities from the Dutch GMS is slightly higher than that of the EGMS. This is evident in both the uplift area in the center, where the difference map shows positive values, and the northernmost and southernmost areas, where the Dutch GMS exhibits slightly stronger subsidence than the EGMS. It should be noted that the comparison of absolute values in this case is not meaningful due to the use of different GNSS reference systems for the calibrations of the Calibrated/L2b products in the EGMS and the Dutch GMS, respectively.

Consequently, a slight general offset in the velocities, as observed in the northern and southern parts of the area, is expected, and is registered.

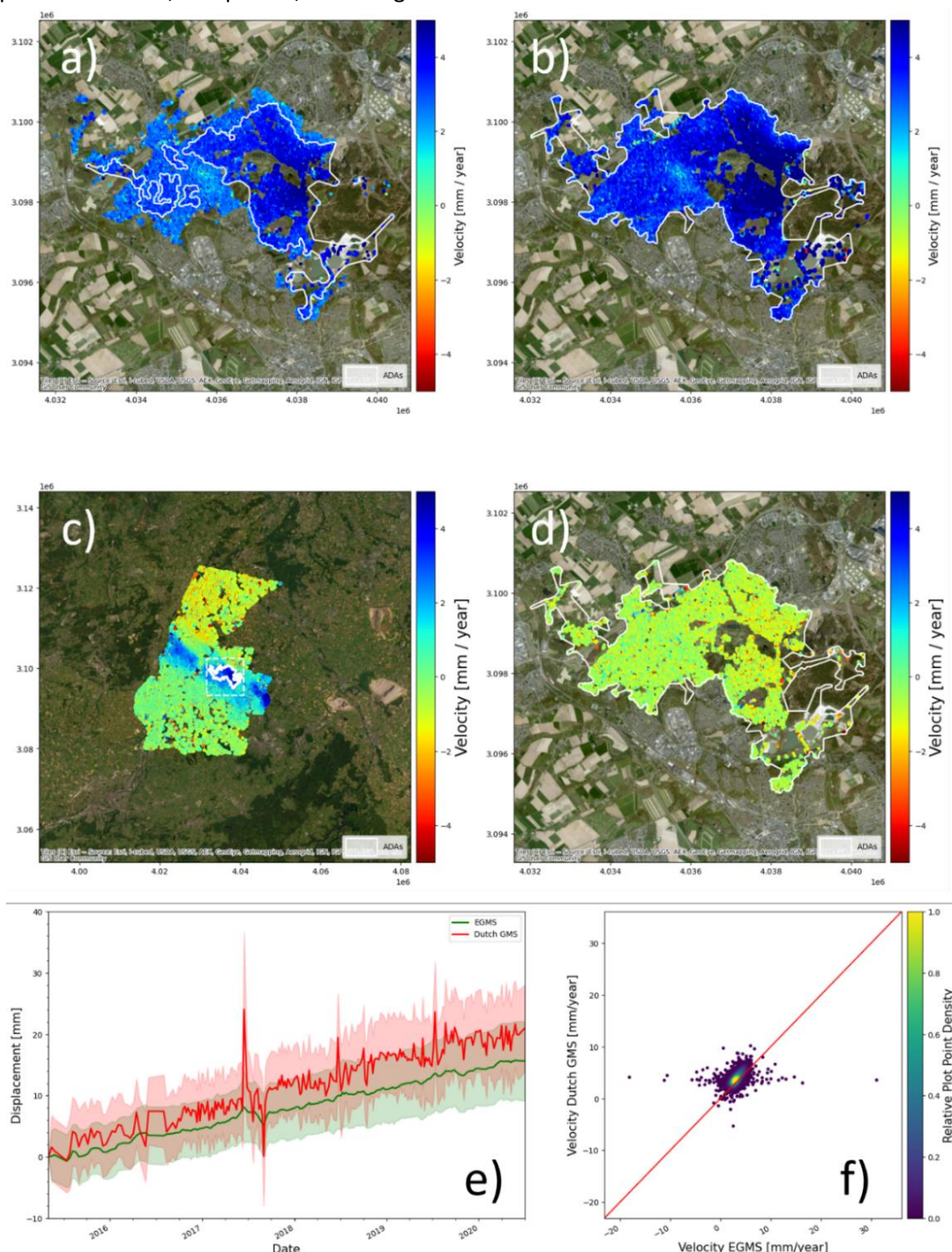


Figure 18: Detailed map of the same L2b product displayed in Figures 16 and 17, with focus on the largest ADA in the centre of the uplift area: ascending (a) and descending (b) active deformation areas (ADAs) derived from EGMS Basic/L2a product – (c) overview of the ADA location; (d) velocity difference ($dvel = vel_{EGMS} - vel_{Dutch GMS}$) between the EGMS and the Dutch GMS; e) average and standard deviation of all the ADA time series; (f) velocity correlation.

Figure 18 shows a detailed comparison for the largest ADA in the centre of the uplift area. Figures 18(a) and 18(b) show the respective velocity maps with the detected ADA. Given that the velocities in the Dutch GMS are slightly higher, the ADA derived from the Dutch GMS are in general larger than the ones coming from the EGMS. The velocity difference map in Figure 18(d)

shows that the velocities of the Dutch GMS are slightly higher than those in the EGMS (negative difference).

Figure 18-e illustrates the time series for both datasets, displaying a clear linear behaviour in both cases. The time series of the Dutch GMS appears slightly steeper due to the higher velocity. The indicated standard deviations for the time series in Figure 18-e suggest a similar amount of noise in both datasets. In Figure 18-f, the spatial correlation of the velocity values is depicted by plotting EGMS velocities on the horizontal axis against Dutch GMS velocities on the vertical axis. Ideally, the distribution of the points should align with the diagonal marked in red, but the distribution of the points is rather compact, indicating a mismatch of 5–10 mm/year for a larger number of points. This misalignment can also be observed in Figure 18-d, where it manifests as a slight noise in the difference map.

Table 4 summarizes the calculated validation measures averaged for all ADA derived from Calibrated/L2b products, along with the resulting IoAs.

Table 4: Limburg IoA results summary

Limburg	Validation Measure	IoA
Spatial overlap [%]	41.22	0.39
Relative Velocity Difference [%]	28.99	1.00
Velocity Correlation	0.42	0.38
Displacement Time Series Correlation	0.76	0.84
Total		0.65

The achieved spatial overlap of 40% is relatively low, primarily due to slightly higher velocities in the Dutch GMS dataset and the presence of rather smooth and wide uplift patterns. The smoothness of the velocity fields means that the size of the detected ADAs is very sensitive to even slight variations in the velocities, resulting in a 40% overlap despite a relative velocity difference for the ADAs below 30%.

The spatial velocity correlation is 0.42, also relatively low, as observed in Figure 18-f. The time series correlation yielded a value of 0.76, indicating that both time series exhibit similar linear behaviour with some variation in trend, as reflected in the velocity differences.

Conclusion for the Limburg validation site:

The comparison results in an IoA of 0.65, which means that considerable differences have been observed. This can mainly be attributed to differences in the calibration process. In terms of usability, this does not pose a limiting factor to the ability of the EGMS to detect such large scale, mining-induced ground motion and both datasets show the same large-scale displacement areas. This evidence rather demonstrate that for proper detection of active displacement areas it is important to adjust the parameterization for the ADA detection to the regional velocity regime.

Lorraine region (France)

Multiple areas covered by segments of the national inventories affected by mining/post-mining activities are examined. One specific study area is situated in the Lorraine region, covering the municipalities of Forbach and Freyming-Merlebach, featuring an abandoned coal mine complex (active until 2004). This region spans approximately 50 km², with the EGMS coverage shown in Figure 19.

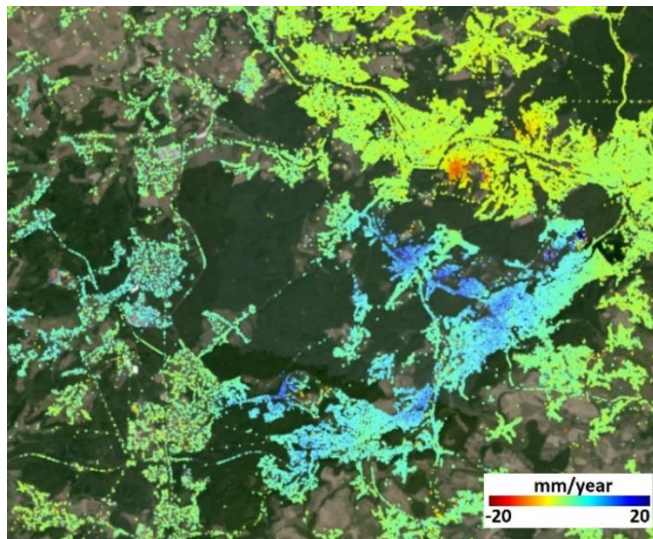


Figure 19: The area in Lorraine region (France) as seen by EGMS (Calibrated/L2b track 37/DESC). It represents residual motion on an abandoned coal mine complex (actually active until 2004).

Figure 20 provides an illustrative comparison in a post-mining site in Lorraine, France. The red area has been derived from historical ground-based terrain motion, while the green area represents the EGMS L2a ADAs (descending track 37). Calculations include area intersection, difference, and union. The goal is to compute the area intersection with respect to the reference area, obtained by averaging the EGMS and inventory areas. The results yield an intersection area of 64%.

*EGMS L2 data products are well suited to detect this type of ground motion:
several mm/year over a few km wide area.*

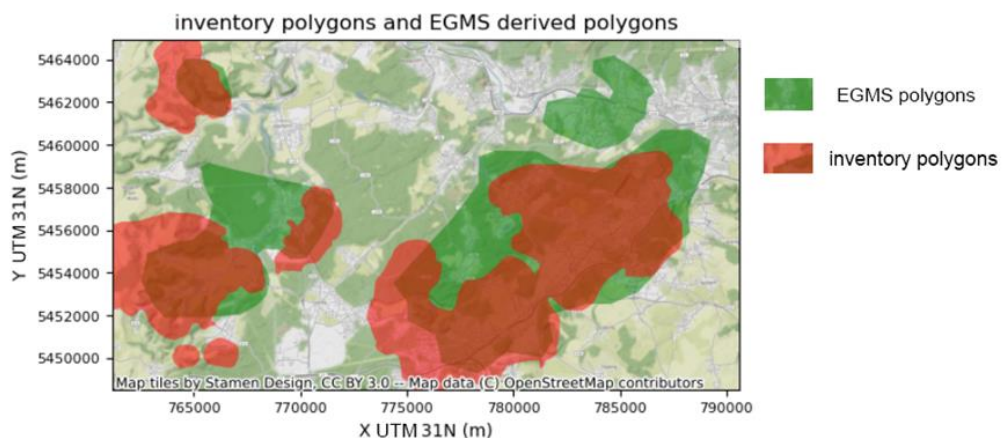


Figure 20: Green area extracted from EGMS Basic/L2a track 37/DESC via the ADA procedure, red area is from national inventory.

IoA: Are the EGMS ADAs similar to the polygons from national inventories?

The number of EGMS-derived polygons considered consistent with the national inventory account for 64% of the affected areas. It is essential to note that EGMS has the potential to map unstable areas not previously identified on the ground, consequently, not included in an inventory. In several instances, even with a low IoA value, the EGMS might be proven useful for improving national inventories.

La Unión (Spain)

The validation site in La Unión, Spain, was specifically selected for its mining activities, encompassing both underground and surface mining, containing tailings dams and waste dump sites. Located on the south-eastern coast of Spain along the Mediterranean, this site was exploited for lead and zinc deposits until 1992. The mining activities were mainly underground until 1960, after which open-pit exploitation started. Over the course of fifty years, the landscape of La Union underwent significant transformations, with surrounding valleys and hills completely covered by mine waste material.

To assess the consistency of the EGMS measurements with this complex mining terrain, the EGMS data over La Unión were compared to ancillary geoinformation. As part of this comparison, automated detection of ADAs in the EGMS was crucial. Figures 21 and 22 show the EGMS velocity maps for the area, featuring Basic/L2a data for both ascending (track 103) and descending orbits (tracks 8 and 110).

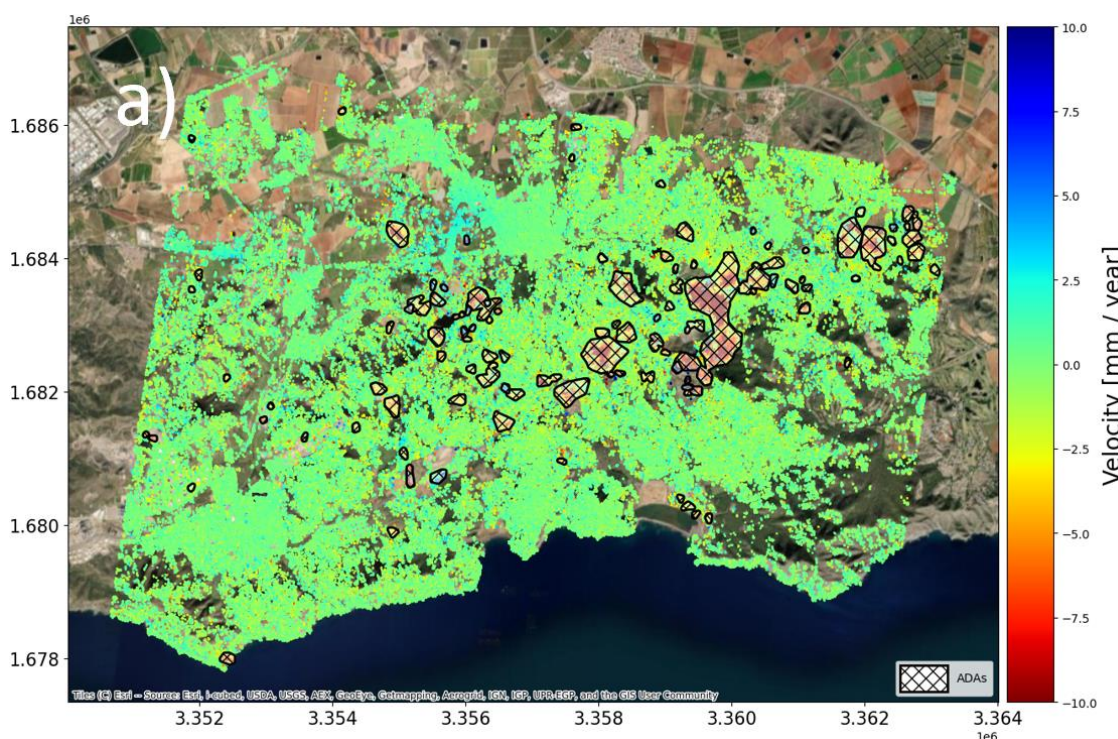


Figure 21: EGMS Basic/L2a velocity maps track 103/ASC in La Unión area with detected ADAs marked as black polygons.

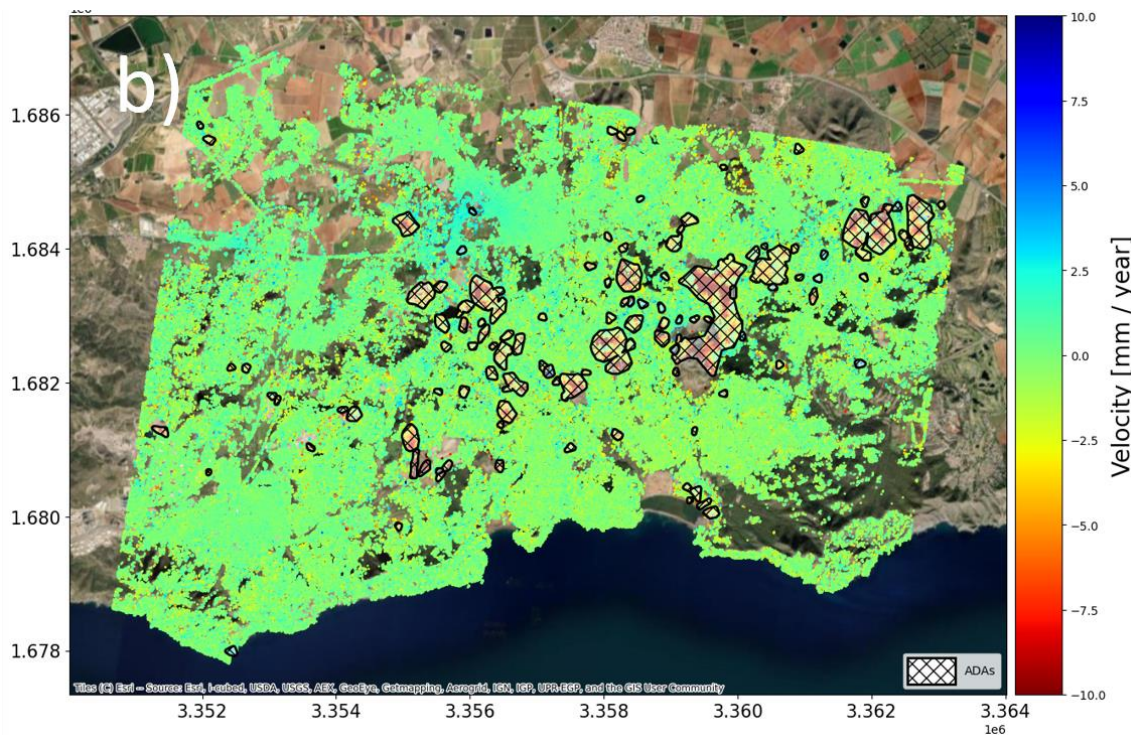


Figure 22: EGMS Basic/L2a velocity maps (tracks 8+110/DESC combined) in La Unión area with detected ADAs marked as black polygons.

Comparison with Corine Land Cover Map:

The comparison with Corine Land Cover (CLC) aims to assess the consistency with land cover related factors causing ground displacement. Figures 23 and 24 show the detected ADAs over the Corine Land Cover categories for both ascending and descending orbits.

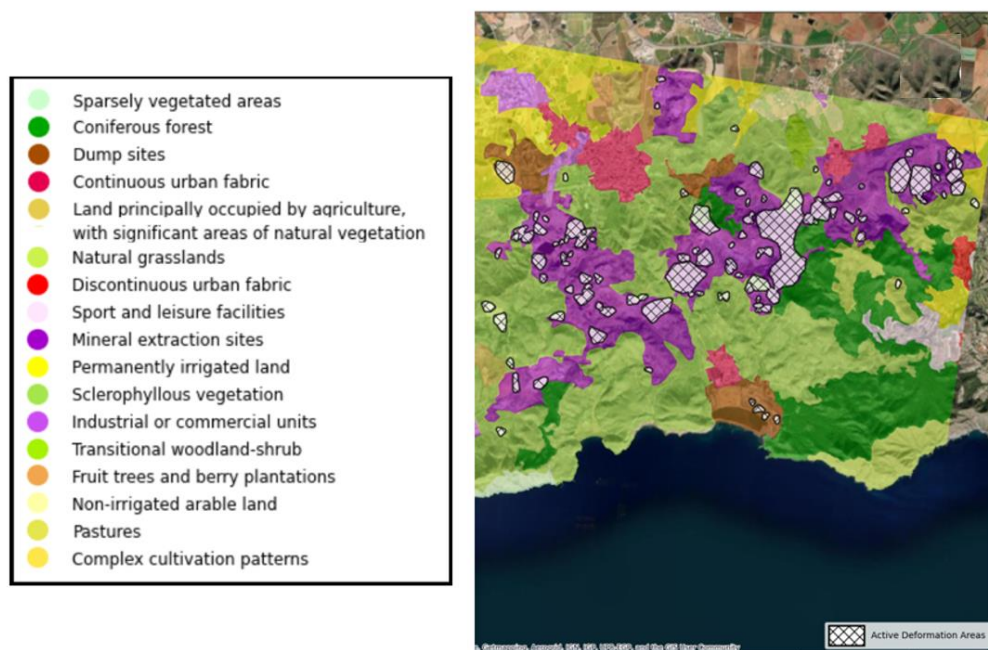


Figure 23: Active deformation areas superimposed on the Corine Land Cover maps for Level 2a products in ascending orbit

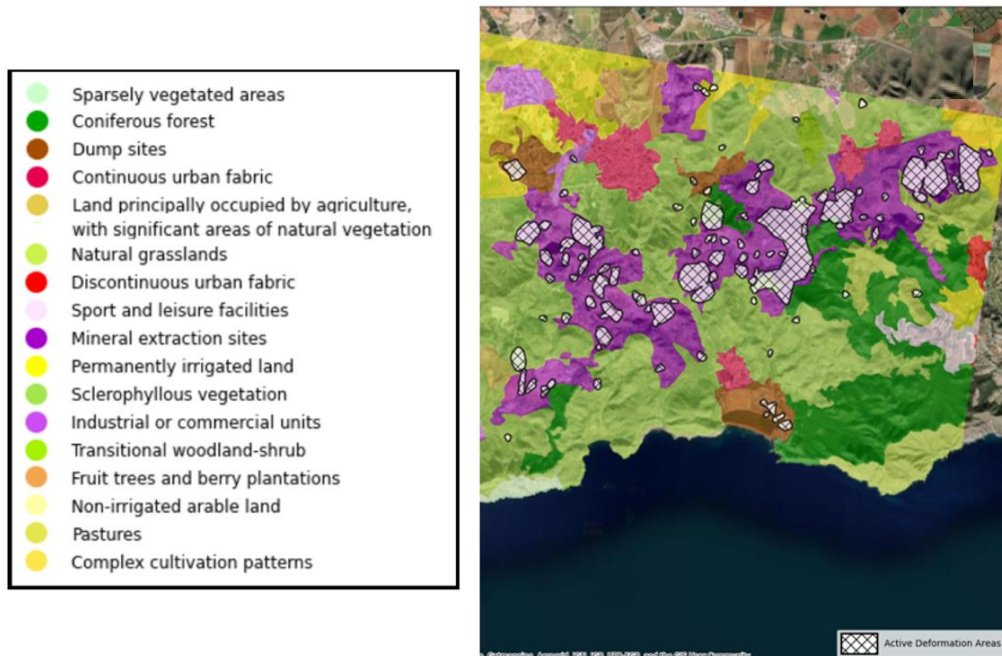


Figure 24: Active deformation areas superimposed on the Corine Land Cover maps for Level 2a products in descending orbit

In addition, Figure 25 shows an overview of the measured areal coverage of thematic units by ADAs (in percent) for all EGMS products. Figure 25 shows a clear correlation between the presence of ADAs and the “Mineral Extraction site” class, i.e., areas that are affected by mining activities, as it was expected for this validation site.

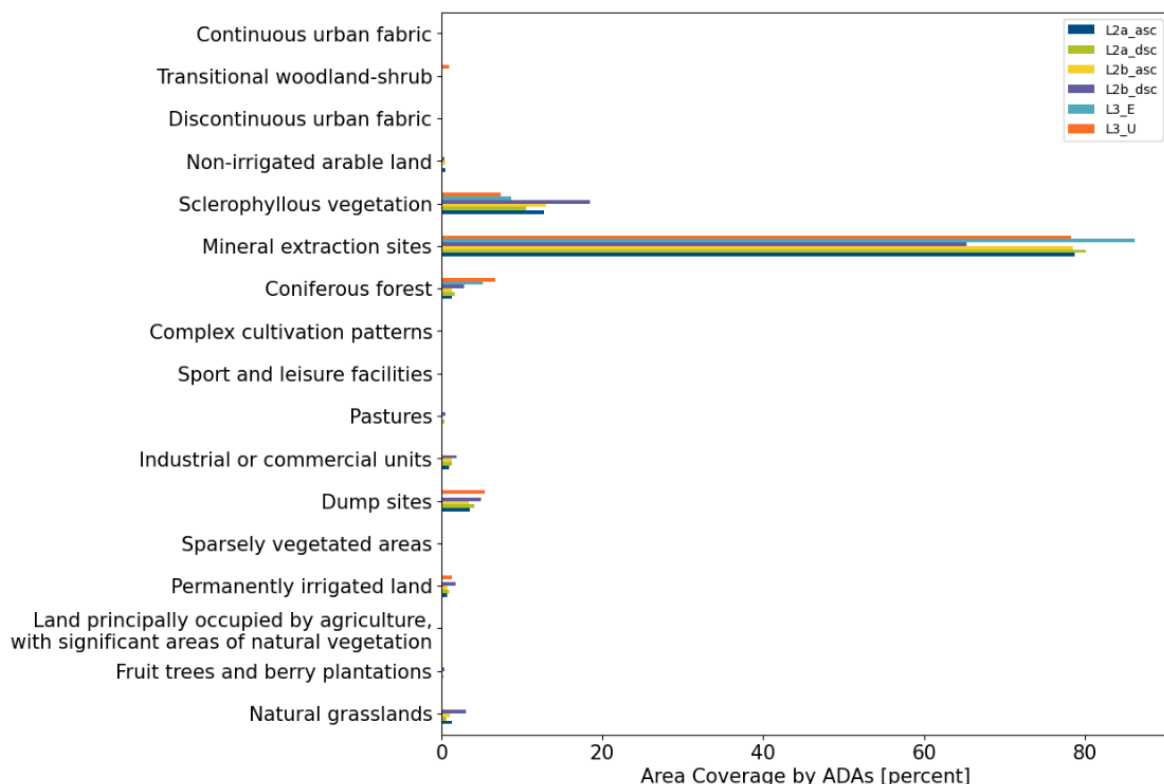


Figure 25: Measured overlap of ADAs with Corine Land Cover categories of the La Union area. Different colour bars represent different EGMS product levels. The measured values represent the overlap of ADAs with the respective Corine Land Cover category in percent of the ADA's total area.

IoA: Do the detected ADAs correlate with expected mostly anthropogenic areas categories in the Corine Land Cover map?

The EGMS products are considered consistent with the Corine Land Cover Map, as the detected ADAs predominantly overlap with areas mapped as mining-related land cover classes. This demonstrates the ability of the EGMS to map active motion (if any) in such areas, within the technical boundaries of the interferometric technique.

Comparison with a mine waste inventory:

The EGMS products were also compared with an inventory of "Mine waste" and "Tailings", where mine waste covers various types of predominantly solid waste materials, and tailings are usually deposited as slurry, mixed with substantial amounts of water. Figure 26 shows the overlap of ADAs detected for Basic/L2a ascending a) and descending b) datasets. In addition, Figure 26 provides an overview of the measured areal coverage of both mine waste and tailings by ADAs (expressed in percentage) for all EGMS products.

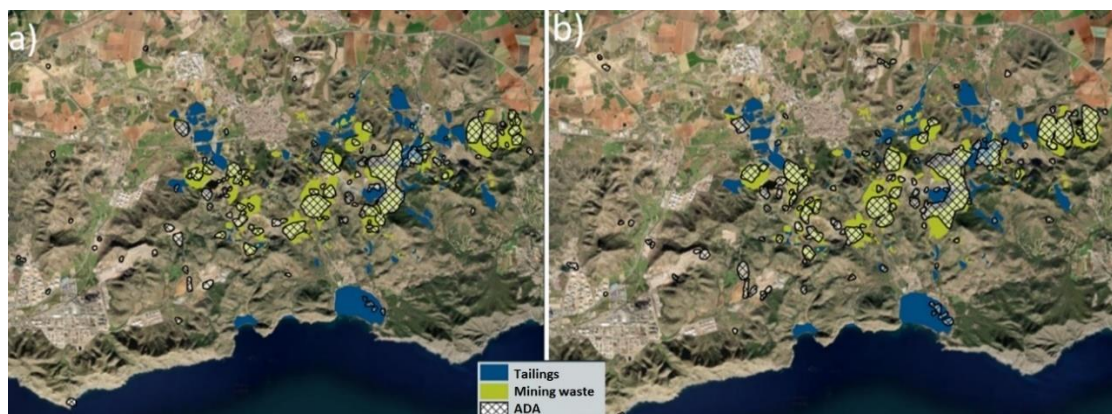


Figure 26: Ascending (a) and Descending (b) EGMS ADA versus mine waste land cover classes

Visual inspection of Figures 26 and 27 reveals that a good number of ADAs overlap with the mine waste areas. However, there is only a very small overlap with tailings zones. The expected overlap with tailing areas, which typically exhibit significant subsidence due to the compaction of the tailings, is not observed. It is plausible that, given the cessation of mining activities in this area approximately two decades before the start of the EGMS dataset, the tailings have consolidated over time, resulting in the absence of significant motion.

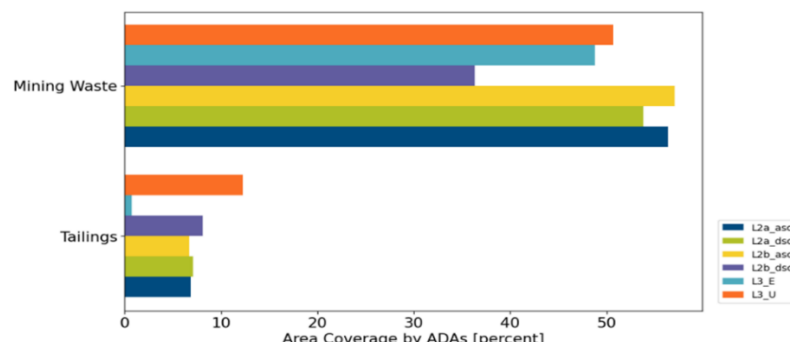


Figure 27: Measured overlap of ADAs with mine waste and tailings storage facilities. Differently coloured bars represent different EGMS product levels. The measured values represent the overlap of ADAs with the respective category in percent of the ADA's total area

IoA: Do ADAs significantly overlap with mine waste categories?

The polygons categorised as “Mining Waste” shows a significant overlap with ADAs detected in the EGMS products, opposite to the “Tailing” polygons, which do not record such correspondence. Yet, the EGMS products are still considered consistent with the mapped mine waste categories because it is plausible to assume that the tailings have been inactive long enough to have consolidated and to not show significant ground motion any longer.

Three additional datasets have been compared to the EGMS products: lithology, fault lines and topography. Since the motion in this region is mainly associated with post-mining phenomena, no significant correlations were found, as expected.

The comparison with Corine Land Cover Map and mine waste categories shows, that the EGMS is capable of mapping individual mining related areas, and it demonstrates the ability of the EGMS to distinguish active and inactive mining waste deposits that are in close proximity.

Silesia (Czech Republic)

The validation site in Silesia, a region shared between Czech Republic and Poland, was selected due to its ongoing and active underground mining. It is one of the largest hard coal mining areas in Europe, with mining activity starting in the 19th century. The development of the mining industry was accompanied by urban growth, and currently, 37 cities collectively host almost three million inhabitants. Figures 28 and 29 show the Basic/L2a velocity maps for both ascending and descending orbits, for which all available tracks have been combined into a single dataset for ascending (tracks 73, 102, 175) and descending (tracks 51, 124), respectively.

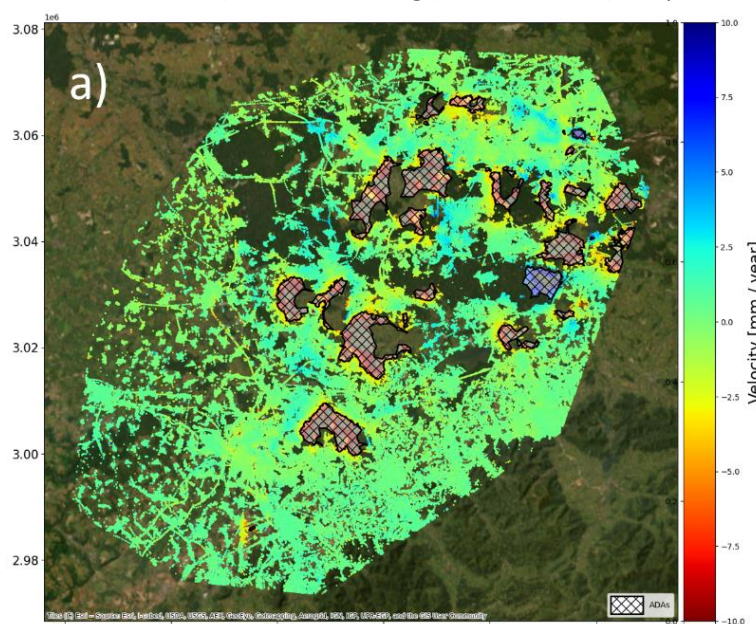


Figure 28: EGMS Basic/L2a velocity maps in for ascending (a) (tracks 73+102+175/ASC) for the Silesia area with detected ADAs polygons.

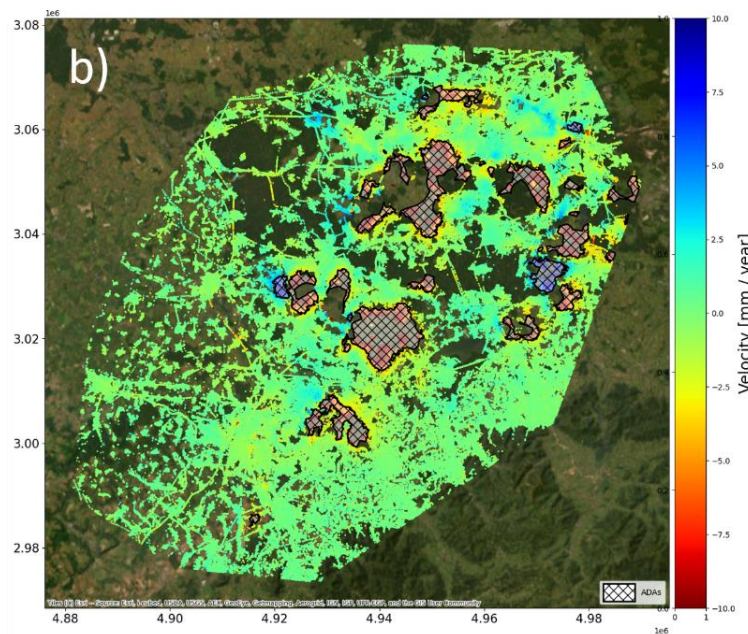


Figure 29: EGMS Basic/L2a velocity maps for descending (b) mode (tracks 51+124/DESC) for the Silesia area with detected ADAs polygons.

Comparison with Corine land Cover:

Like the La Unión site, a comparison with Corine Land Cover was conducted at the Silesia site to assess the consistency of ground displacements measured by the EGMS with land cover categories. Figures 30-a and 30-b show the detected ADAs alongside the land cover categories.

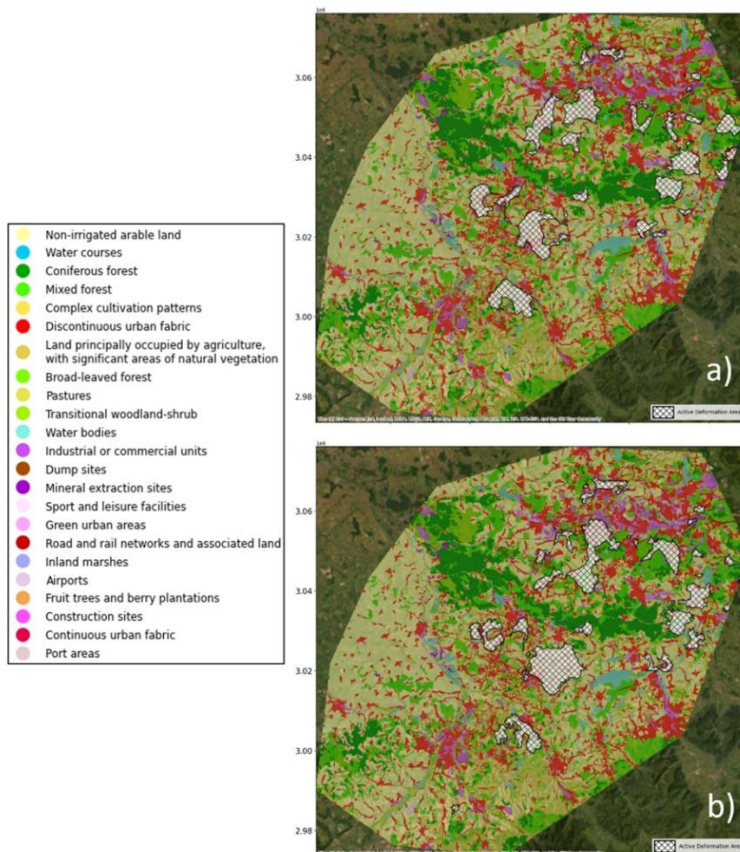


Figure 30: Active deformation areas (ADAs) superimposed on the Corine Land Cover map for Level 2a products in ascending (a) and descending (b) orbits in the Silesia region.

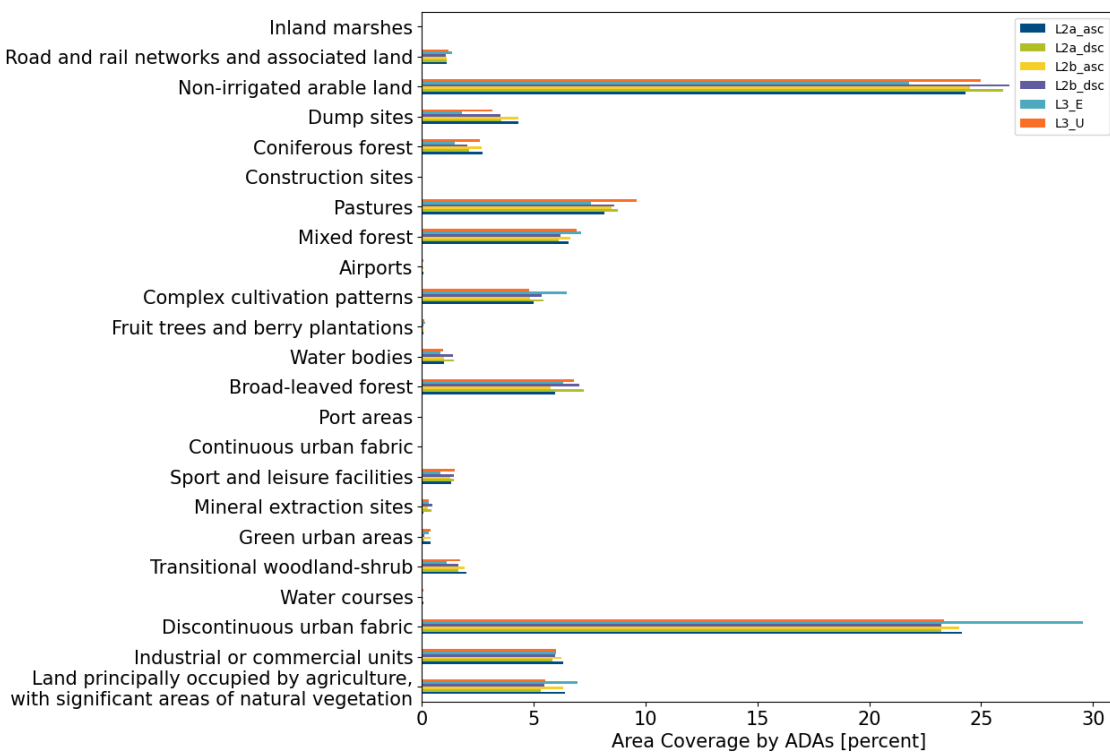


Figure 31: Measured overlap of ADAs with Corine Land Cover categories of the Silesia area. Differently coloured bars represent different EGMS product levels. The measured values represent the overlap of ADAs with the respective Corine Land Cover category in percent of the ADA's total area.

In addition, Figure 31 shows an overview of measured areal coverage of thematic units by ADAs (in percent) for all EGMS products. Visual examination of the maps in Figure 31 reveals no apparent correlation between the ADAs and any CLC category. This lack of correlation is consistent with subsidence in this area primarily being caused by underground mining activities, resulting in surface deformation unrelated to the land cover on top of the mined area.

Nevertheless, the observed overlap between ADAs and CLC classes in Figure 31 indicates a higher overlap with two CLC categories, namely "Discontinuous urban fabric" and "non-irrigated arable land". This can be attributed to these categories being dominant in the area, making an overlap with these categories more likely.

IoA: Do the detected ADAs show any unexpected correlation with the Corine Land Cover Map?

The number of detected ADAs only reflects the relative coverage by the different Corine Land Cover categories and there are no unexpected correlations.

Comparison with mining-related areas:

Another dataset that has been compared is an inventory of Czech mining-related areas. As previously mentioned, the mining activities in this region are mostly underground. The inventory does not distinguish between different categories, so a single category "Mining Areas" is compared to the ADA locations. Figure 32 shows the overlap of ADAs detected for Basic/L2a in ascending (73,102,175) and descending (51,124) datasets with the mining areas.

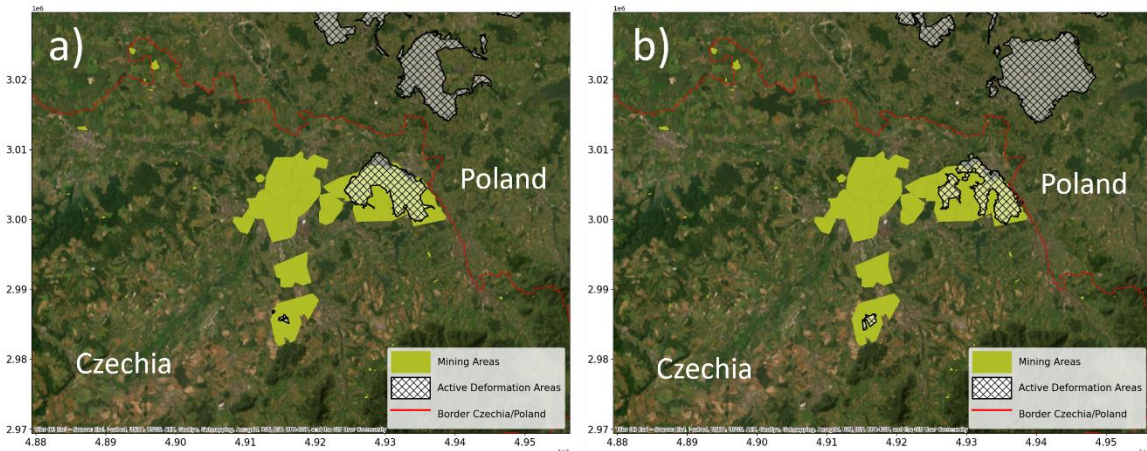


Figure 32: Locations of mining-related areas (green) plotted together with ADA locations a) 51+124/DESC b) 73+102+175/ASC (white). The mining-related areas dataset only contains areas within the Czech territory, but not in Poland.

Both maps show a good overlap with mining-related areas. In particular on the eastern side, the boundaries of the ADA and the mining area exhibit a very good correlation. Additionally, the small ADA further to the south correlates with a mining area. The absence of ADA coverage over some mining areas can likely be explained by different types of mining activity and/or activities having ceased in the past with no associated on-going ground motion. However, detailed information on the status or type of mining activities is not available. Another explanation could be a lack of EGMS MPs due to fast and non-linear displacements. However, a comparison with the point distribution in the velocity maps shown in Figures 28 and 29 indicates that this is unlikely in the area covered by the mining related areas map.

IoA: Do the detected ADAs correlate with mapped mining related areas?

All major detected ADAs overlap a mining related area. Absence of moving MPs over some mining related areas is most likely related to mining activities that do not or do no longer cause displacements.

Three additional datasets have been compared to the EGMS products: fault lines, a geologic map and topography. These datasets have mostly been investigated for any unexpected correlations in this area. With the subsidence primarily being related to mining activity and the avoidance of risk prone fault areas, no correlations were expected.

Conclusion for the Silesia area:

EGMS is capable of mapping ground motion related to subsurface mining, within the technical boundaries of the product, and that the ability to detect areas with ground displacements is not significantly affected by the land cover on the surface. Non-linear deformation patterns affect the MP density and therefore the ADA boundaries.

Urban

Thyborøn (Denmark)

Thyborøn, located on a sandy barrier facing the North Sea, is vulnerable to flooding, particularly during storm surges from the adjacent Linford, due to its low elevation (1.0–2.5 m). Subsidence in this region is attributed to the overall sedimentary structure of the sand barriers, with a significant part of the hamlet constructed on highly compressible landfill layers. For validation in Thyborøn, data produced by DTU were used since the GMS of Denmark only provides data until 2020. DTU provided Basic/L2a products. The focus area is the harbour, which is dominated by a single ADA. In general, a slight offset between the two datasets is evident, as observed in the displacement maps in Figure 33-a and 33-b, as well as in the difference map in 33-c. This offset is likely a result of different reference point selections.

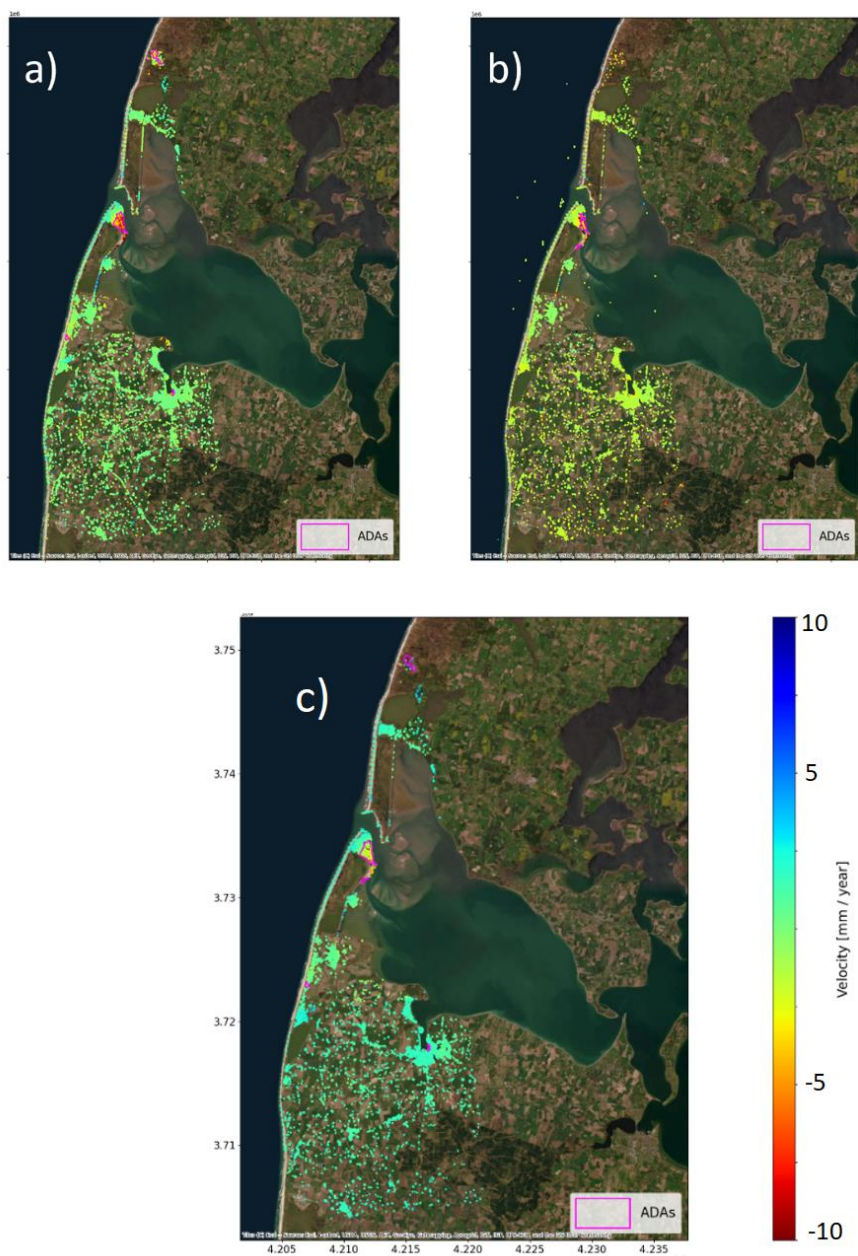


Figure 33: Comparison of Calibrated/L2b velocities from track 88/ASC for (a) the EGMS and (b) DTU-derived InSAR map; (c) velocity difference ($dvel = vel_{EGMS} - vel_{DTU}$). ADAs are marked by magenta polygons.

Figure 34 focuses on the Thyborøn harbour area, illustrating the most significant ADA with subsidence exceeding 10mm/year. The figure shows that the EGMS subsidence velocities are higher than those derived by DTU. Additionally, the EGMS data exhibit a higher MP density, resulting in a better coverage of the area. It is worth noting that both datasets have been resampled to the same spatial grid and time period, but not referenced to the same reference point.

The averaged time series in Figure 34-e display nearly linear trends, with different slopes reflecting the different velocities emphasized earlier. The associated standard deviations appear very similar, indicating a comparable level of noise in the data. The velocity distribution in Figure 34 f) exhibits an almost linear pattern, with a shift towards lower subsidence values for the DTU dataset, which is consistent with the general slight offset between the velocity values of the two datasets that was observed in Figure 33 above.

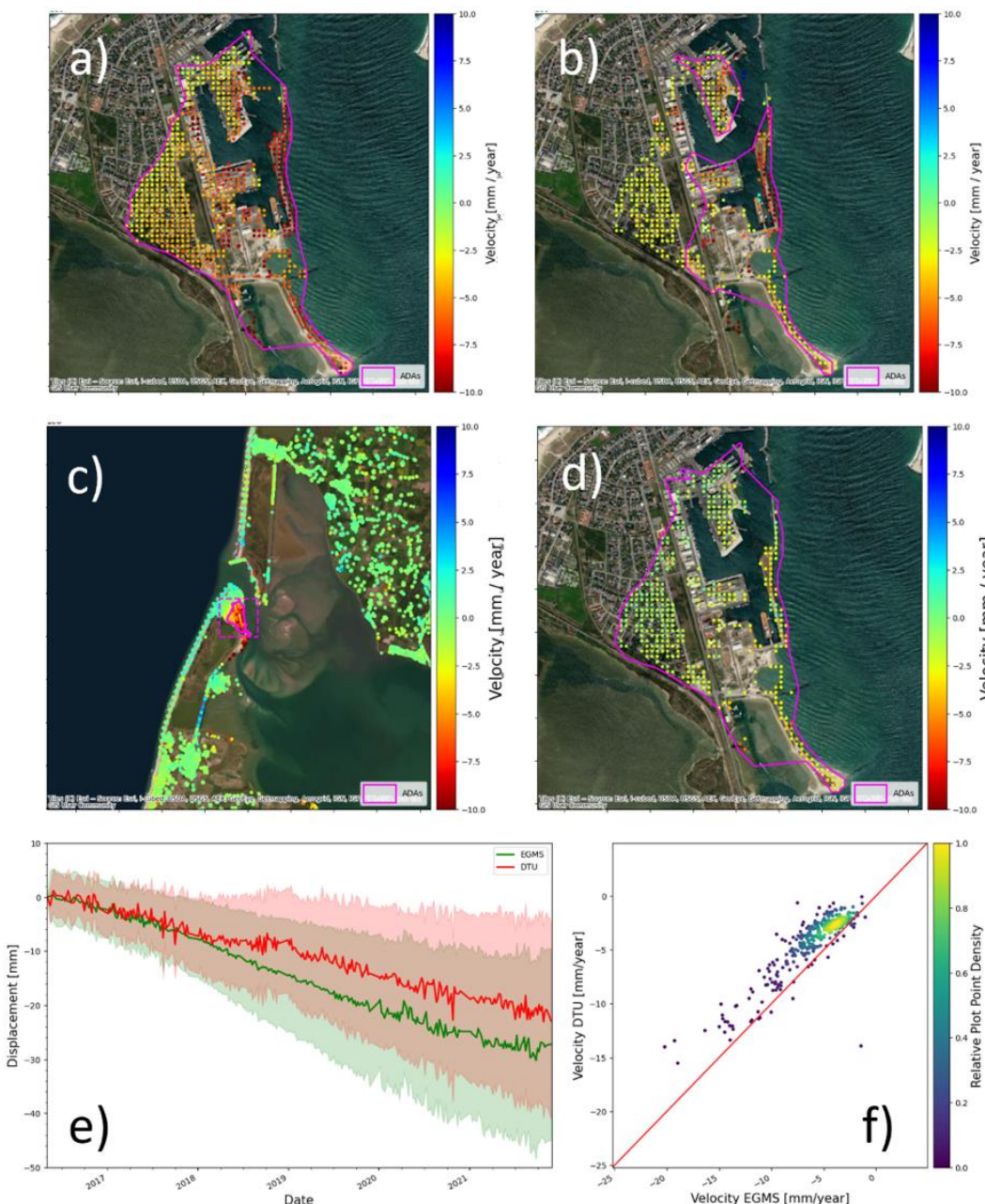


Figure 34: Zoom-in of the Calibrated/L2b product visualised in Figure 34, with focus on the largest ADA in the centre of the uplift area: (a) EGMS velocities; (b) DTU velocities; (c) overview of the ADA location; (d) velocity difference ($dvel = vel_{EGMS} - vel_{DTU}$).

Table 5: Validation measures and IoAs for Thyborøn, Denmark.

Thyborøn	Validation Measure	IoA
Spatial overlap [%]	59.87	0.60
Relative Velocity Difference [%]	40.73	0.96
Velocity Correlation	0.88	0.82
Displacement Time Series Correlation	0.92	0.91
Total		0.82

It can be concluded that while a slight velocity offset is observed over the entire area, most likely caused by different reference point definitions. The ADAs derived from EGMS and DTU results show similarities in the harbour area. The observed differences are expected since different processing workflows/chains have been used by EGMS and DTU to produce the compared products. It can be concluded that the EGMS allows the identification of subsidence at the local scale, coherently with one of the expected fields of application.

Oslo (Norway)

The main validation site for urban subsidence and the impact of engineering/construction works is the Municipal area of Oslo. Over the past 10 to 15 years the area surrounding the central station in Oslo has undergone extensive building and infrastructure development. The construction activities have resulted in significant settlements in the area, primarily induced by the reduction of pore pressure, mainly attributed to water pumping associated with drilling activities. Figure 35 shows the EGMS velocity maps (Basic/L2a product) for the area in both ascending (35-a) and descending orbits (35-b), for which all available tracks have been combined into a single dataset for ascending (tracks 44, 146) and descending (tracks 37, 66, 139).

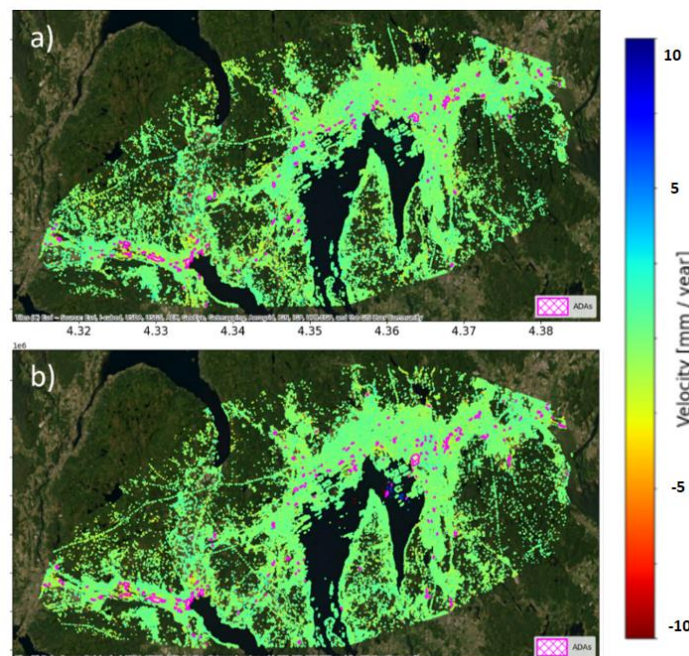


Figure 35: EGMS velocity maps in for 44+146/ASC (a) and 37+66+139/DESC (b) mode for the Oslo area with detected ADAs marked as pink polygons.

Comparison with Corine Land Cover:

The comparison of displacement velocity patterns with land cover maps has been done to assess the consistency with land use related causes for ground displacement. Figure 36 a) shows an overview of the metropolitan area of Oslo, with detailed views of Drammen and Oslo City regions presented in Figure 36 b) and c), respectively.

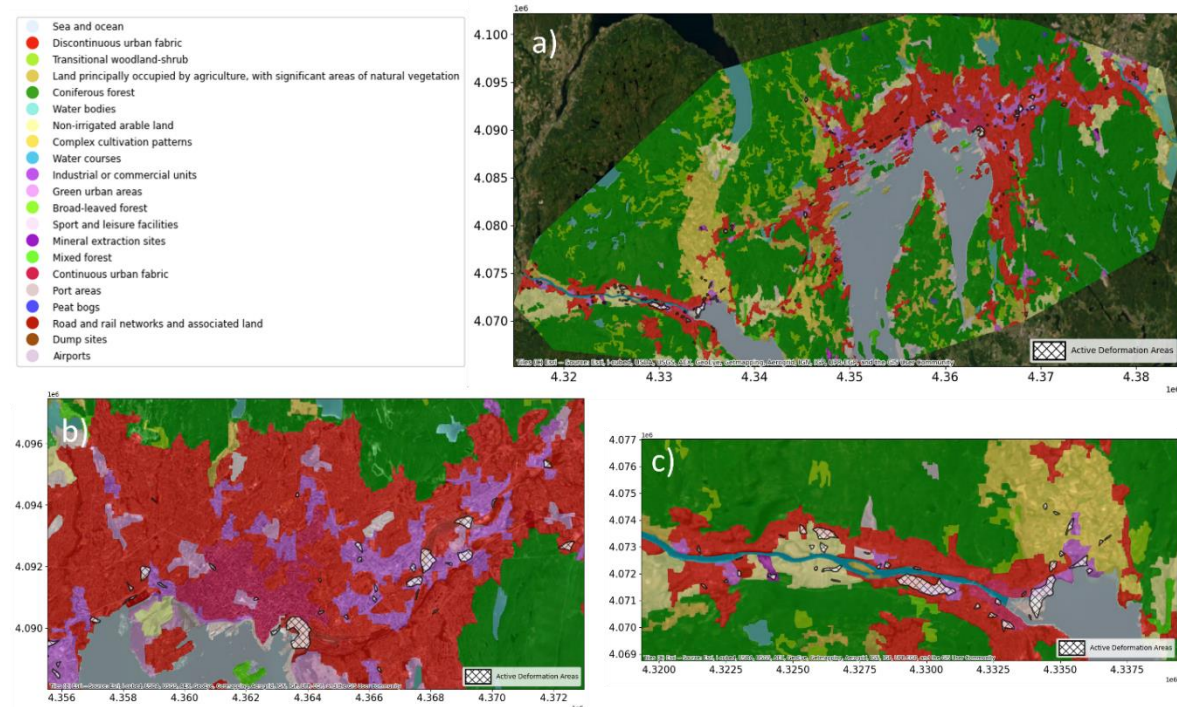


Figure 36: Comparison with Corine Land Cover for the Oslo municipal region. a) Corine Land Cover with ADAs overlain; b) Zoom-in of Drammen region; c) Zoom-in of Oslo City region.

Figure 37 provides an overview of the measured areal coverage of thematic units by ADAs (in percentage) for all EGMS products. A clear correlation is evident, indicating subsidence primarily occurring in anthropogenic areas, especially industrial and urban fabric, as expected for this validation site.

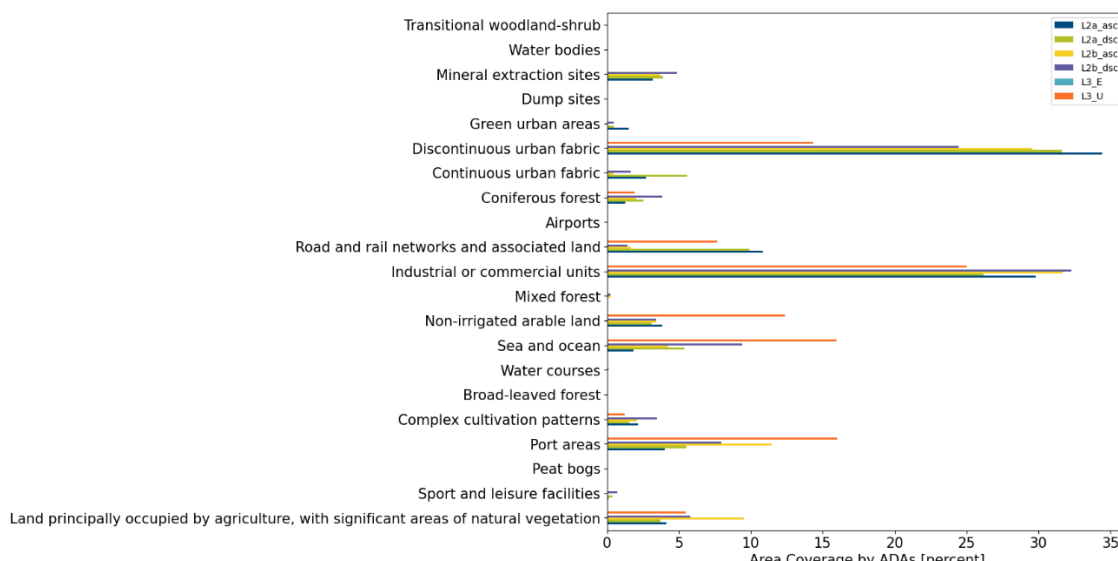


Figure 37: Corine Land Cover area coverage with active deformation areas. Different colour bars represent different EGMS product levels. The measured values represent the overlap of ADAs with the respective Corine Land Cover category in percent of the ADA's total area.

IoA: Do the detected ADAs correlate as expected mostly with anthropogenic areas?

The ADAs detected in the EGMS products mostly overlap with urban and industrial areas as classified by the Corine Land Cover map.

Comparison with Quaternary Geology Map:

The comparison with geological data allows verifying if the ADAs derived from the EGMS are consistent with the local geological or geomorphological features.

Figure 38 shows the comparison of a quaternary geology map with the ADAs detected for the Oslo metropolitan area. All products, except for Ortho/L3 East/West product, where no ADAs were found in the area, exhibit a clear correlation between the locations of ADAs and the presence of anthropogenic filling, and/or marine and fluvial deposits. These are typically compressible soils with geotechnical characteristics that make them prone to long-term compaction, resulting in subsidence recorded by the EGMS. Subsidence in the area is related to soft overburden, often in combination with construction activities that reduce pore pressure in these materials.

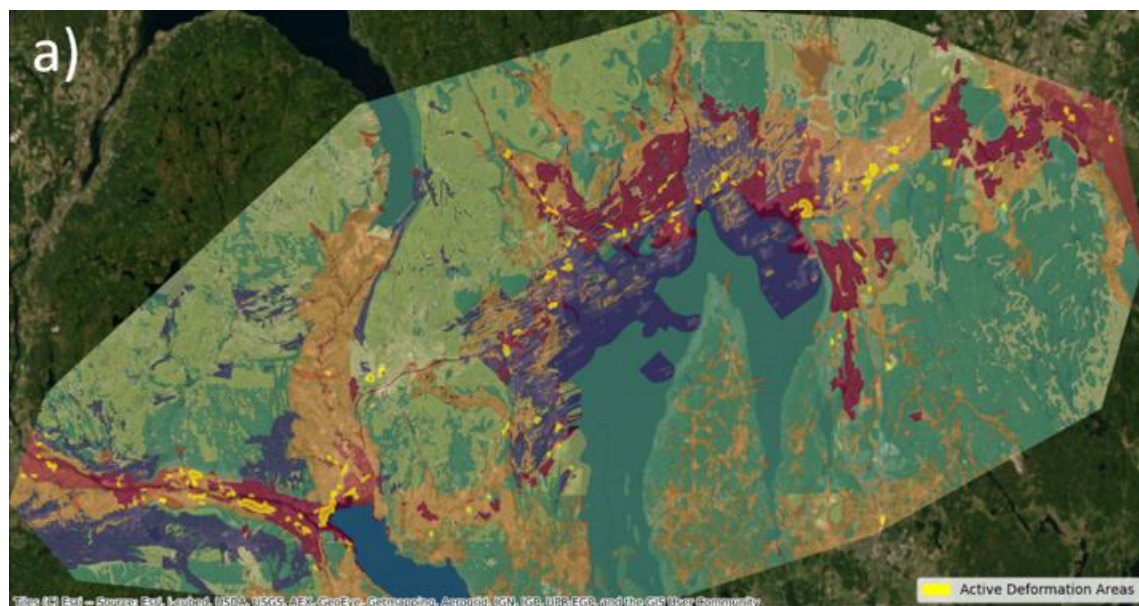


Figure 38: Comparison of detected ADAs with the quaternary geology for the Oslo metropolitan area. (a) Map showing in yellow the ADAs from ascending Level 2b tracks overlain onto the quaternary geology.

IoA: Do the detected ADAs correlate with soft layers?

The ADAs detected in the EGMS products mostly overlap with sedimentary layers (marine and fluvial deposits) and anthropogenic material. This is coherent with the initial hypothesis.

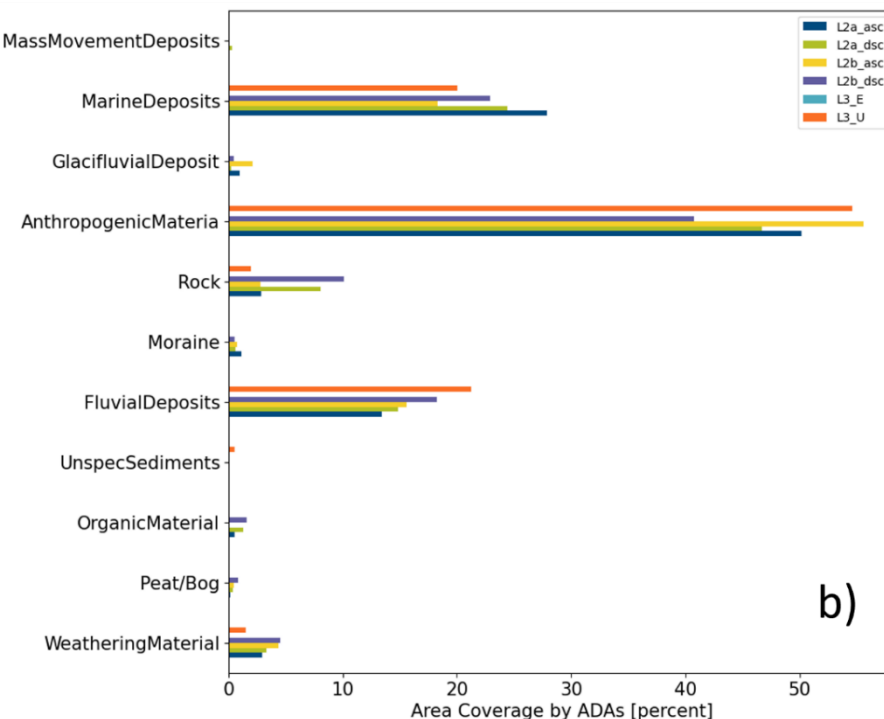


Figure 39: (b) Bar plot showing the overlap of the different geological units by ADAs. Differently coloured bars represent different EGMS product levels. The measured values represent the overlap of ADAs with the geological unit in percent of the ADA's total area.

Comparison with Depth to Bedrock Map:

Figure 40 depicts the thickness of the overburden layer “depth to bedrock” for Oslo compared with the ADAs detected for the Basic/L2a ascending tracks (44, 146). In areas with soft overburden layers, the thickness of these layers is expected to have an impact on the magnitude of subsidence. Assuming the same urban setting, an area with the maximum thickness of compressible soil will experience the highest subsidence rates. However, the presence of new buildings may accelerate this process. While the depth to bedrock map does not cover all identified ADAs, there is a clear correlation in several locations between the thickness of the overburden and the location and extent of the ADAs. This correlation is particularly evident for the two larger ADAs near Oslo Central station in the centre of the map.

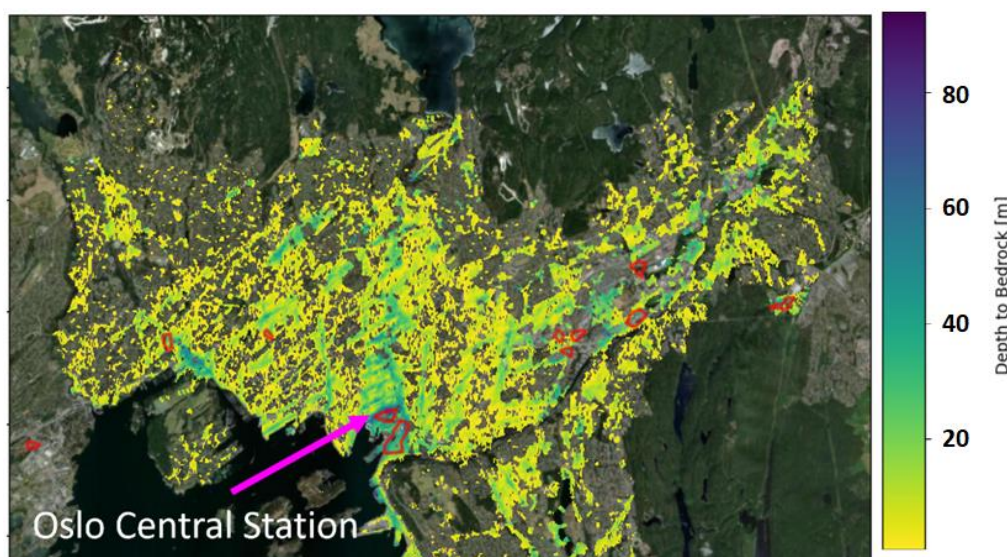


Figure 40: ADAs (red polygons) detected in EGMS Level 2a ascending (all tracks combined) plotted with soft soil thickness.

IoA: Do the detected ADAs show a correlation with areas of higher depth to bedrock?

There is a clear correlation of ADAs with areas of increased depth to bedrock. In case of the Oslo Central station, the ADAs correlate well with the shape of the areas with deeper bedrock.

Two additional datasets, a bedrock map and topography, have been compared to the EGMS products. The findings from both datasets confirm that ADAs are mostly located in areas hosting thick sedimentary sequences. The topography analysis reveals that ADAs are almost exclusively situated in flat areas.

The high degree of consistency demonstrated across all the EGMS datasets underlines the EGMS's capability to reliably map anthropogenic ground deformation phenomena within an urban environment.

Po delta (Italy)

The Po River delta, covering an approximate area of 400 km², is a complex ecosystem shaped by sedimentary processes and influenced by human activities such as ground water pumping.

Figure 41 shows a comparison of displacement velocities for the Po River delta from the EGMS, and the regional GMS provided by the Regione del Veneto (RDV, Veneto Region). The comparison reveals discrepancies across a broad area in the Po River delta. Existing literature has consistently reported subsidence in the Po River Delta [Faris et al, 2014; Faris et al, 2022; Cenni et al, 2021], and therefore, it is reasonable to infer that, for this area, the EGMS provides a more accurate reflection of the situation compared to the regional GMS.

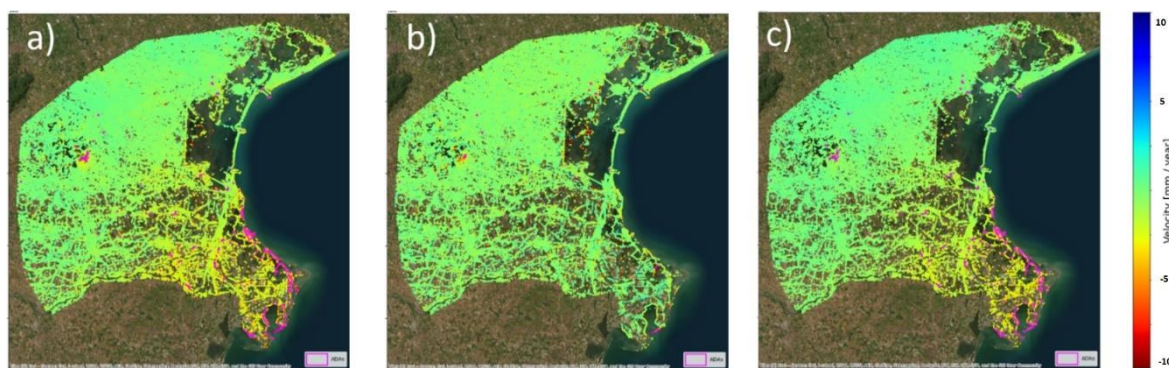


Figure 41: Comparison of displacement velocities for the Veneto validation site: a) EGMS (multiple tracks combined/resampled); b) Regione del Veneto GMS; c) Velocity difference between a) and b)

Despite the velocity differences observed in the Po River delta, resulting in a very low overlap in identified ADAs (see Table 6), the relative velocity difference for the identified ADAs remains within an acceptable range at approximately 50%. The velocity and time series correlation also indicate relatively good agreement, which can be attributed to the rather smooth and "large-scale, but low amplitude" nature of the velocity difference and the strong linearity of the time series in both datasets. The resulting IoA for the comparison with the data provided by the Regione del Veneto is 0.70.

Table 6: Validation measures and IoAs for Po River Delta

Veneto	Validation Measure	IoA
Spatial overlap [%]	34.26	0.08
Relative Velocity Difference [%]	47.98	0.93
Velocity Correlation	0.65	0.79
Displacement Time Series Correlation	0.78	1.00
Total		0.70

Conclusion for the Veneto area:

The comparison for the Veneto area results in an IoA of 0.7, which means that differences between EGMS and RDV products were found. However, these differences are confined to the area of the Po River delta, and based on literature, it can be concluded that the EGMS products are able to capture the large-scale deformation of the Po Plain which cannot be captured by the regional dataset because of the smaller size of the processed area. The ability of the EGMS to detect both large and detailed scale ground motion patterns is confirmed.

Tagus Valley (Portugal)

The Lower Tagus Valley in Portugal has been selected for examination, with a particular emphasis on fault systems. Historically associated with damaging earthquakes impacting the Greater Lisbon Area, the region presents seismic hazard that pose risks to both population and infrastructure (see e.g., Carvalho et al, 2017). Additionally, potential effects on various projects, such as CO₂ storage, geothermal endeavours, and underground energy storage, need consideration (Pereira et al, 2013). Beyond earthquake activity, subsidence is suspected to result from the compaction of a clay-rich aquitard, led by the over-exploitation of adjacent aquifers.

The comparative analysis of EGMS products focused on fault lines, considering previous studies that reported ground displacements either related to or correlated with the presence of fault lines due, for example, to their influence on local geology and acting as hydrogeological barriers (Heleno et al, 2011). However, it has to be noted that the fault lines have been mapped through geological interpretation and therefore they are not classified as seismogenetic sources. Therefore, ground motion may be caused by other factors, e.g. anthropogenic activities. As already mentioned above, it should also be noted that a correlation of ground deformation with a fault line does not necessarily mean that the fault is the direct cause of the observed deformation. A fault may also act as a geological “barrier” for e.g. the groundwater flow, easing or not the extraction of water and thus acting or not as predisposing factor for subsidence.

Figure 42 shows an overview of fault lines and subsidence for the entire Tagus Valley validation area. It is important to note that low thresholds for ADA detection (ADA velocity < 2mm/year) were employed to ensure enough ADAs for comparison.

The results revealed several ADAs exhibiting a clear correlation with the presence of lineaments, which act as a factor controlling the local geological asset. The zoom-in on two specific sites in Figure 42 (left-hand side) show a very good correlation in both subsidence and heave patterns.

This pattern of correlation repeats across the entire fault line inventory, where several more of such correlations can be found. However, also an example for a fault line crossing an ADA can be observed (see the upper right zoom-in of Figure 42).

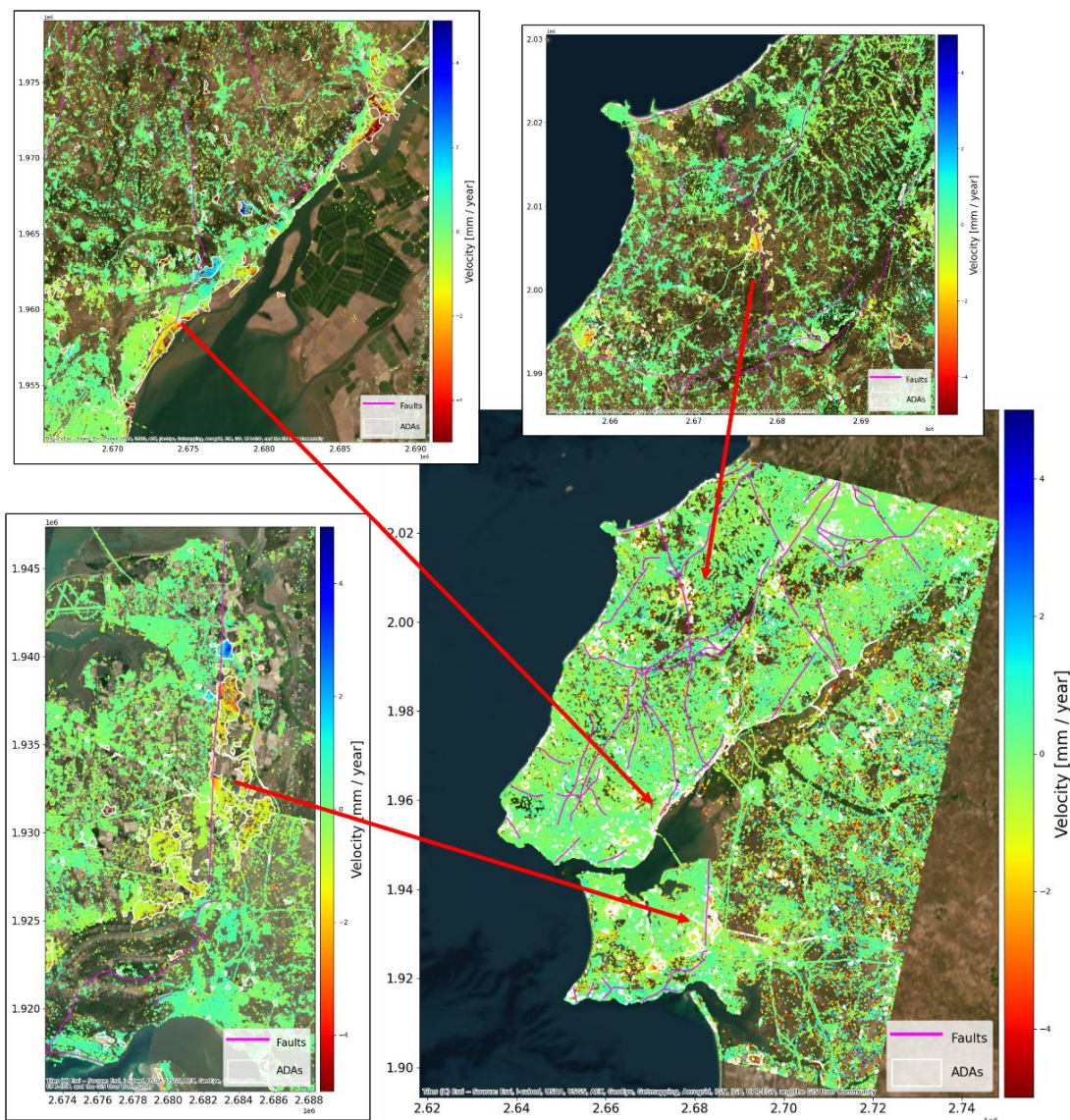


Figure 42: EGMS velocity maps (tracks 45/147/ASC) for the Tagus Valley with fault line (magenta) and detected ADAs (white polygons). The zoom-ins show the locations indicated by the red arrows.

IoA: Do you see the expected effect of fault lines on displacement patterns?

Several ADAs show a correlation between their location and the position of a fault line. However, this does not necessarily indicate that the faults are generating the motion.

Three additional datasets have been compared to the EGMS products: CLC, a geological map and topography. These datasets have been investigated for any unexpected correlations; however, none were observed. Correlation between the presence of fault lines with displacements detected by the EGMS is observed. Such correlation demonstrates the ability of

the EGMS to detect rather small displacements connected to the presence of faults as factors controlling the local geological and hydrogeological asset.

Groundwater exploitation

Lorca (Spain)

The Alto Guadalentín valley in Spain has been selected as a validation site due to the extensive subsidence resulting from prolonged ground water extraction, marking the largest subsidence area of this kind in Europe. The basin contains a multi-layer aquifer system spanning approximately 277 km², subject to water exploitation over the past 50 years. This exploitation has led to a decline in pore water pressure, triggering a gradual compaction of the sediments and subsequent lowering of the ground surface.

Figure 43 depicts the soft soil thickness dataset available for the Alto Guadalentín valley, which has been clipped at the 5m thickness contour. The excessive ground water extraction in this region has led to a very strong subsidence larger than 100km². Figure 43 also compares the soft soil data with the detected ADAs, derived from EGMS Basic/L2a ascending (tracks 45 and 147) and the EGMS displacement velocities.

The ADA almost exactly aligns with the 5m thickness contour, demonstrating a very strong correlation between the soft soils thickness and measured subsidence velocity. This correlation is particularly evident in the central region of the ADA, where thickness and subsidence rates peak, and near the southwest end of the ADA, where a slight thickness increase coincides with an increase in subsidence rates.

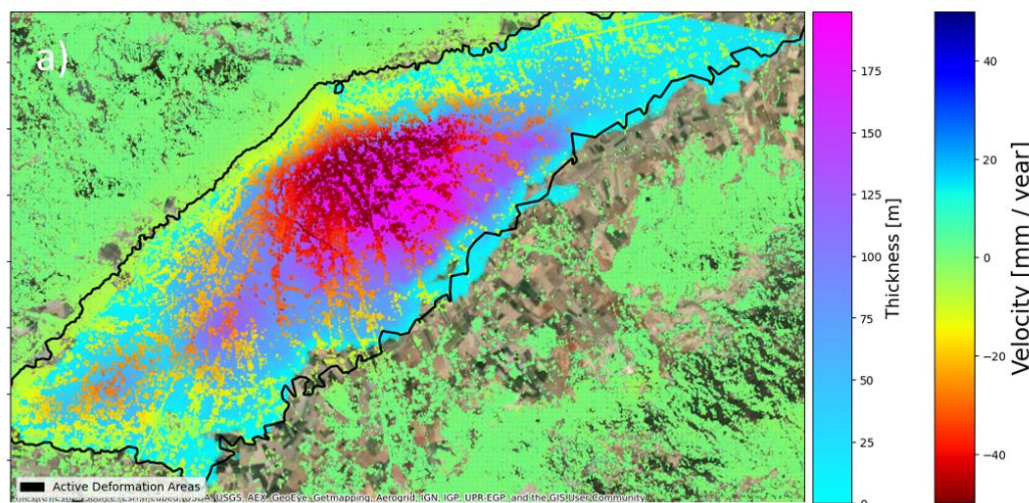


Figure 43: EGMS Basic/L2a ascending (all tracks combined) and detected ADAs (black line) co-plotted with soft soil thickness.

IoA: Do the mean velocity values of the EGMS correlate spatially with soft soil thickness?

The major ADA shows a clear correlation with the outline of the area with increased soft soil thickness (>5 m). Also, local maxima in the soft soil thickness map correlate well with local maxima in the subsidence rates mapped by the EGMS.

Figure 44 also illustrates a comparison between the detected ADA and the EGMS displacement velocities (Basic/L2a ascending and descending datasets) with a ground water model derived from piezometric levels (this will be assessed in the accuracy section 3.2.2). It has to be noted that this ground water model is referred to 2012, a few years before the start of the EGMS time series. Nevertheless, the expectation is that patterns in the subsidence field should correlate with those in the piezometric levels, as they reflect the degree of ground water exploitation.

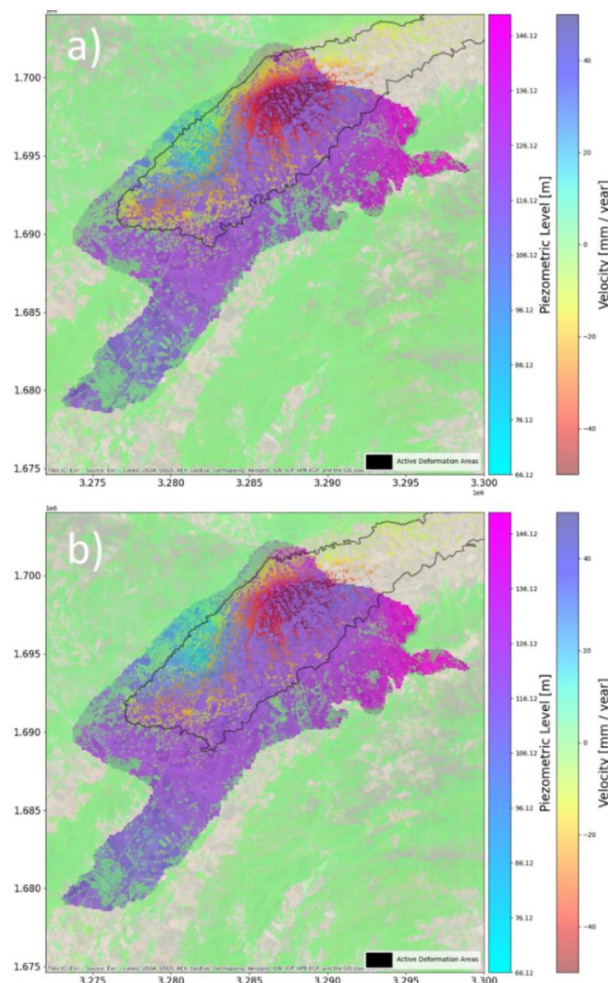


Figure 44: EGMS velocity maps in for Basic/L2a ascending (a) and descending (b) mode (all tracks combined) compared with a ground water model given as piezometric levels for the Lorca area.

IoA: Do the piezometric levels from the ground water model show a correlation with areas of higher velocities in the EGMS datasets?

Although some correlation can be observed between piezometric levels and subsidence, the peaks in both datasets are clearly shifted, i.e., the area with lowest piezometric level is located slightly west of the area of maximum observed subsidence in the EGMS.

Three additional datasets were compared to the EGMS products: CLC, well locations and topography. These datasets were investigated for any unexpected correlations; however, none were observed.

The observed correlations of displacements detected by the EGMS, and soft soil thickness map and the ground water model clearly demonstrate the ability of the EGMS to map ground displacements caused by ground water extraction in very high detail.

Volcanism

Etna Volcano (Italy)

The validation site at **Mount Etna** was selected due to its active volcanism, being the largest active volcano in Europe. The area is particularly interesting for its abrupt surface deformation phenomena, e.g., resulting from the earthquake connected to the onset of the eruption that took place from 24–27 December 2018. Mount Etna is a highly dynamic volcanic system characterized by summit eruptions from five craters and fissural eruptions mainly clustered along three rift zones extending from the summit toward northeast, south, and west, respectively (Cappello et al., 2013). Given the specific purpose of this analysis, a separate and ad-hoc InSAR processing was conducted by IREA, resulting in the availability for all products levels for comparison with EGMS products.

Figure 45 shows the comparison of Basic/L2a displacement velocities, revealing an overall good spatial agreement between the datasets. Consequently, the detected ADAs exhibit notable similarities in size and form. Despite variations in coverage, particularly in the crater region due to the different definition of measurement points in the processing algorithms, the overall agreement in covered areas is very good. A detailed examination of the velocity maps for the ADA on the eastern flank shows that velocity values are in good agreement, with some differences found close to the summit and in the southern part of the ADA, closer to the Mediterranean Sea.

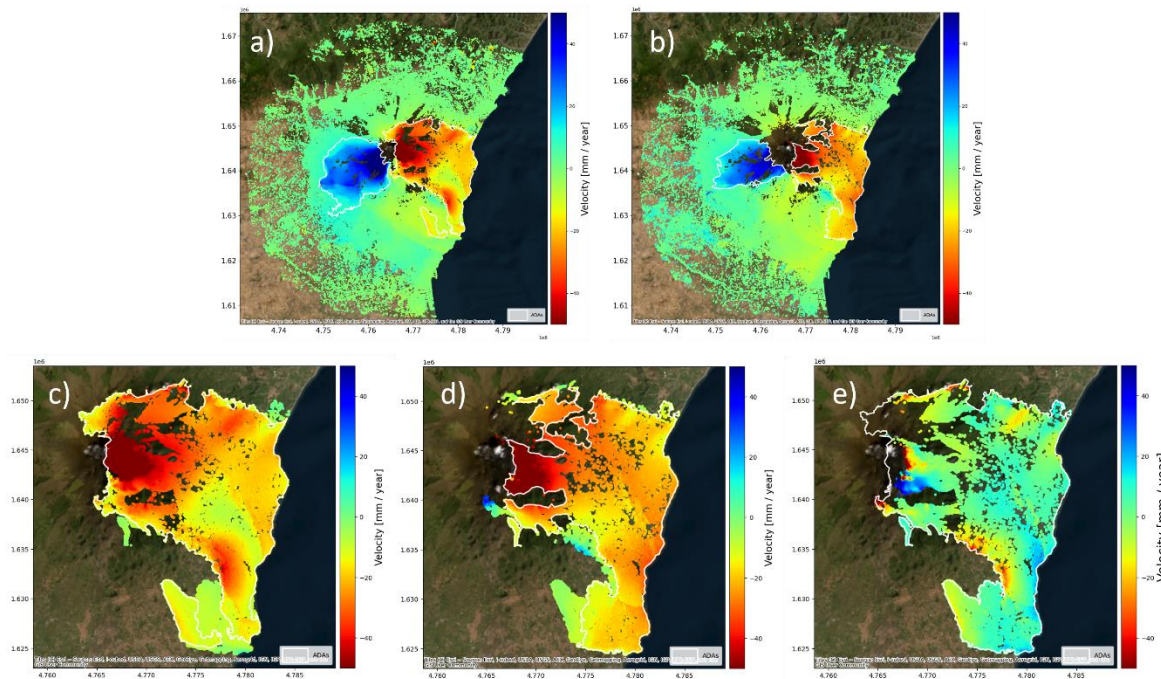


Figure 45: Comparison of EGMS velocities with velocities provided by IREA for the Basic/L2a product track 44/ASC: (a) EGMS velocities; (b) IREA velocities; (c) EGMS velocities eastern ADA; (d) IREA velocities eastern ADA; e) velocity difference eastern ADA ($dvel = vel_{EGMS} - vel_{IREA}$). ADAs are marked by white polygons.

The displacement time series for the same ADA, illustrated in Figure 46 a), also show the high level of agreement between the two datasets. This includes the sharp drop in the time series representing the earthquake connected to the onset of the eruption that occurred in December 2018. Only towards the end of the observed period, a certain mismatch can be observed, where the EGMS data suggests continued decrease, while the displacements stabilise in the IREA dataset. It remains unclear the cause of such mismatch.

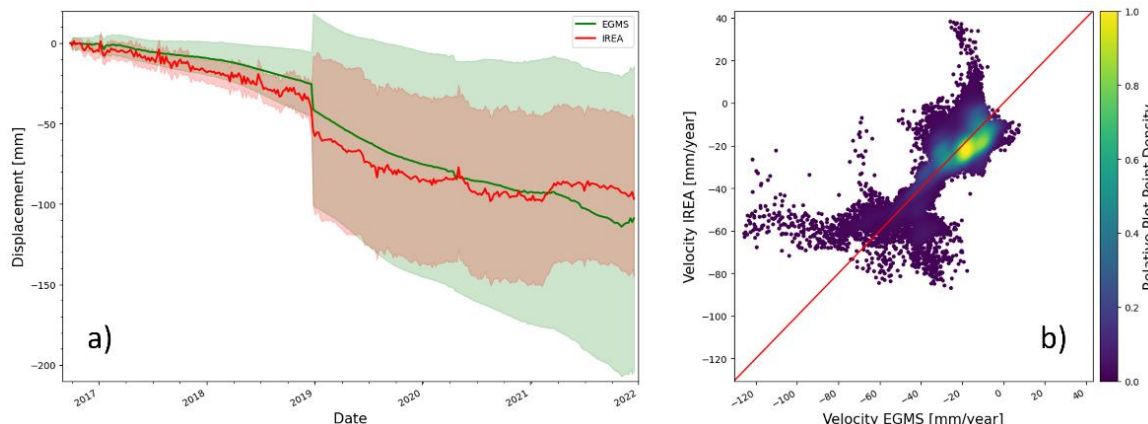


Figure 46: Time-series and velocity correlation for measurement points within the ADA shown in the previous figure. (a) average and standard deviation of displacement time-series; (b) velocity correlation.

Table 7 shows the summary of all validation measures averaged for all products and the resulting IoAs. The table demonstrates that a good match is observed for all validation measures. Notably, the spatiotemporal overlap and the robust time series correlation result in IoAs of 1.0, indicative of a very good match. While the relative velocity difference and velocity correlation IoAs are slightly lower, these variations are expected given the dynamic nature of the volcanic system.

Table 7: Index of Agreement (IoA) for Etna

Etna	Validation Measure	IoA
Spatial overlap [%]	88.89	1.00
Relative Velocity Difference [%]	70.24	0.85
Velocity Correlation	0.74	0.89
Displacement Time Series Correlation	0.88	1.00
Total		0.94

This observation can be attributed to the smaller vertical velocity component compared to the horizontal component in the volcanic context, potentially making vertical component more sensitive to differences in the underlying LOS products.

Conclusion for Etna Volcano:

The comparison with the IREA products results in an IoA of 0.9, reflecting that the datasets match very well despite the dynamic character of the volcanic system and the very non-linear time series. This demonstrates that the EGMS is capable of reliably mapping displacements under such difficult conditions.

3.2 Consistency/Accuracy

This section is conceived to evaluate the accuracy of the EGMS portfolio while studying ground motion in certain thematic areas. Specifically, the goal is to evaluate the EGMS accuracy within the boundaries of several applications, i.e. to estimate how much the data can describe, quantitatively, a certain ground motion phenomenon. Figure 47 shows an overview of the validation sites. The full descriptions of the data and sites can be found in [D3.1-Validation Data Collection](#) and [D5-Validation_Areas](#).

Table 8: Overview of validation sites (Consistency/Accuracy)

	Validation with GNSS data	Validation with in situ data	Position and displacement validation with CR
Landslides	Not evaluated	Tyrol (AT)	Indre Nordnes, Jettan and Gamanjunni (NO)
Mining and post-mining	Not evaluated	Turow (PL) Lorraine (FR)	Not evaluated
Urban / Anthropogenic	Jutland (DK) Gran Canaria (ES)	Not evaluated	Thyborøn (DK)
Groundwater exploitation	Lorca (ES)	Lorca (ES)	Not evaluated
Seasonality (Basic/L2a products only)	Lorca (ES), Gran Canaria (ES) Jutland (DK)	Not evaluated	Not evaluated

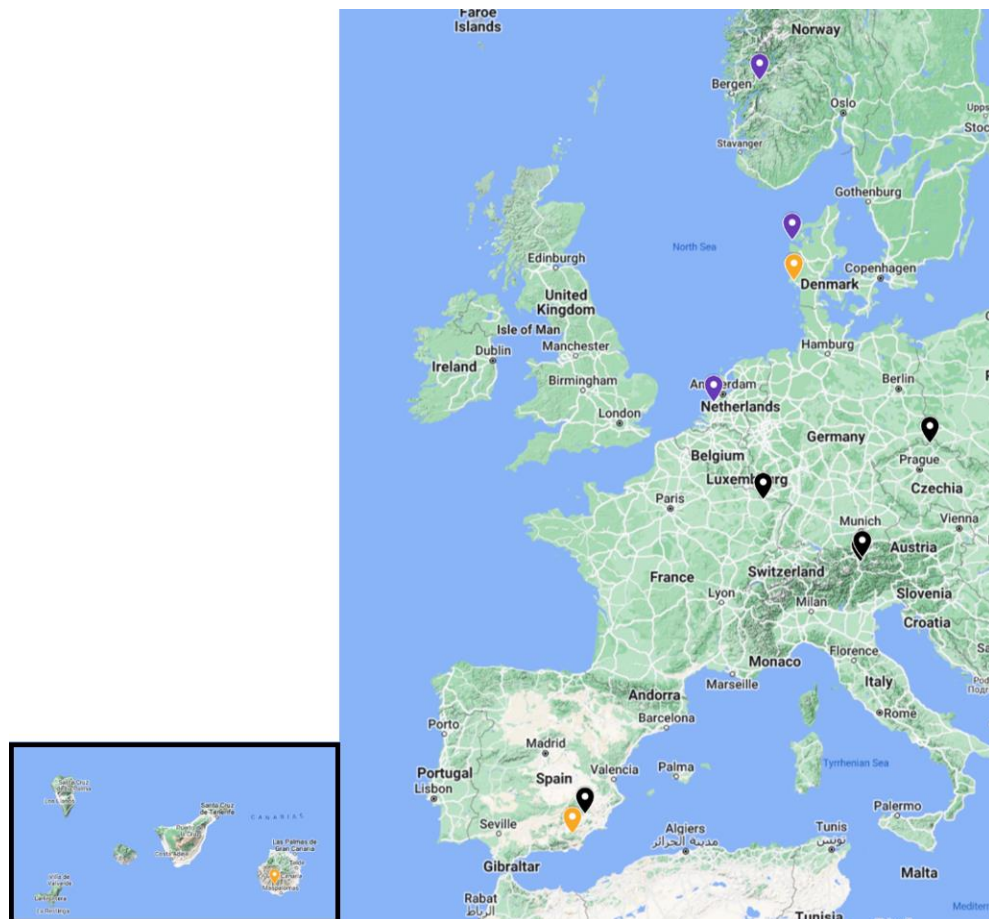


Figure 47: Validation objectives and thematic areas versus sites (Accuracy). The colours refer to the different activities reported in the previous table. (basemap: google)

In these sites, the EGMS portfolio is compared to other high resolution and in-situ data sources such as:

- GNSS observations (velocity components and time series).
- Geodetic data acquired by in-situ landslide monitoring stations.
- Levelling data acquired by in-situ campaigns over abandoned mining.
- Piezometric data (groundwater level measurements).
- Artificial Corner Reflectors (CRs) deployed on the ground to reflect in an optimal way the radar signal back to the satellite together with precise measurement of the CR location.

3.2.1 Methodology overview

Three validation activities were carried out in different validation sites (Figure 47). The full description of each methodology can be found in [D6.1-Validation_Methodologies](#). A summary with the main aspects follows:

- **Comparison with GNSS data:** The goal of this activity is to validate the geocoding and ground motion time series of the EGMS products with GNSS measurements. Test statistics are applied to compare EGMS time series and velocities against GNSS data to judge whether the differences are significant or not. Some of these test statistics are adapted into the Indexes of Agreement. The following steps have been followed to validate EGMS products with GNSS data:
 - **Temporal interpolation:** The comparison requires the interpolation of GNSS time series to InSAR acquisition dates, to ensure that the same time interval is covered. A 12-day interpolation window which weights the inverse of the time difference is used.
 - **Time reference:** to align GNSS and EGMS time series to the same reference date (also known as reference date).
 - **Projection of GNSS time series to LOS:** Given the observation geometry, GNSS displacement is transformed to radar LOS for EGMS product levels L2a/Basic and L2b/Calibrated.
 - **GNSS spatial referencing:** For level L2a/Basic data, a GNSS station is selected as reference station per validation site. The time series difference between the reference and the rest of the stations is then calculated. For level L2b/Calibrated and L3/Ortho products, the velocity differences are calculated between the GNSS reference frame, and the reference frame (i.e. the A-EPND velocity model) used in the L2b/Calibrated and L3/Ortho products and subtracted from the GNSS time series.
 - **InSAR MP selection:** MPs are selected to be compared with GNSS based on distance (MPs are selected within a 100m radius from the GNSS station) and height criteria.
 - **Spatial interpolation:** Using only the selected InSAR MP, spatial interpolation is performed to the GNSS location. The interpolation error has also been

estimated, considering the provided MP accuracy. Double differences are used for L2a/Basic products only because they are referred to a virtual reference point. This is not needed in L2b/Calibrated and L3/Ortho products because they are both spatially relative to the same reference system, i.e., ETRF 2000.

- **GNSS-InSAR comparison:** The correlation between GNSS and InSAR time series is calculated together with the standard deviation of the differences in the time series. Only the part of the time series where InSAR and GNSS overlap is selected and the BLUE (Best Linear Unbiased Estimation) [Teunissen, 2000a, Teunissen, 2000b] is applied, which also provides the variance of the estimated parameters.
- **Comparison with in-situ data:** The objective of this activity is to evaluate in-situ measurements such as levelling data, piezometers, and geodetic monitoring against the EGMS ground motion data. Two workflows have been designed to evaluate EGMS time series and their associated velocity:
 - **In-situ vs EGMS velocity comparison:** In order to compare the velocities, the in-situ XY measurements are converted to LOS. Then, 50 or 100 m buffers are taken to collect the InSAR MPs surrounding the in-situ measurements. Based on the averaged MPs velocity values the accuracy and precision of the EGMS in comparison to the in-situ measurements is evaluated.
 - **In-situ vs EGMS time-series comparison:** The same pre-processing employed for the velocity analysis is applied. Then aggregation is performed both for InSAR and in-situ time series (6 days, monthly, yearly). Outlier and seasonality extraction are applied to evaluate how trends, accelerations, deceleration, and seasonality impact on the TS inter-comparison. Smoothing of both time series is performed since the goal is not to evaluate the different known accuracy of two measurement techniques but rather to observe their general agreement to characterize the deformation phenomena.
- **Evaluation of XYZ with CRs:** The purpose of this activity is to evaluate the precision of the EGMS time series (location, height, and measured motion) and it has three main focuses:
 - **Height estimation (Z):** For this task, the CRs with known heights derived by the levelling campaigns are used. If not, GNSS measurements in correspondence of the CRs are considered. The differences between orthometric and geometric heights are considered negligible, given the small distances between CRs. A 100m buffer is taken to collect all MPs surrounding each CR. Then, a comparison between the estimated relative heights of the CR and the MPs closest to the CR location is performed. Statistical testing is used to decide if the differences can be judged to be significant, considering their corresponding standard deviations.
 - **Geo-positioning accuracy (XY):** The product specifications indicate that the geo-positioning accuracy shall be below 10 m. To verify this, the GNSS local observations have been used given the high accuracy of their horizontal

component. The accurate position of the CRs is known. Utilizing a 25-meter buffer, all proximate MPs to each CR are isolated, followed by a meticulous selection of MPs with similar time series behavior. Finally, the distance (offset) between the CR and the nearest MPs is calculated.

- **Quality of the EGMS time series:** To evaluate the quality of the EGMS time series displacements, the GNSS stations are used at the chosen CR sites. The same procedures described in “comparison with GNSS data” are applied.

3.2.2 Index of Agreement overview

For each of the validation activities and methodologies summarized above, reproducible IoAs have been derived. Table 9 summarizes each of the normalized indexes together with the EGMS product levels that are evaluated:

- **IoA for GNSS** – there are three indexes of agreement: IoA1 for time series analyses, IoA2 for velocity assessments, and IoA3 for evaluating seasonal signal patterns. Additionally, two statistical tests have been derived to test the similarity of the time series and velocity estimations between EGMS and GNSS. For the seasonal effects, two other values are estimated to perform a valuable interpretation. Three additional metrics are computed for the seasonal signal component to facilitate a comprehensive interpretation: the standard deviation, mean, and root mean square (RMS) of the detrended signals—post linear trend removal. These metrics are designated as IoA4, IoA5, and IoA6, respectively. It is important to note that all IoA metrics are normalized across the entire spectrum of GNSS stations and product datasets, enabling an aggregated evaluation of the EGMS products. This normalization process involves calculating each IoA metric using the extremal (minimum and maximum) values observed across the EGMS data in the area of interest and the station readings. However, this normalization procedure may introduce bias in representing specific locations or products. As will be evident in subsequent time series graphical representations, this normalization can result in certain site stations or products being disproportionately represented, potentially leading to the underrepresentation of some in favour of others or vice versa.
- **IoA for in-situ**– three indexes that evaluate time series correlation, error, and agreement between EGMS and in-situ data have been defined. A fourth index has been averaged within the base index to establish a general sense of agreement and to enable site intercomparison.
- **IoA for CRs** – The IoAs for CRs are the same as for the GNSS time series comparison concerning the time series agreement. An additional IoA for the geo-positioning accuracy has been estimated.



Table 9: Index of Agreement (IoA) for Accuracy/Precision

IoA	Methodology	Short description of how the index is calculated	Approach	EGMS products
IoA1 – Time series: correlation	Validation with GNSS	Time series correlation (after normalization described in the previous sections)	Correlation	L2a/L2b/L3
IoA_test_time-series – Overall model test for time series	Validation with GNSS	The overall model test (OMT) procedure compares the means of explained and unexplained variation (between EGMS and GNSS) in the model in order to determine if the explained variation.	Statistical test	L2a/L2b/L3
IoA2 – Velocity: velocity differences	Validation with GNSS	Percentual difference between the EGMS and GNSS velocities	Difference between measures (%)	L2a/L2b/L3
IoA_test_velocity – Velocity t-test for velocity difference	Validation with GNSS	Statistical test used to compare means of two groups (EGMS, GNSS)	T-test	L2a/L2b/L3
IoA3 – Seasonality: Correlation of detrended signals	Validation with GNSS	Correlation (after detrending described in the previous sections)	Correlation	L2a
IoA – Seasonality: Standard deviation of differences of the detrended signals	Validation with GNSS	Measure indicating how much EGMS and GNSS differ after removal of linear trends (velocity model).	Error	L2a/L2b/L3
Seasonality: Mean of differences of the detrended signals	Validation with GNSS	Mean of differences of the detrended signals (GNSS)	Mean difference	L2a/L2b/L3
Seasonality: RMS of differences of the detrended signals	Validation with GNSS	RMS of differences of the detrended signals (GNSS)	RMS	L2a/L2b/L3
Time series/velocities correlation	Validation with in-situ	Comparison between deformation time series (EGMS / Insitu)	R ²	L2a/L2b/L3



Time series/ velocities Error	Validation with in-situ	Error or difference between deformation time series (EGMS / Insitu).	Mean Absolute Error (MAE)	L2a/L2b/L3
Time series/ velocities agreement	Validation with in-situ	Time-series quality assessing how well the EGMS time series agree with the insitu measurements.	Index of Agreement (d)	L2a/L2b/L3
Normalized mean of (corr, error, agg)	Validation with in-situ	Combined index averaging the 3 indexes defined above with equal weight.	Combined Index	L2a/L2b/L3
Time series quality and velocity of time series with CR	Validation with GNSS at or close to CR	Quality assessment of how well the EGMS time series agree with those at the CR locations. The latter have been performed using GNSS, therefore the IoA are the same as described above (IoA1, IoA_test_time-series, IoA2, IoA_test_velocity, IoA3).	Same six IoA as for GNSS	L2a
Positioning accuracy estimates	Position/Displacement validation with CR	X, Y, Z accuracies or geo-positioning and height accuracies. How close the estimated EGMS heights and locations are to the measured CRs heights and locations.	Position difference, weighted error	L2a

EGMS products:

L2a = Basic

L2b = Calibrated

L3 = Ortho

3.2.3 Validation results per thematic area

Landslides

Navis (Austria)

Kerschbaumsiedlung is a residential area located on the western part of the municipality of Navis, in Austria, on the south slope of the mountainous region of the Misljoch. Since 2012, GPS surveying has demonstrated that part of this slope is moving up to 3 cm/y. Twelve buildings out of a total of 84 are affected by the slope movement. The landslide motion is caused by the presence of normal faults, tension cracks and trenches taking place in the landslide crown (i.e. the upper portion). The described terrain features are unambiguous signs of deep-seated rock slope deformation.

Brewer and Marlow (1983) introduced a map style which incorporates *slope* and *aspect* values in a unique map. Figure 49 provides an example of this map; three slope categories are mapped with difference in saturation and are combined with eight aspect categories, rendered with an orderly progression of colors. As depicted in Figure 48, Navis is exposed principally south, south-east, and southwest. Furthermore, the kinematic of the deep-seated structure existing in Kerschbaumsiedlung is moving slowly mostly towards the south as shown in figure 49.

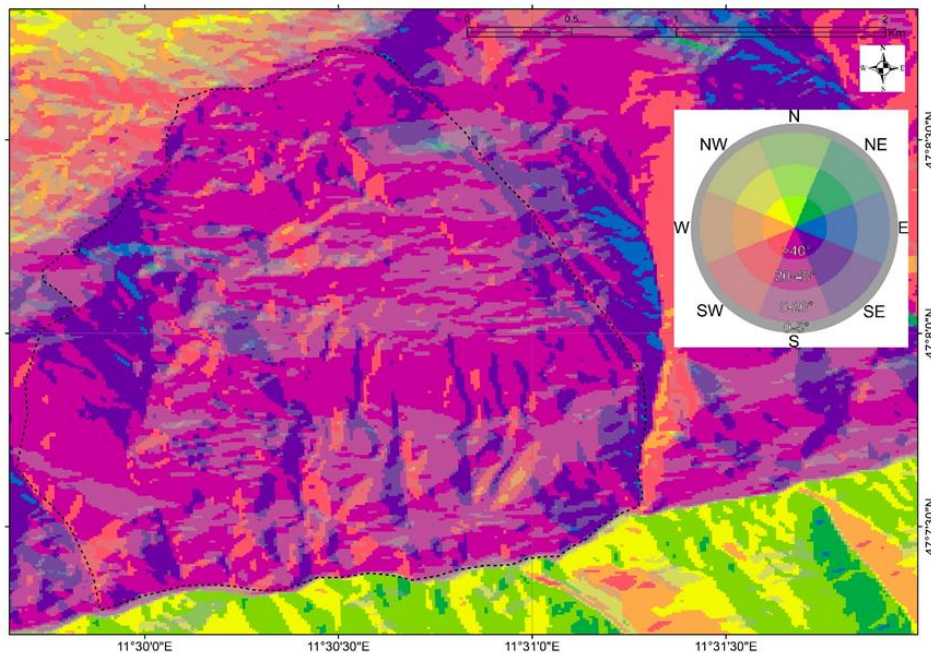


Figure 48: Aspect – Slope map for Navis (Tyrol/Austria) with the color-coding indicating the general surface orientation

In August 2013, an Automatic Tracking Total Station (ATTS) system was deployed in 80 points spread all over the Navis landslide. The data used for the validation comes from six stations. The ATTS system measures X, Y and Z components of motion, the displacement is automatically derived every day (mm/day) and the stated device accuracy is about ± 5.4 mm/y.

To highlight the density and the proximity of the EGMS data to the in-situ stations, in a close view of the Navis area is shown in Figure 49, which includes the buffer drawn around each station.

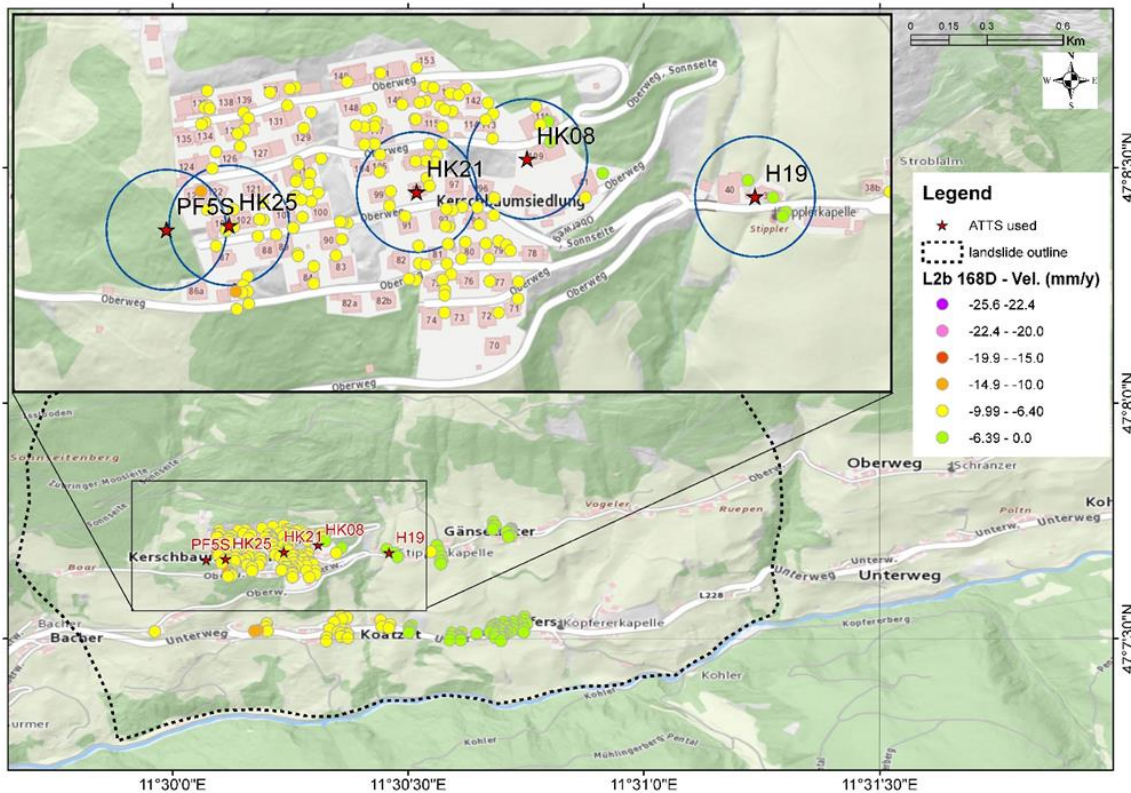


Figure 49: EGMS Descending L2b data distribution in Navis and position of the in-situ stations.

Figure 50 shows the 3D daily time series for the ATTS station TS1 – PF5S used for the validation, in the case study of Navis, where the strongest direction of motion is towards the south with 40 mm cumulative displacement in 5 years (2016-2021).

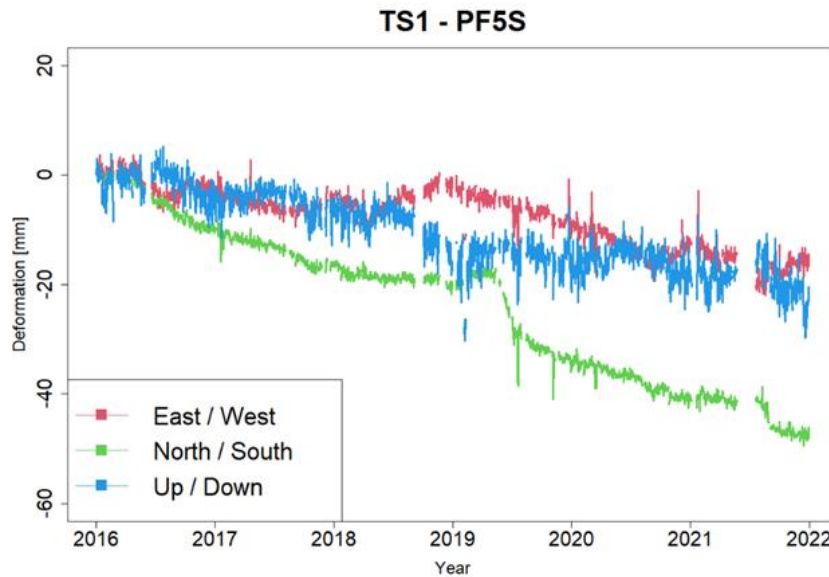


Figure 50: ATTS time series for station TS1 – PF5S.

Figure 51 shows the findings for the velocity inter-comparison for all the EGMS datasets, which resulted with an almost identical score for Basic/L2a and Calibrated/L2b (track 117 in ascending orbit and 168 in descending orbit). The performance for the errors was always above 0.75. The correlation results reached instead medium-high scores (0.7 to 0.9) with the only exception of the L3 East-West data. On the other hand, the lowest scores were the ones for the agreement, which were above 0.25 only for the two descending datasets.

As for the velocity, overall Calibrated/L2b performed slightly better, and the worst score was the agreement. The Ortho/L3 Up-Down performed exactly at the same level of the two descending products, whereas the worst performance was obtained for the Ortho/L3 East/West. In conclusion, the two descending datasets, even if lower in precision (correlation score), maintained a lower error (0.9) and were more accurate (agreement).

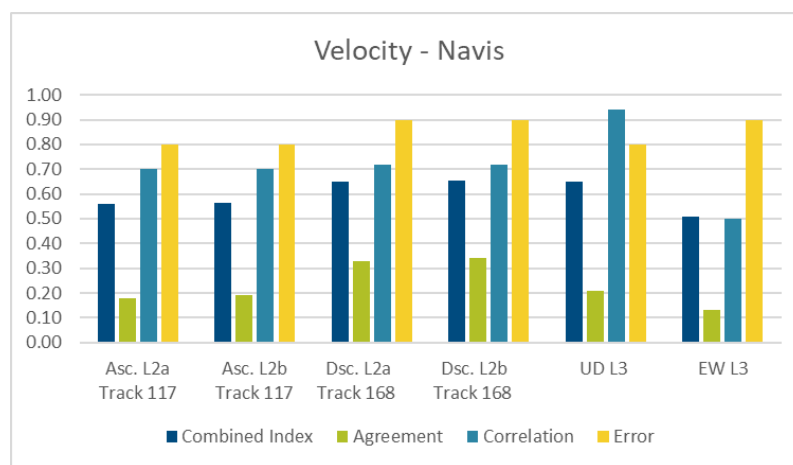


Figure 51: Velocity results for the Navis case study

The overview of all the IoA results for the time series is shown in figure 52. Here it is clear that the Basic/L2a descending product outperformed the rest of the datasets. However, an exception could be observed for the Ortho/L3 Up-Down where the highest correlation reached 0.62; this score helped the vertical product to reach an adequate combined index of 0.56, very close to the descending Calibrated/L2b (0.57). Ortho/L3 East-West was the product with the lowest performance, with a combined index of 0.39.

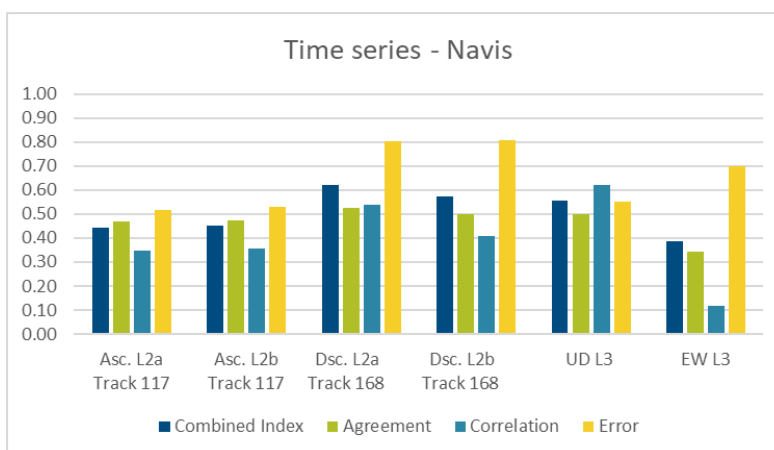


Figure 52: Time series results for the Navis case study

Figure 53 shows the plot of the TS1-PF5S ATTS station against the EGMS MP, chosen because of his lowest Mean Absolute Error (MAE) in comparison to the in-situ TS. Figure 53 is an example of time series validation for the descending Basic/L2a Track 168 which reached the best results for the combined index.

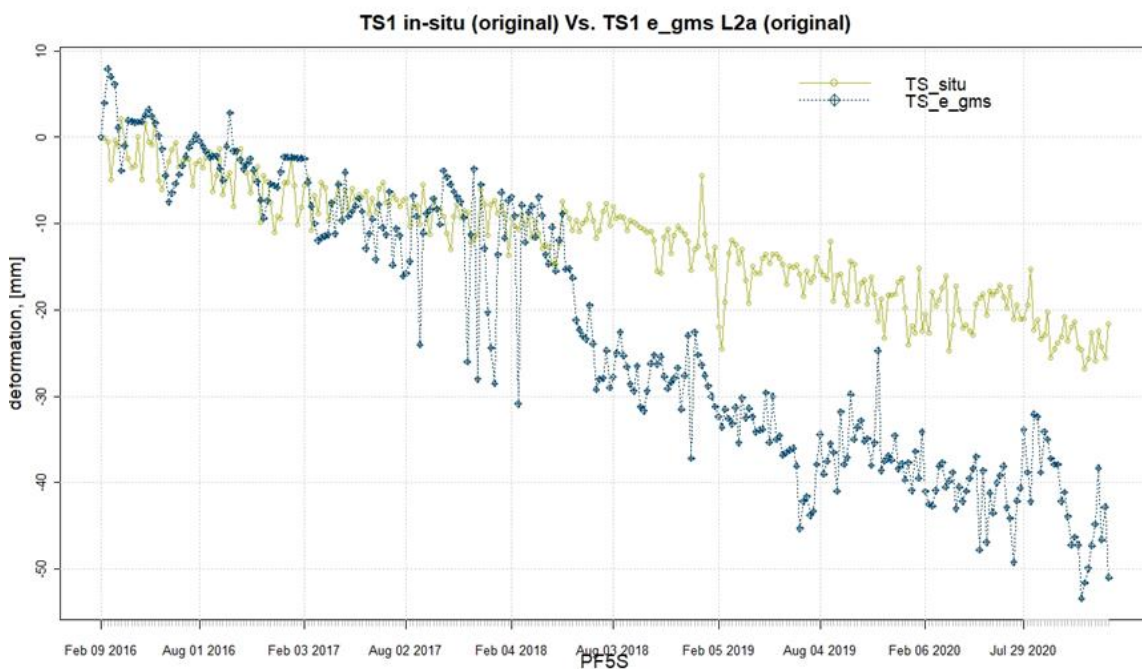


Figure 53: Comparison plot of in-situ TS1-PF5S against the closest EGMS MP that falls within the 50 m buffer around the ATTS.

The site of Navis reached a medium level of agreement in terms of velocity and time series between the in-situ and the EGMS data.

Which are the factors that affect negatively the EGMS performance in Navis?

The first factor is the south exposition of the study site (Figure 48) which can be considered the worst-case scenario for SAR applications given the flight direction and acquisition geometry.

The second factor is the main direction of motion recorded at the in-situ station, which is towards the south. The conversion of the velocity and time series from the 3 components of the in-situ measurements (East-West, North-South, Up-Down) to LOS in this case study was made under the assumption that, being the south direction of displacement the strongest component, it obliterates the rest of the motion (up-down and east-west). Therefore, the north-south deformation rate was considered to be zero. That limitation explains why in Figure 53 the EGMS detects an excess of deformation, in comparison to the in-situ data, which could represent the missing southward component of motion.

In cases like Navis, the eligibility criteria to be used to perform an analysis with the EGMS data shall be the following:

- Selection of the Basic/L2a product in one LOS direction (ascending or descending) compatible with the aspect and slope.
- Prioritization of the most representative LOS products in terms of coherence and density of MPs.
- Avoidance of the Ortho/L3 products (at least the EW component).

Vögelsberg (Austria)

Vögelsberg village is situated on a northeast-facing slope at the lower Watten valley in Tyrol, Austria. Since the summer of 2015, nine buildings have been affected by structural damage. Because of those concerns, in April 2016 the same ATTS system already in use in Navis was deployed in this area. The currently active and slowly moving rockslide (approx. 0.2 km²) is embedded in the lower sector of a bigger (approx. 4.6 km²) deep-seated gravitational slope deformation (DSGSD). Although the ATTS monitoring system stopped in August 2021, two damaged buildings were equipped with automatic crack-meters in May 2021 and those measurements are still on-going. The Vögelsberg slope/aspect map in Figure 54 shows the exposition toward the east/north-east and slightly steeper slope in comparison to Navis.

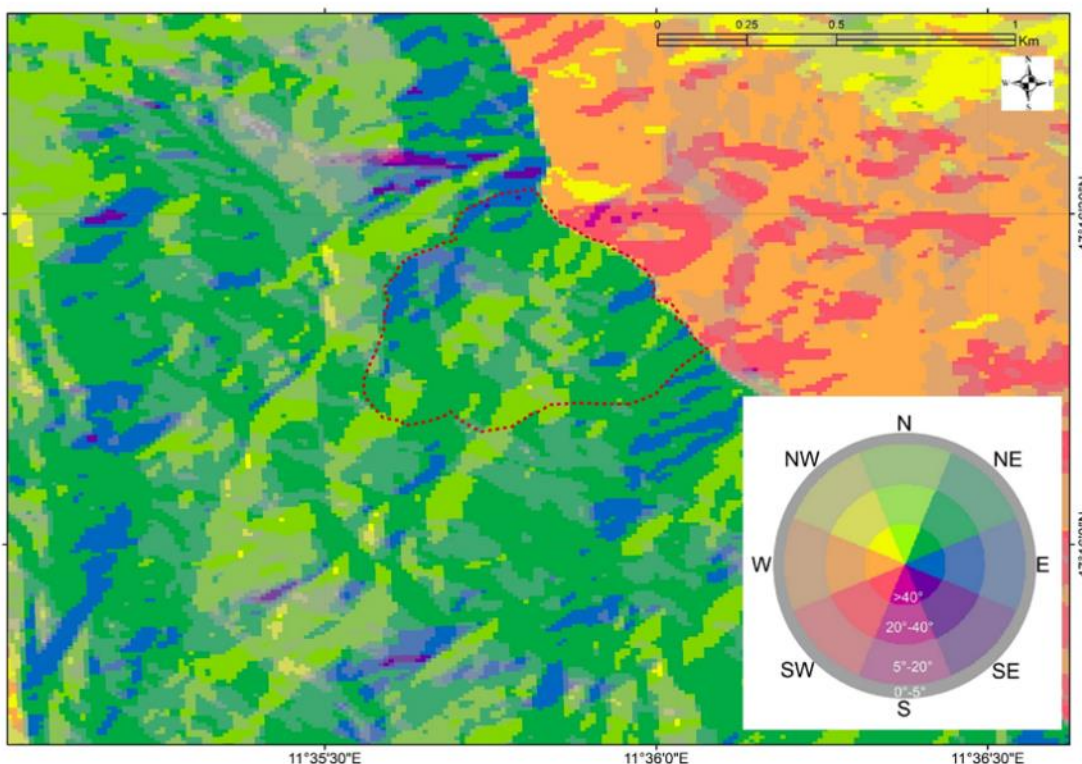


Figure 54: Aspect – slope map for Vögelsberg.

The data used for the validation consists of three stations, the ATTS system measures XYZ or 3D components of deformation and it corresponds in terms of accuracy and measuring rate to the system installed in Navis.

Figure 55 depicts the Vögelsberg landslide, where the buffers around each station and the MP density for the Basic/L2a ascending data are highlighted. Figure 56 shows the XYZ daily time series for one of the two stations (the ATTS station TS2 – D5_1) used for the validation. In this

case, the strongest direction of motion is towards the north (with 200 mm), followed by a vertical negative cumulative displacement of 100 mm in 5 years (2016-2021).

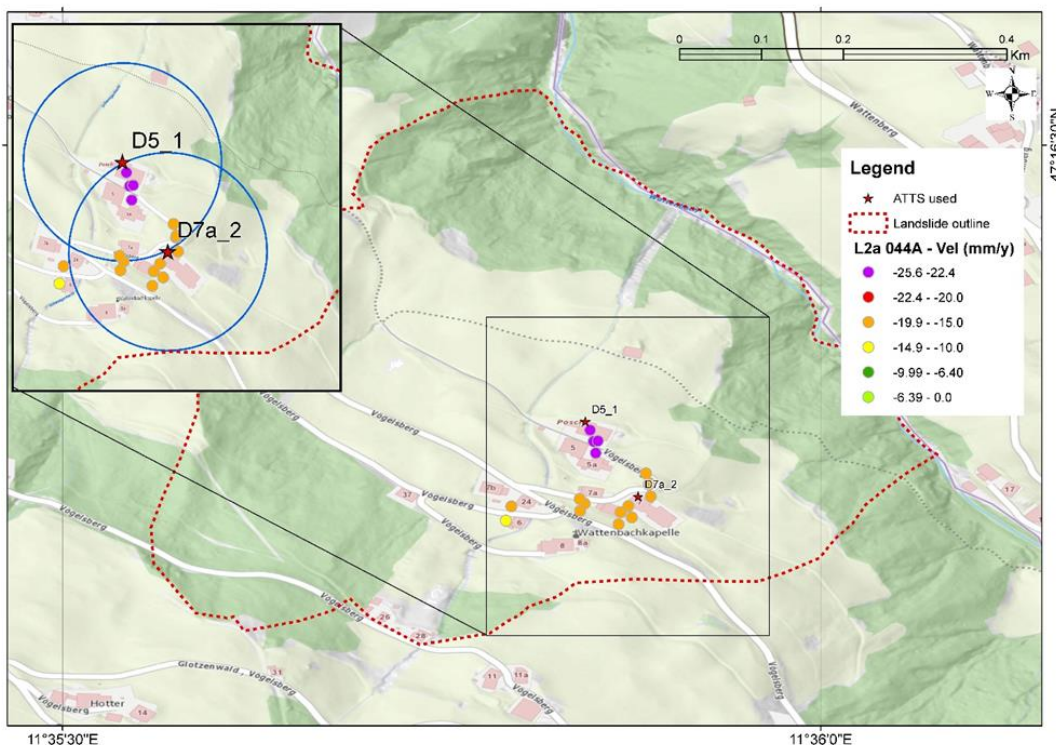


Figure 55: EGMS Ascending Basic/L2a data distribution in Vögelsberg and position of the in-situ stations.

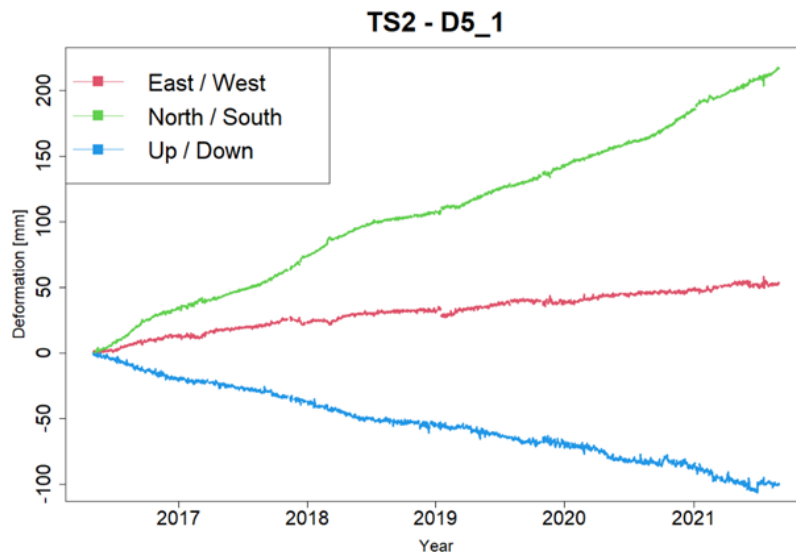


Figure 56: ATTS time series for station TS2 – D5_1.

Figure 57 shows the results for the Vögelsberg study case concerning the validation of the EGMS velocities. Considering only the velocity value, Calibrated/L2b performs slightly better when dealing with a favourable ascending acquisition geometry (track 44), corresponding to a high IoA. Conversely, slightly worst results were obtained with the analysis made with the opposite acquisition geometry (descending, track 168). The validation of the velocity for this case study demonstrates that only the combined use of precision (correlation) with R^2 and error (MAE) was not satisfactory to fully evaluate the EGMS. In fact, at Vögelsberg, being the two metrics for the velocity in all datasets almost identical, the only way to differentiate all the six products (Figure

57) was to use the IoA which combined Ortho/L3 (up-down) and Basic/L2a and Calibrated/L2b ascending.

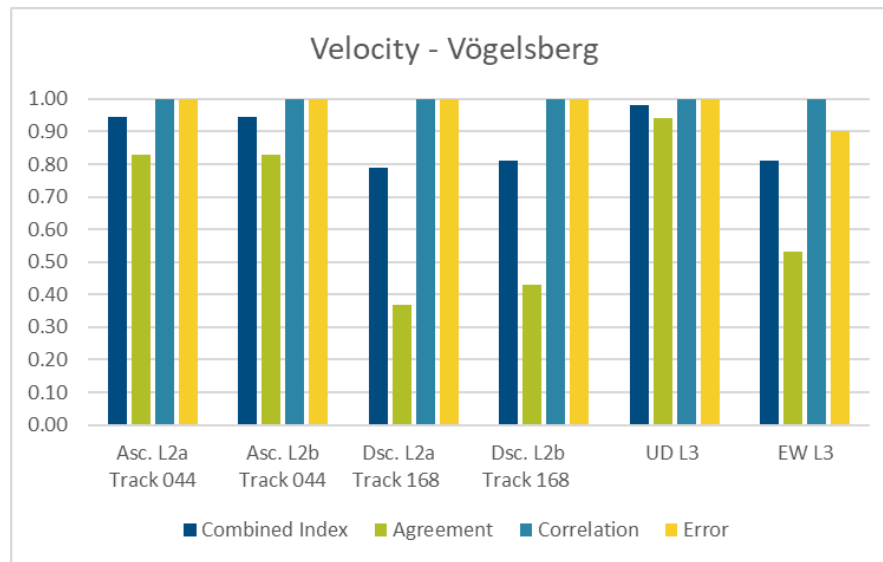


Figure 57: Velocity results for the Vögelsberg case study.

Concerning the evaluation of the overall time series (Figure 58), the results are considerably robust across the six different products. For the two ATTS stations inter-comparisons, the IoA is never lower than 0.7; the Ortho/L3 (East-West) product showed the lowest performance.

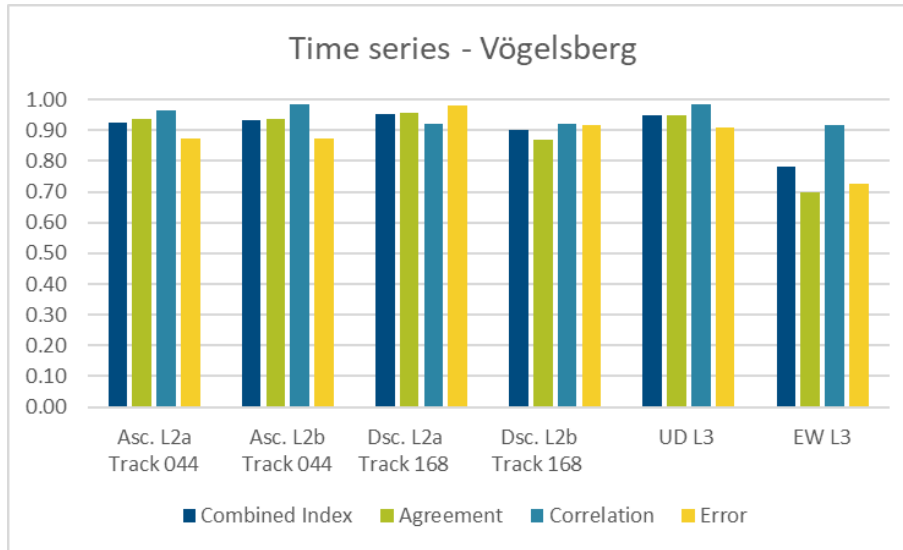


Figure 58: Time series results for the Vögelsberg case study.

Figure 59 shows the plot of the TS2-D5_1 ATTS station against the EGMS MP, chosen because of his lowest MAE in comparison to the in-situ TS. This is an example of time series validation for the ascending Basic/L2a Track 044 which reached very good results for the combined index.

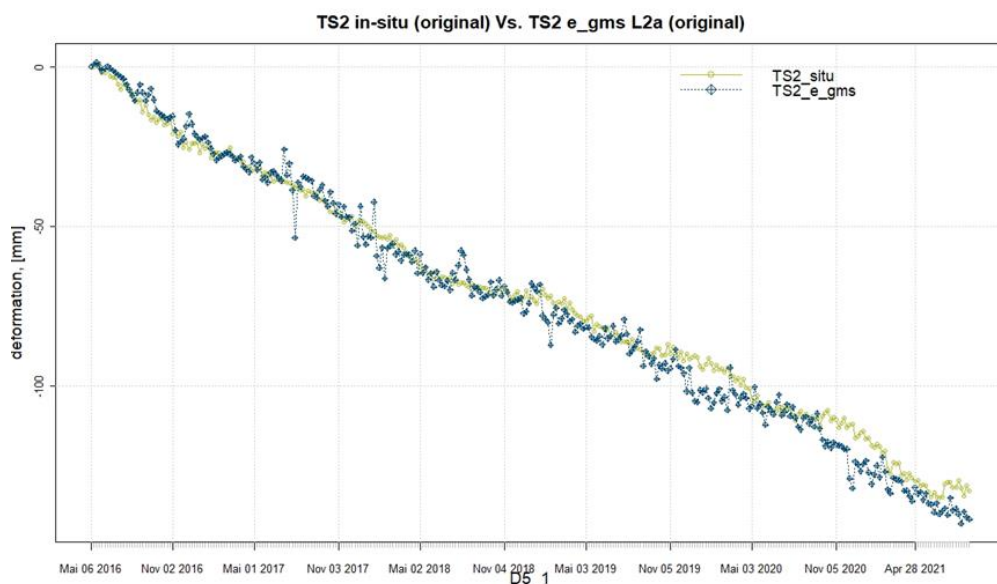


Figure 59: Comparison plot of in-situ TS2 against the best EGMS MP that fell in the 100 m buffer around the ATTS D5_1.

The Vögelberg case study resulted in a confirmation of the EGMS reliability, precision, and accuracy of the deformation measurements for all the six EGMS products tested. In fact, even an active landslide, exposing north-east (Figure 54) and experiencing most of the motion towards the north (Figure 57), if compared to state-of-the-art in situ monitoring devices, can be successfully studied in terms of accuracy and precision using L2 (Figure 59) and L3 EGMS products with the exception of Ortho East/West (as demonstrated in the case of Navis).

Indre Nordnes, Jettan and Gámanjunni (Norway)

The test sites in Norway correspond to landslide prone mountain areas located in the Troms and Finnmark County, located in northern Norway. Indre Nordnes and Jettan are two unstable mountain ranges located on the east side of the Lyngenfjord. Gámanjunni is an unstable mountain section, or a compound slide¹, located on the east side of Manndalen.

These locations are part of a cluster of deforming rock slopes in the region, which are influenced by the geological history, bedrock structure, fluid flow, permafrost, and weathering processes [Vick et al, 2021, Rouvet et al., 2021].

These rock slopes pose a potential hazard of triggering displacement waves or rock avalanches that could affect nearby settlements and infrastructures [Hermanns et al, 2018]. Because of the high risk of landslides, several monitoring systems have been deployed to acquire continuous,

¹ Complex or compound slide is a category within the types of landslide movements. According to the Varnes classification [Varnes, 1978] of landslide types Hungr et al., [2014] defined a rock compound slide as the “sliding of a mass of rock on a rupture surface consisting of several planes, or a surface of uneven curvature, so that motion is kinematically possible only if accompanied by significant internal distortion of the moving mass.”

real-time, or periodic, with weekly intervals, measurements. A total of five CRs have been installed together with continuous GNSS measurements at or nearby the CR locations at the three test sites. The GNSS time series have been analysed and compared with the MPs located near the GNSS locations.

From the five existing stations and the possible three EGMS products to be analyzed, decisions were made considering the following constraints:

Only the Basic/L2a product was compared with existing measurements because the original GNSS data were not converted to a comparable coordinate system to perform the Calibrated/L2b evaluation.

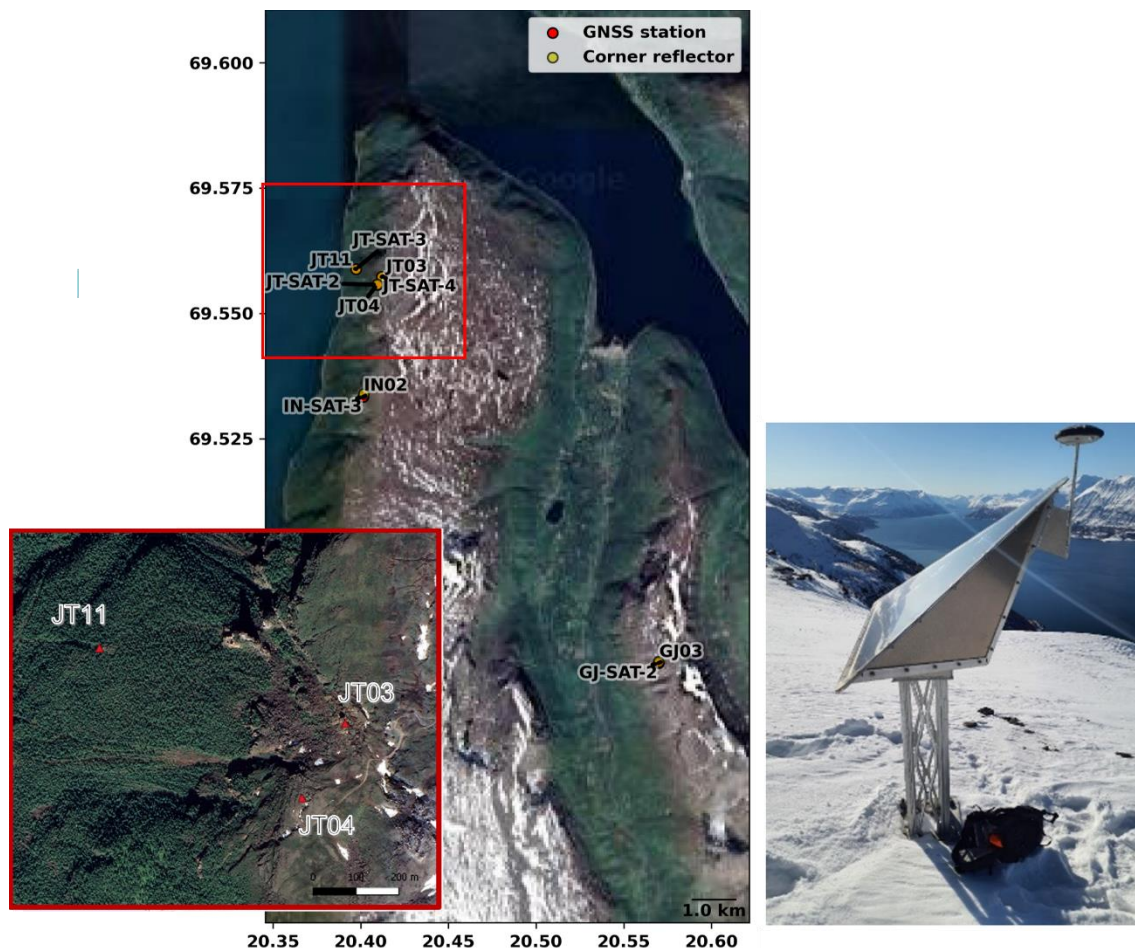


Figure 60: Map of the Norwegian CR site with Indre Nordnes (one CR with 'IN' initials), Jettan (three CRs with JT initials) and Gámanjunni (one CR with GT initials) mountains with satellite background. The Google Maps satellite inset figure shows the Jettan mountain survey with CR stations JT-SAT-4, JT-SAT-3 and JT-SAT-2, of which, at the westernmost the CR (JT-SAT-4) is located within a highly vegetated area. The ID numbers were kept as used by NVE, and the corresponding GNSS stations do not have 'SAT' in the name. On the right bottom corner an image of one of the CRs is shown.

The locations of the CRs in Norway are depicted in Figure 60. The GNSS station JT11 has been selected as the reference station to evaluate the performance of the Basic/L2a products (track 168 descending). It should be noted that the GNSS stations' locations are different from the locations of the CRs, with distances between 2 and 60 m apart. Therefore, the GNSS measurements may or may not mirror CR measurements, especially for GNSS stations beyond

the minimum resolution of the EGMS products (i.e. 20x5 m) or further away from the CRs. While there might be better procedures to validate the time series at a CR location, given that the GNSS stations are meters apart from the CR, the 100m radius makes it comparable and possible to estimate the standard deviations of the EGMS MPs.

Figure 61 shows the double differences between EGMS and GNSS close to each CR for all stations using station JT11 as a reference. The winter acquisitions are not processed in the EGMS products to retain coherence, which can be observed by the gap of observations during winter. The time series shows a good fit with the GNSS observations falling within the error bars of the EGMS MPs.

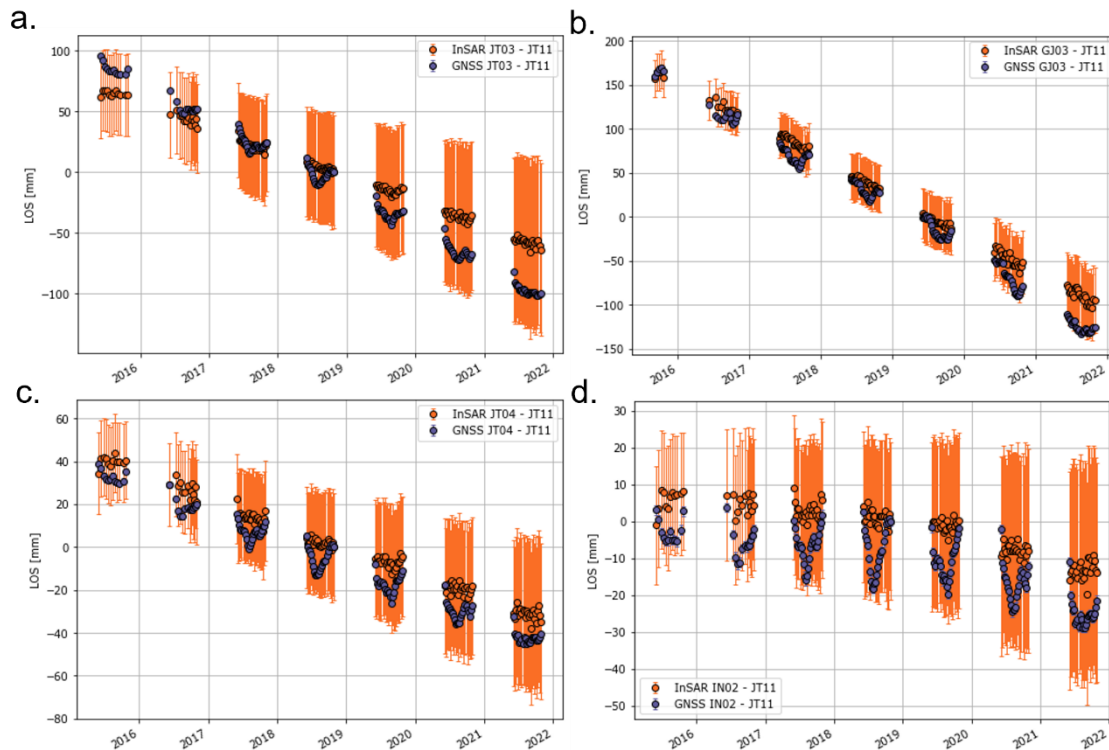


Figure 61: Examples of time series double differences between three of the stations for track 168/DESC. Station IN02 is the reference station. Acquisitions during wintertime were not processed to avoid loss of coherence due to snow cover. The error bars of the EGMS MPs were derived using all the datapoints falling within the search radius. Stations a) JT03 b) GJ03 c) JT04 d) IN02

Another way to visualise the fit between the double differences is by subtracting the double differences time series of the GNSS from the ones of the EGMS. The results are presented in Figure 62, where the differences in time between GNSS and EGMS are compared.

Ideally, the subtraction between the double difference time series should be around zero. In this figure, it is better observed that the linear displacement rate (or velocity) is either under or overestimated whenever these differences are not around zero. Stations JT04 and IN02 have time series differences around zero, indicating an excellent agreement. Stations JT03 and station GJ03 show an underestimation of the EGMS with respect to the GNSS of approximately 30 mm in 6 years of observations (c.a. 5 mm/year). The results of the differences between EGMS and GNSS time series generally fall within a one-sigma deviation or one standard deviation from the mean, with few punctual exceptions at station GJ03.

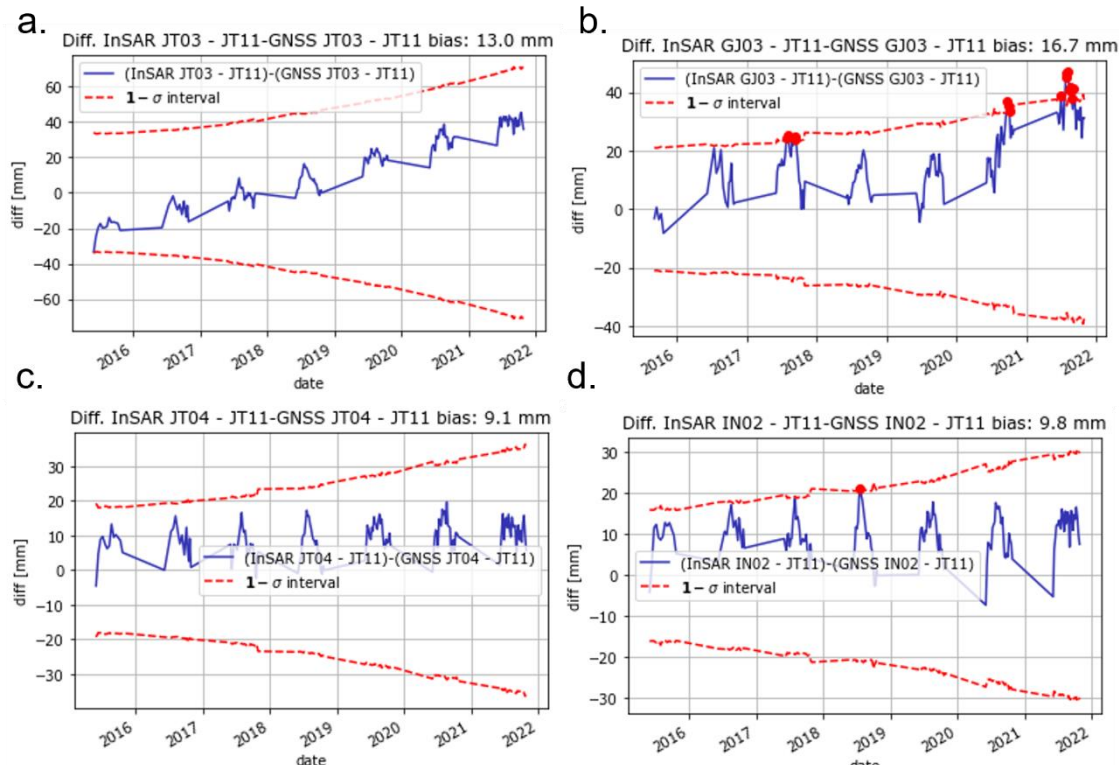


Figure 62: Subtraction between the EGMS and the GNSS double differences time series for the four stations using JT11 as a reference (blue line). Red lines indicate a one-sigma deviation interval or one standard deviation from the mean.

Figure 63 demonstrates the correlation of double difference velocities between EGMS and GNSS for all stations. This graph corroborates the results shown in previous figures. The velocity estimation at station GT03 and JT03 slightly deviates from the ideal correlation (black filled line), indicating that the EGMS velocities are lower than those measured by GNSS. For station JT03 the difference of the velocity between EGMS and GNSS is about 10 mm/year while for GT03 is lower, about 7mm/year. The EGMS velocity at stations JT04, JT11 and IN02 almost matches the GNSS estimation.

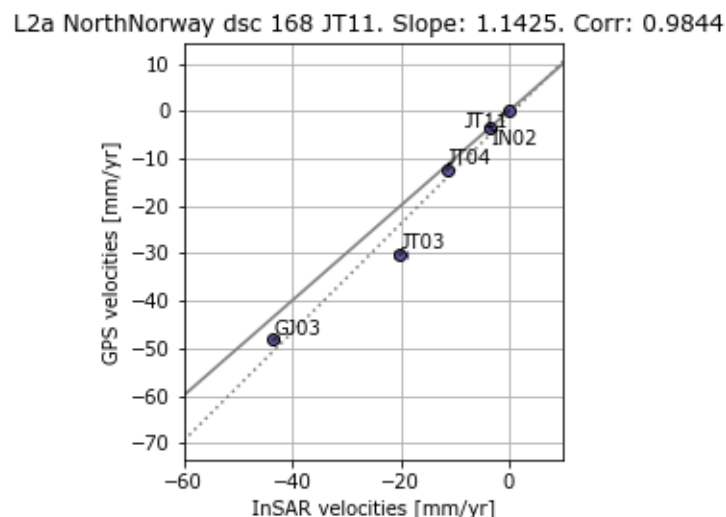


Figure 63: Correlation between EGMS/GNSS velocities. Station location falling within the black full line indicates perfect agreement between the estimated double difference velocity of the EGMS with the GNSS. Dashed line indicates the best fit line between all stations

Overall, the velocity correlation for all studied stations is 0.98, indicating that the Basic/L2a product time series generally align well with the GNSS stations. For such thematic area as landslides, only L2a products should be used and, to avoid problems with referencing, double differences should be performed. If there are not enough GNSS stations or no stations at all, double differences between InSAR observations can be performed between MPs outside and inside the location of a potential landslide. The optimal track orbit (ascending or descending) should be used depending on the slope direction.

For this validation site, the correlation of velocity estimation between EGMS and the GNSS measurements close to the CR is close to 1 (Fig. 66), indicating a near-perfect correlation. The most significant estimated difference in velocity is at station JT03 (Fig 66), with an estimated difference in velocity between EGMS and GNSS of approximately 10mm/year, still within the one-sigma standard deviations of the EGMS (Fig. 65a). This indicates the usability of the EGMS for landslide monitoring in high latitude mountain environments.

Mining and post-mining

Turow (Poland)

Turow is the second largest active coal mine in Poland. The mine is depleting water supplies, consequently generating subsidence in Germany and Czech Republic. The extensive network of water boreholes for the monitoring of Turow helps to monitor mining impacts in the surroundings of the open-pit lignite mine. Only 16 out of the 36 stations match the monitoring period of the EGMS (shown in Figure 64).

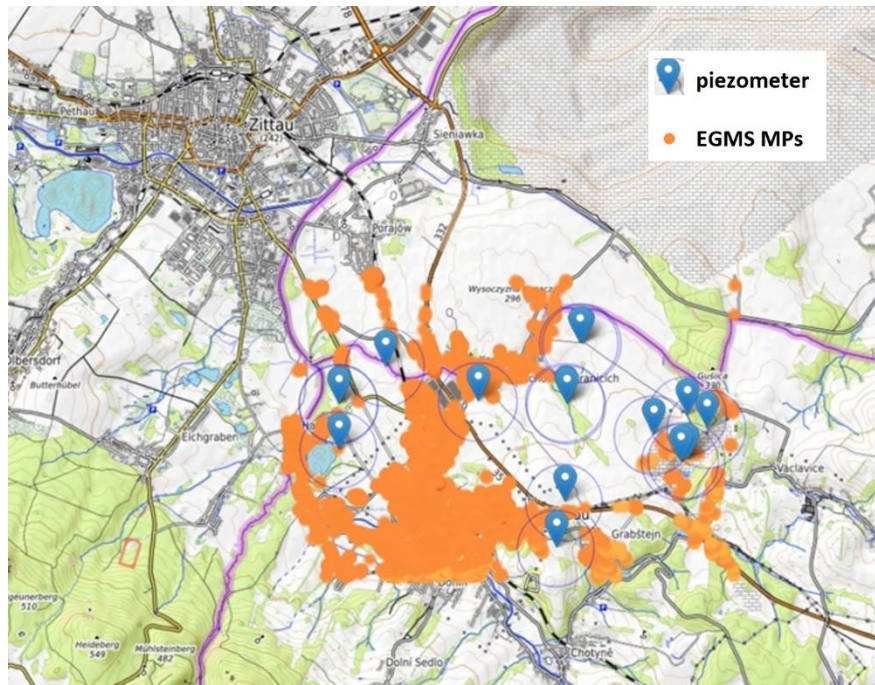


Figure 64: Turow validation site showing the Basic/L2a Ascending EGMS product, the piezometer position, and the drawn buffer.

The ground water levels are measured regularly twice a year. The measurement is expressed in meters above sea level of the heads of the water table for each time step. In the Turow case, the method proposed by Boni et al., 2016 was applied for comparison purposes, expressed in the following equation:

$$S = \text{Vel(EGMS)}/\text{Vel(piezometer)}$$

Where S is the storage coefficient, Vel (EGMS) is the minimum EGMS velocity calculated for the MPs falling inside the buffer around each station, and Vel(piezometer) is the piezometer velocity.

Finally, the $\Delta d = S \times \Delta h$ relation was used to calculate the new monthly deformation rate (for the time series) adjusted for the head of the groundwater change. The buffer used around the single boreholes was 500 m. An example of the adjusted piezometer TS4 – H-2a (in mm/y) plotted against the best matching (in terms of lowest MAE) MPs that fell inside the 500 m buffer is shown in Figure 65. Figure 66 follows the same approach for piezometer H-8a.



Figure 65: Comparison plot of in-situ time series against the best EGMS MP that fell within the 500 m buffer draw around the piezometer H-2a.

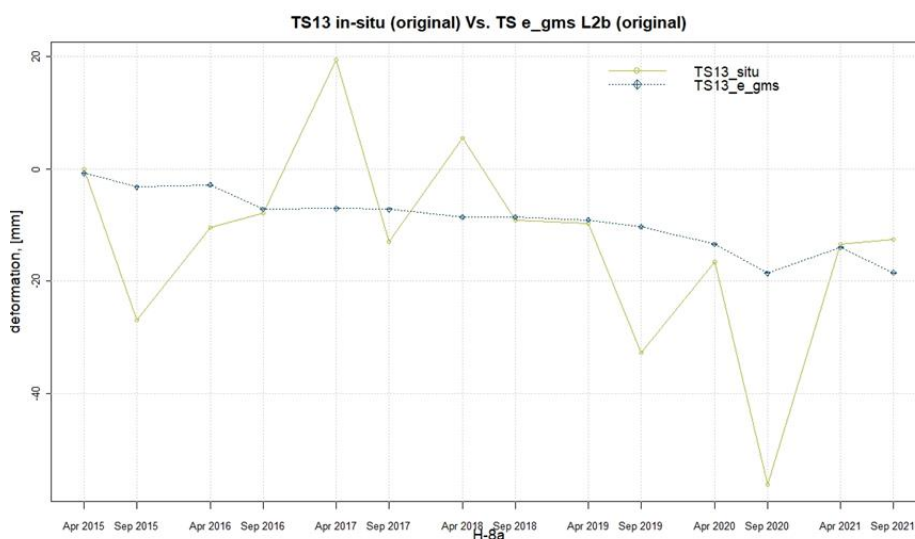


Figure 66: Comparison plot of in-situ time series against the best EGMS MPs that fall within the 500 m buffer draw around the piezometer H-8a.

For the Turow area, only the piezometric time series were validated against the EGMS products, because the velocities were only used for the calculation of the storage coefficient. For this study case, two sets of ascending data (track 073 IW1 and track 146 IW2) were available.

In Figure 67 it is clearly visible that track 073 is performing better than the other. For all the time series the errors are always higher than the rest of the metrics (considering that high error score corresponds to low MAE). All products scored very high in all the IoAs with the Basic/L2a ascending track obtaining the highest score.

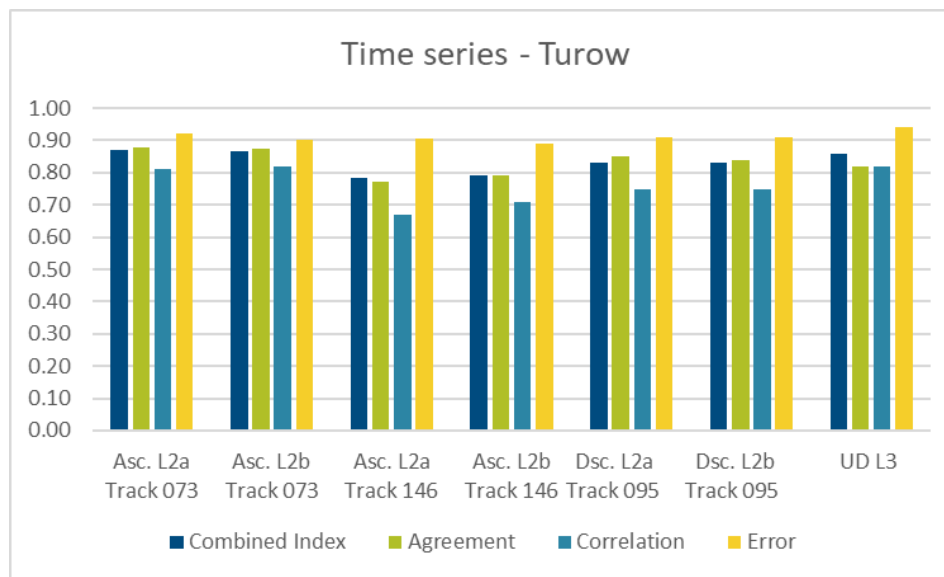


Figure 67: Time series results for the Turow case study.

Overall, the combined index indicated high consistency and agreement for all the time series evaluated with the only exception of H-8a (refer to Figure 67) where the original curve did not show a linear trend as the rest of the data.

Another interesting finding is that the accuracy of the EGMS for monitoring subsidence phenomena increases if, in the studied area, a track with lower viewing angle, such as track 073 ascending IW1 (near beam), is available.

Lorraine (France)

The commune of Freyming-Merlebach is located in the region of Lorraine (France), at the boundary with Germany. Concerns started to rise because the area was experiencing uplifts due to natural water filling in formerly exploited underground coal mines. A very large number of annual levelling measurements (>850 points) is used to validate the EGMS. The EGMS velocity was validated against each in-situ measurement, whereas only ten levelling stations with the highest uplift rate were considered for the time series validation.

In the Lorraine test case, the levelling measurements accuracy is around ± 20 mm/year, and the measurement is vertical (expressed in mm/y), that is why the EW displacement is not considered for the validation.

Correlation is the lowest metric observed in Figure 68. The reason behind this is that there is no linear dependency between insitu and EGMS velocities. Agreement metric shows a high value for all products and tracks.

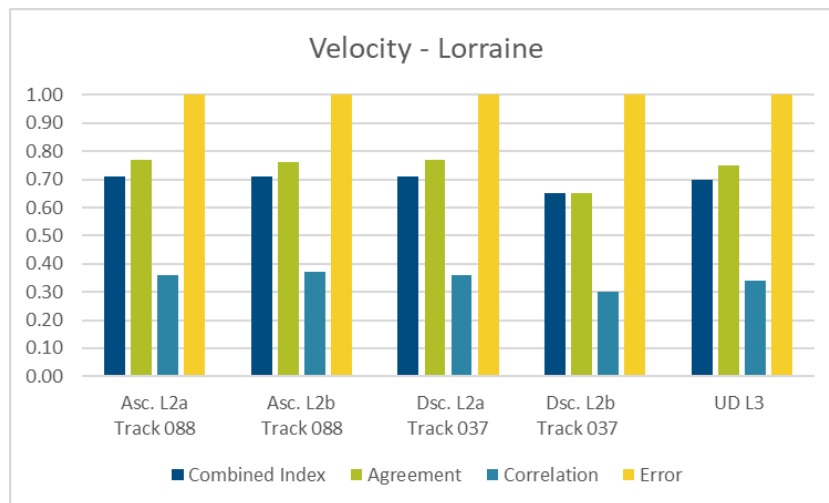


Figure 68: Velocity results for the Lorraine region.

The time series results for the 10 strongest velocities MPs that fall inside the levelling buffer are shown in Figure 70. The descending and the Ortho L3 vertical products are the ones with the highest IoAs. Probably the fact that the descending data (track 037) were acquired at a lower incidence angle than the ascending data (track 088) eased the validation of a traditional levelling approach that is mostly evaluating the vertical component of displacement.

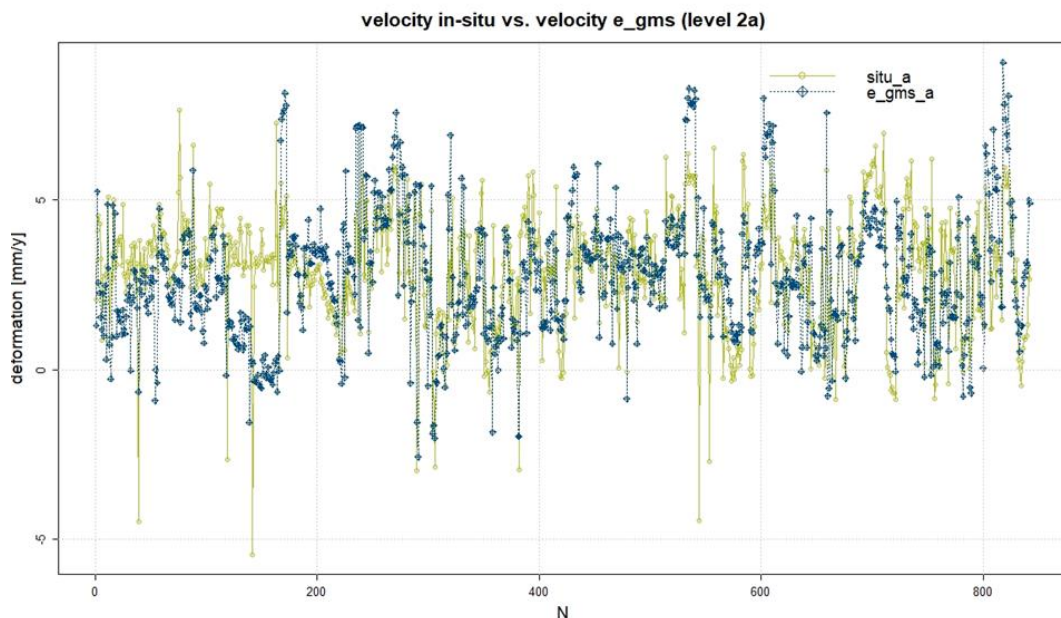


Figure 69: Plot showing the mean velocity of the whole population of levelling points against the maximum value of EGMS MPs that fall inside the 50 m buffer.

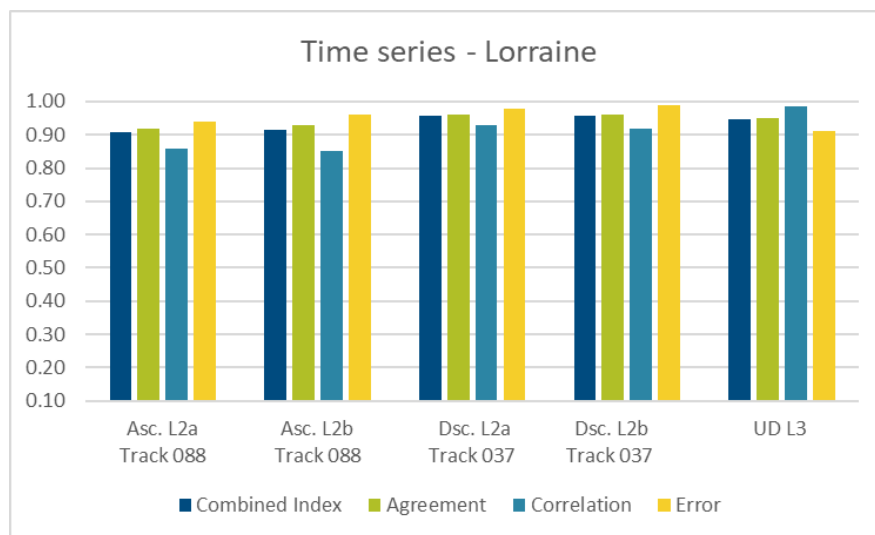


Figure 70: Time series results for the Lorraine case study.

Figure 71 shows an example of time series plot for one of the ten levelling stations that registered a high rate of uplift.

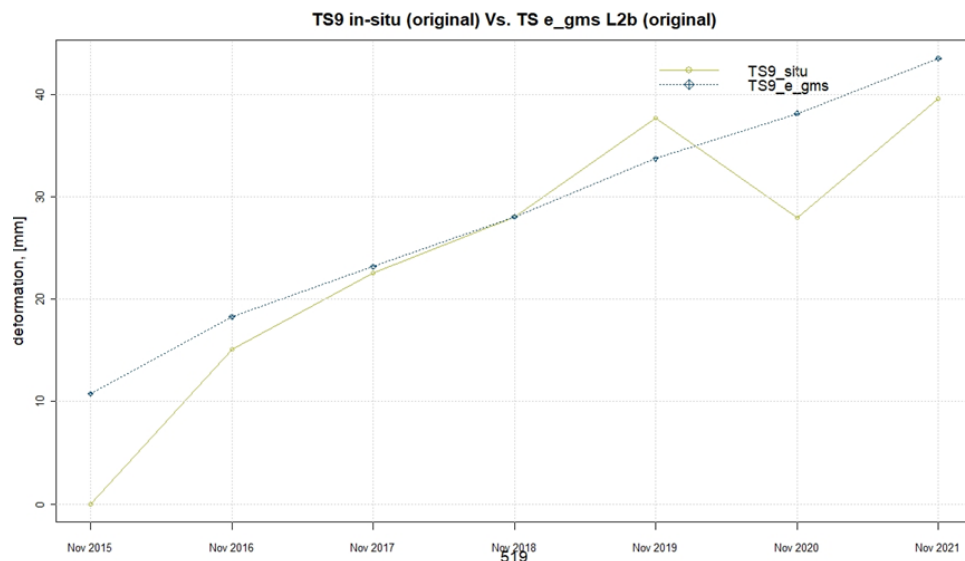


Figure 71: Time series plot of an in-situ data (station number 519) that has shown a high-rate positive velocity.

Overall, the combined index scored for each EGMS product above 0.91, which demonstrates the consistency of the EGMS with yearly levelling measurement of ground uplift in post-mining areas.

Urban

Jutland peninsula (Denmark)

Jutland is a large peninsula that contains the mainland regions of Denmark. It separates the North and Baltic seas, and borders Germany to the south. Along the west coast, the sedimentary sequence is mostly composed of sand and clay. Jutland's terrain is flat, with a slightly elevated ridge down the central parts. The highest hills (~150 m a.s.l.) are in the east. The west has a very low topography with some areas being below the average sea level. This area has been monitored with GPS stations since around the year 2010 (Figure 72). The phenomenon that is targeted by the GPS monitoring network is coastal subsidence.

Although Denmark is uplifting around 1 mm/year due to the post-glacial rebound, large parts of the coastal regions are subsiding due to local phenomena. For example, the harbour in Esbjerg (Jutland region) registers active subsidence. Other subsidence phenomena have also been reported in the town of Thyborøn, as reported in a previous chapter.

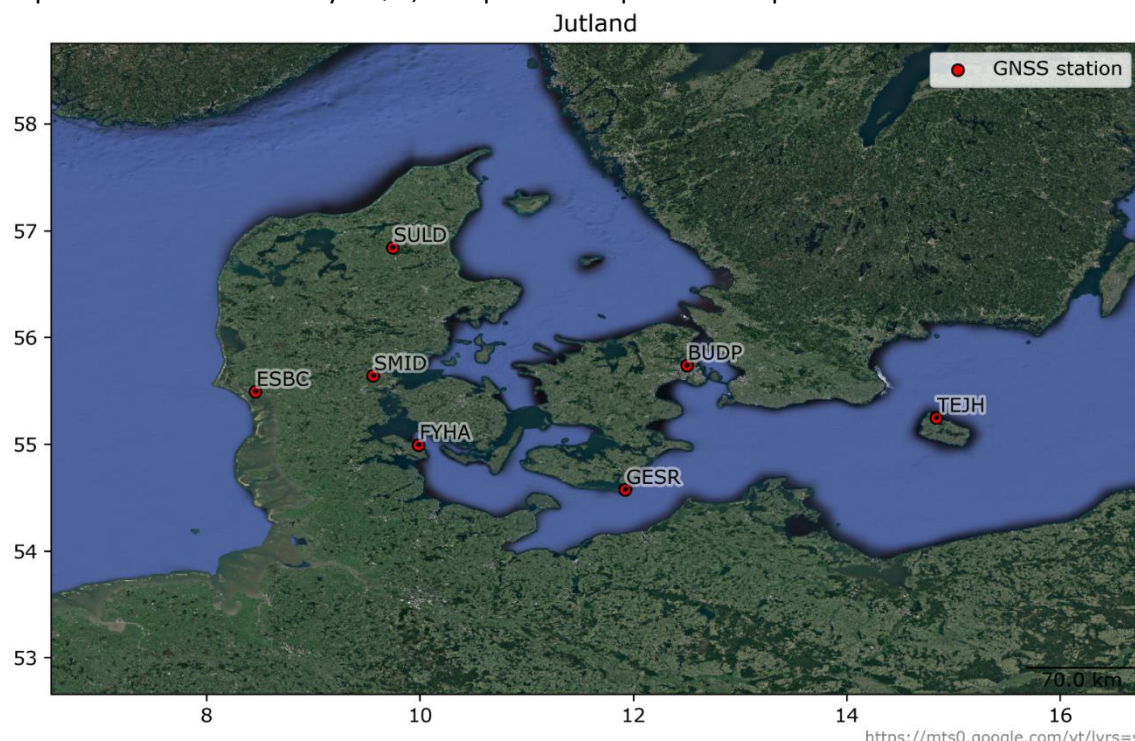


Figure 72: Jutland peninsula in Denmark and the GNSS stations used at this test site.

In Jutland, at some station locations, few MPs were observed within the applied 100 m radius around the GNSS stations. Because of this, there were less than three MPs at some locations in rural areas, and therefore, it was impossible to derive standard deviations of the EGMS time series. Therefore, the following stations were excluded from the analysis: TEJH, BUDP and GESR.

Figure 73 displays different station examples of EGMS MPs comparisons around each GNSS station. Figures 73-a and 73-b show the double differences with reference to FYHA station for Basic/L2a products for descending track 066 and ascending track 117 respectively. Figures 73-c and 73-d show the single differences instead for Calibrated/L2b products for descending (c) and ascending (d) tracks, respectively.

The time series and velocities in Denmark show an excellent fit between the GNSS and the EGMS MPs around the GNSS stations. The GNSS time series fell within the estimated standard deviation of the EGMS time series. Figure 73-c shows the station with the worst fit between the EGMS and GNSS, station SULD, where at some instances in time, the GNSS displacements fall outside the estimated GNSS standard deviations. However, the velocity difference is minimal, lower than 1.5 mm/yr.

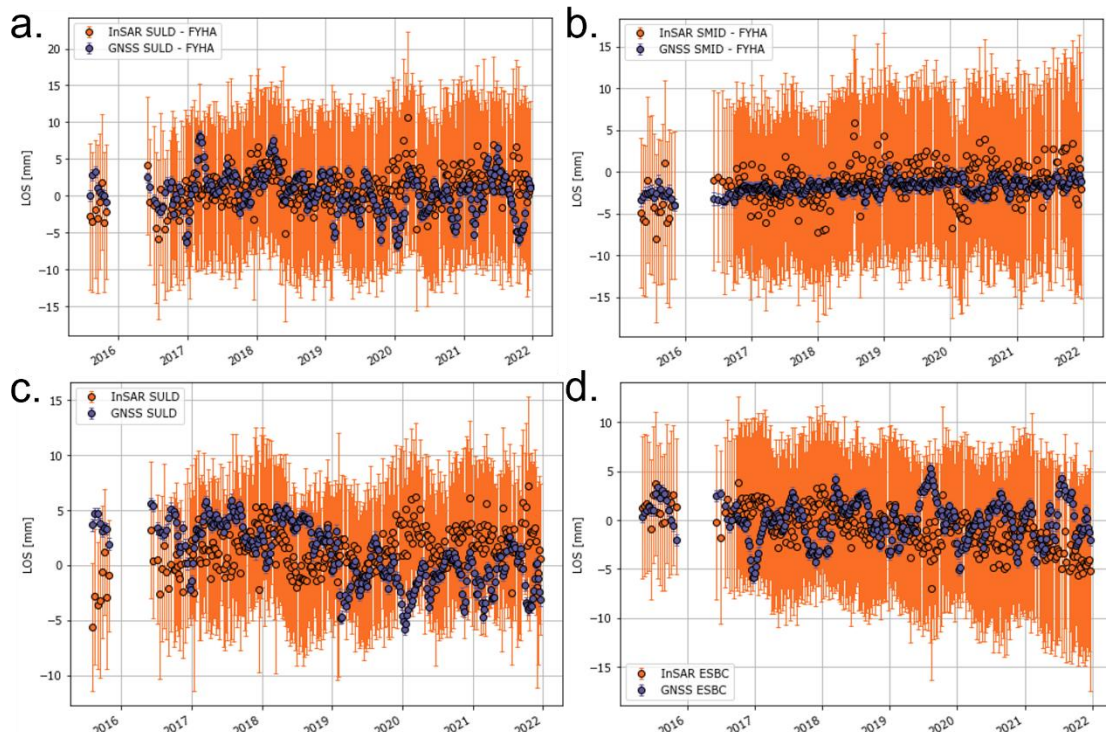


Figure 73: a) and b) Examples of double differences between pairs of GNSS station FYHA and Basic/L2a products for descending-066 (a) and ascending-117 (b) tracks. c) d) Example of single differences between EGMS and GNSS of Calibrated/L2b products. (c) descending track (066) and station SULD, and (d) is the ascending track (117) and station ESBC.

The overall model test (OMT) for the time series and t-test for velocity differences give a positive outcome for nearly all stations, suggesting a similarity between EGMS and GNSS time series.

Figure 74 shows the time series of the only stations that did not pass the velocity test from all stations and analysed products.

The left-side of the figure compares a single station with surrounding EGMS MPs, while the right-side displays differences between GNSS and EGMS within a 1-sigma interval. The stations SULD and SMID fail the t-student test for velocity for the ascending track of the Calibrated/L2b products. Still, the estimated velocity differences between GNSS and EGMS is minimal and in the order of 0.5-0.7 mm/year.

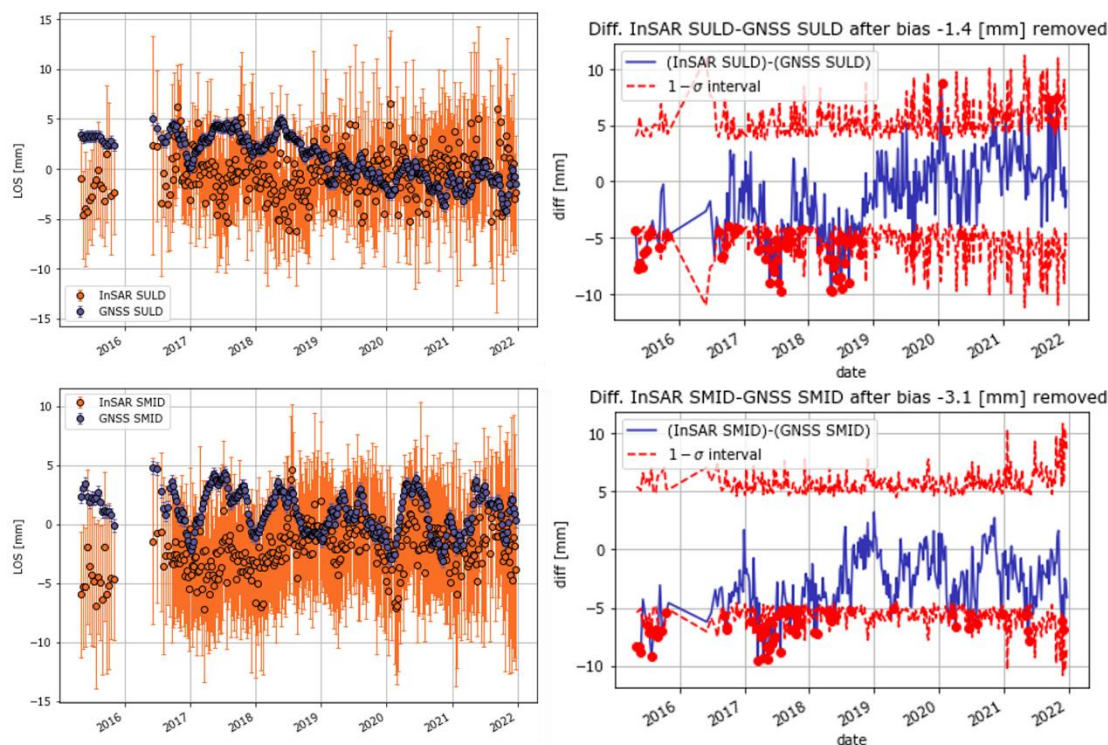


Figure 74: Examples of single station Calibrated/L2b products, highlighting comparisons for ascending track 044 between EGMS and GNSS for station 'SULD' (top) and the corresponding time series differences. The same is done for station 'SMID' for the same track (bottom).

Figure 75 shows the bar charts of the IoAs of the available ascending and descending tracks for both the Basic/L2a and Calibrated/L2b products and the East and Up L3 products. All stations passed the time series test (IoA_1_test) for all tracks of the Basic/L2a products and Calibrated/L2b products, and only station SULD failed the velocity test. However, the velocity difference between EGMS and GNSS for SULD stations is between 0.6 and 1.5 mm/year depending on the track for Basic/L2a products, and between 0.4 and 1.4 mm/year for Calibrated/L2b depending on the track.

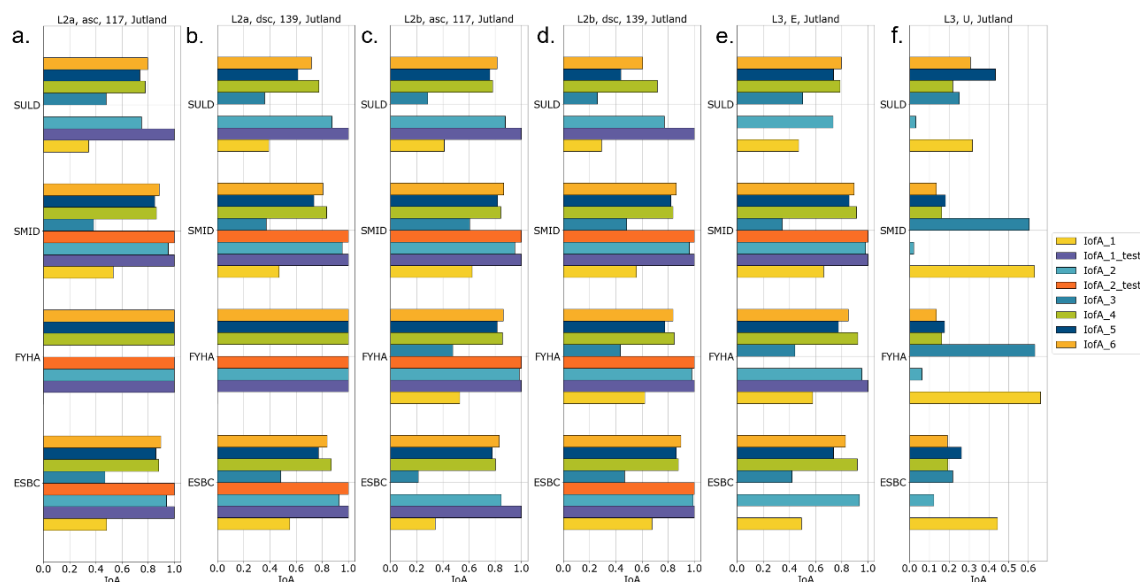


Figure 75: Index of Agreement for Basic/L2a, Calibrated/L2b and Ortho/L3 EGMS products for one of the available ascending and descending tracks. Each of the subplot title indicates the product followed by the type and number of tracks.

The worst performance is shown by one of the L3 products (E42N36 tile) failing the velocity and time series tests except for station SMID. The maximum estimated velocity difference for L3 East-West products is 1.5 mm/year, and 0.69 mm/year for the L3 Up-Down products.

Overall, the seasonality index (IoA_3) or the correlation of detrended signals indicates an acceptable but not excellent correlation of seasonal effects between EGMS and GNSS. Therefore, seasonal effects should only be interpreted, with some care, for Basic/L2a products.

Calibrated/L2b time series have undertaken calibration with GNSS, and consequently, the time series have changed. Seasonality using GNSS comparison with Basic/L2a products should be carefully interpreted because of the nature of the double-difference estimations. Two reasons could be hypothesised:

- if there is remaining seasonality after removing the trends, the reference station might display inverse seasonality with respect to the other station.
- if there is no remaining seasonality, there are no seasonal effects, or the seasonal effects are in phase between the analysed stations, a single time series might be processed to extract the peaks and amplitudes of the seasonal signals and ensure that no seasonal effects were present in the spatial reference of the EGMS products.

Figure 76 showcases examples of the correlation of estimated velocities between EGMS and GNSS using all stations per evaluated product. This figure reinforces previous observations of the velocity differences: the correlation coefficients indicate a good agreement between GNSS and EGMS estimated velocities for most of the EGMS products and tracks, except for the SULD station; track 117 of the Calibrated/L2b products show the worst correlation considering all the stations. The reason for that difference will need to be investigated.

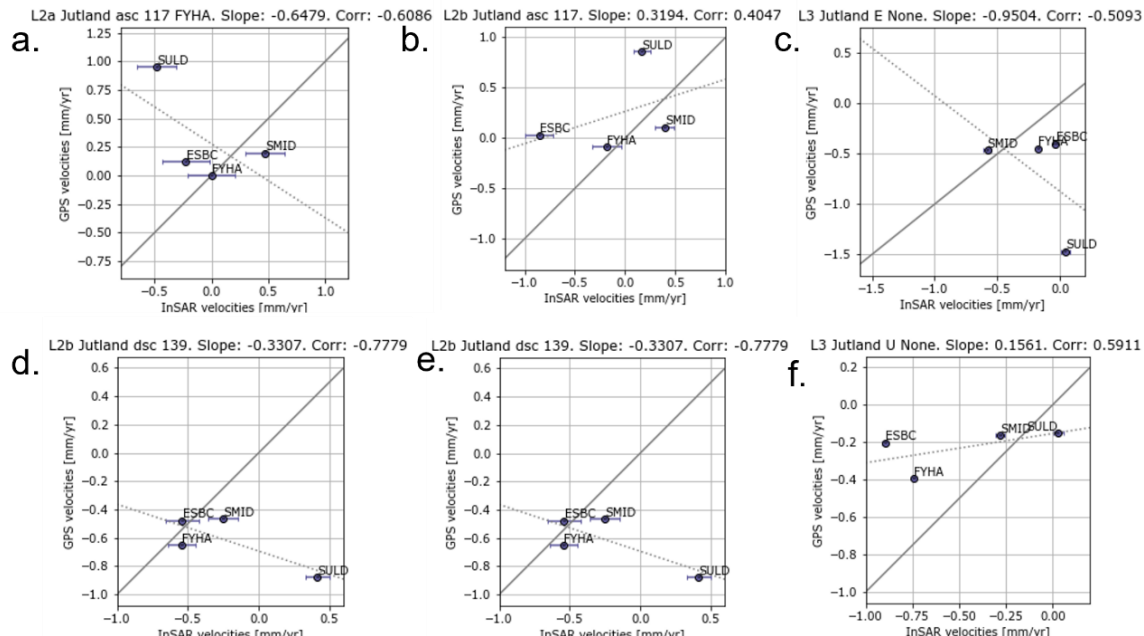


Figure 76: Correlation between EGMS/GNSS velocities for the three EGMS products. Station location falling within the black full line indicates perfect agreement between the estimated double difference velocity of the EGMS with the GNSS. Dashed line indicates the best fit line between all stations. a) b) L2a-117 c) L3-EW d) e) L2b-139 f) L3-UD

The time series of the GNSS stations and the EGMS MPs around the GNSS stations is similar. The velocity differences highlighted by the IoA are minor, with the highest differences in the order of 1.5 mm/year, indicating an overall good fit, except for station SULD.

Thyborøn (Denmark)

In the west coast region of Denmark, Thyborøn holds significant interest due to its unique geographical features. This area is a focal point of a thematic investigation centred on subsidence, primarily resulting from consolidation phenomena. The location, mainly constructed on landfill and soft sediments, exhibits notable subsidence rates exceeding 7 mm/year, particularly in its south-eastern parts.

Recent measurements in Thyborøn include CRs linked to a levelling network (Figure 77). This network serves to calibrate satellite-based deformation measurements, offering crucial data for this study.



Figure 77: Map of Thyborøn Peninsula and the three CRs observable in the EGMS time series the image in the right bottom corner shows an example of the type of CR deployed in Thyborøn.

Three out of 8 CRs are visible in the EGMS product being validated. The three CRs are made from 60x60x120 cm square aluminium/iron plates with double geometry, suitable for both ascending and descending satellite paths. Moreover, there have been two levelling campaigns relevant to this release of the EGMS (2015-2021). Consequently, for the current EGMS comparison, Thyborøn has been primarily utilized for assessing the geo-positioning accuracy.

The geolocation accuracy of the Basic/L2a and the Calibrated/L2b products was evaluated in the Thyborøn site. For both products, the estimated accuracy is below the geolocation accuracy requirement of 10 m.

In the next validation iteration that will include the 2022 update, the remaining CRs should become visible, and it will be therefore possible to include the 2022 levelling campaign.

Gran Canaria (Spain)

The island is a populated outermost Spanish region and one of the most popular touristic destinations in Europe. More than two million people live and work in the archipelago, resulting in an average population density three times greater than the rest of Spain. The Canary Islands are one of the major volcanic oceanic island groups of the world and have a long magmatic history, which began at the bottom of the ocean more than 40 million years ago. This volcanic archipelago is constructed on the passive continental margin of the African Plate on Jurassic oceanic lithosphere and comprises seven main volcanic islands that form a chain extending for some 500 km across the East Atlantic Ocean.

The aim is to validate data acquired in volcanic regions. Most of the historical eruptions in the Canary Islands have been short lived (from few weeks to few months) basaltic, strombolian to violent strombolian eruptions, which have generated scoria cones of different sizes and lava flows of different extent. Sixteen historical eruptions have been documented in the Canarian Archipelago to date. The last event occurred in September 2021 in La Palma and lasted 85 days. It covered with lava flows more than 1228 Ha and destroyed around 1700 buildings. Because of the availability of GNSS stations, the validation focus has been on the island of Gran Canaria (Figure 78).



Figure 78: Grand Canaria and GNSS stations distribution

In the analysis of Basic/L2a and Calibrated/L2b products (ascending track 162), all stations pass the overall model test (OMT) for the time series (IoA 1) except for the AGUI station for the L2b descending track. There is a notable agreement between the EGMS and GNSS stations, with AGUI being the station where the fit is poorer with velocity differences in the order of 1.8 mm/year for the Basic/L2a products and 1.3 mm/year for the Calibrated/L2b products. Station ALDE shows the most negligible velocity differences for both tracks out of all the Gran Canaria GNSS stations.

Figure 79 illustrates the worst and the best performance for the time series comparison for the Basic/L2a and Calibrated/L2b products.

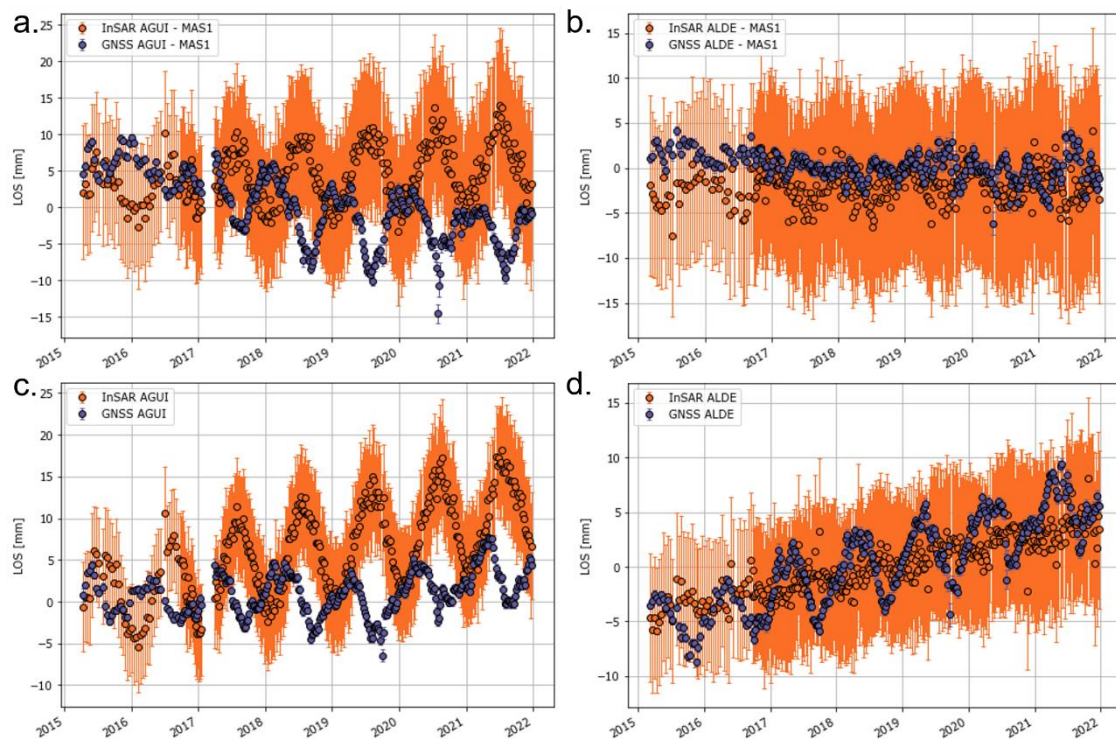


Figure 79: a) and b) Examples of double differences between pairs of GNSS stations and Basic/L2a products for 162/ASC track. c) d) Example of single differences between EGMS and GNSS of Calibrated/L2b products. Subplot a) and b) are examples of the worse fits (station AGUI) and c) and d) are examples of the best fits (station ALDE). Reference station: 'MAS1'.

In both figures 79-a and 79-b, the AGUI time series single differences accurately capture the linear trend or velocity but fail the IoA_{test_1} due to anticorrelation in seasonal effects. Consequently, station AGUI has one of the lowest IoA4 values, the IoA for the correlation of detrended signals. Station ALDE on Figure 79-b and 79-d exhibits the lowest velocity differences on ascending and descending tracks for Calibrated/L2b products. This is clearly visible as GNSS captures the seasonal deformation pattern whereas EGMS displays a clear linear rate of displacement.

Overall, the agreement between EGMS and GNSS stations is similar between Basic/L2a and Calibrated/L2b products. In the case of Calibrated/L2b products, four out of five stations for the ascending track and two out of five for the descending track do not pass the velocity test. However, note that the stations that do not pass the velocity test have velocity differences in

the order of 0.6 to 1.2 mm/year, and the station AGUI has the worst performance for the descending track with 1.4 mm/year.

Figure 80 depicts the Ortho/L3 products comparison in the East-West (top row) and vertical direction (bottom row). The Ortho East/West product exhibit higher IoAs than the Ortho Vertical product (Figure 81), consistently across all stations. This can be observed from the best (MAS1, ALDE) and worse results (AGUI) in Figure 80.

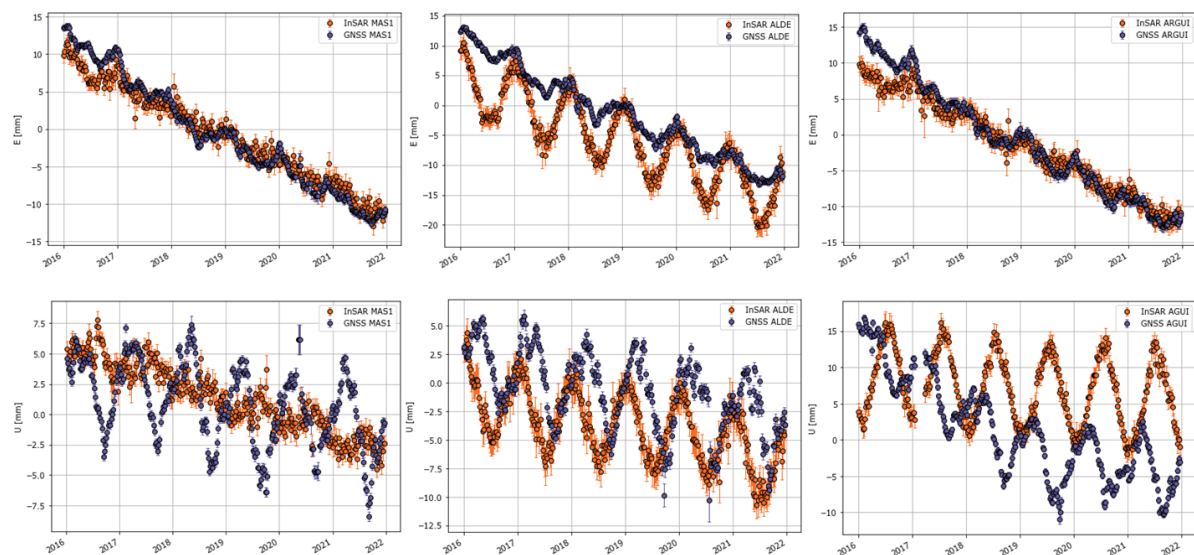


Figure 80: Ortho/L3 products comparison in the East-West (top row) and vertical direction (bottom row)

Figure 80 shows, with the exception of AGUI for the Ortho Vertical product, that the time series seem to fit nicely, at least for the velocity value. Bigger differences are appreciated in the time series trend and seasonality. The most significant velocity differences in East-West Ortho/L3 products are 0.9 mm/year at TERR, followed by ARGUI, with a 0.7 mm/year difference between EGMS and GNSS.

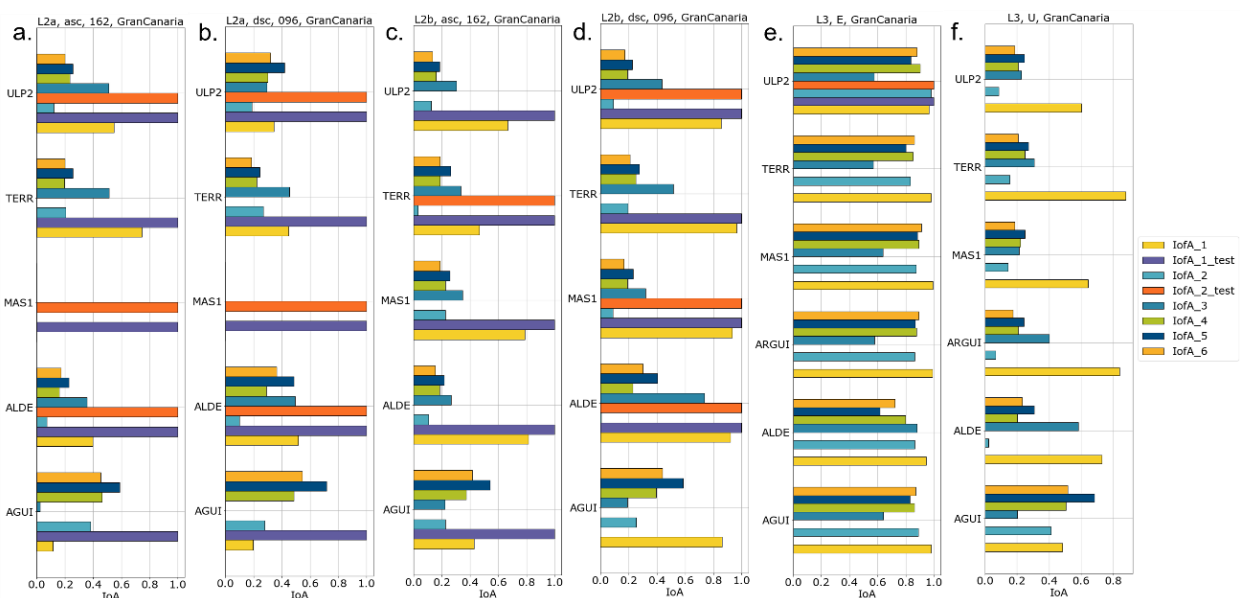


Figure 81: Index of Agreement for Basic/L2a, Calibrated/L2b and Ortho/L3 EGMS products for one of the available ascending and descending tracks. Each of the subplot title indicates the product followed by the type and number of tracks.



For the Ortho/L3 products in the Vertical direction of displacement the most significant velocity difference is approximately 2.3 mm/year at station AGUI, as shown in Figure 80. TERR follows with velocity differences of around 0.8 mm/year. Generally, the EGMS Ortho Vertical time series appear smoother over time than the GNSS time series, with more pronounced anti-correlation than the East/West component. This is expected given the spatial and temporal averaging (resampling to a coarser grid and to a common 6-day temporal sampling) performed to derive these products. GNSS data show seasonal effects at all stations with an amplitude signal of roughly 10 mm, which is only slightly captured by the EGMS at the stations AGUI and ALDE.

The seasonality index (IoA_3) or the correlation of detrended signals indicates an acceptable but not excellent correlation of seasonal effects between EGMS and GNSS. However, as seen for the GNSS stations in Jutland, seasonal effects should only be interpreted, with care, for Basic/L2a products.

The general assessment for the Gran Canaria test site is positive, with a good fit between most of the GNSS stations and the EGMS time series around those stations. The time series of the EGMS sometimes mimics the GNSS, having mostly one station (AGUI) as an outlier. The largest velocity difference has been estimated at AGUI GNSS station and corresponds to 2.1 mm/year for Basic/L2a products, 1.4 mm/year for Calibrated/L2b products, and 2.3 mm/year for Ortho/L3 Up-Down. Because of the nature of the InSAR and GNSS processing (choice of the spatial reference, resampling in time, average in space, atmospheric corrections, and how the GNSS was processed), seasonal effects should not be interpreted for Calibrated/L2b and for Ortho/L3 products. They should additionally be carefully interpreted for Basic/L2a products.

Overall, the agreement between EGMS and GNSS stations is similar between Basic/L2a and Calibrated/L2b products. In the case of Calibrated/L2b products, four out of five stations for the ascending track and two out of five for the descending track do not pass the velocity test.

However, note that the stations that do not pass the velocity test have velocity differences in the order of 0.6 to 1.2 mm/year, and AGUI has the worst performance for the descending track with 1.4 mm/year.

This means that the EGMS can accurately measure moderate ground motion; however, the data shall be carefully treated when the seasonal or any other trend variation is analysed at the scale of the single MP.

Groundwater exploitation

Murcia Region (Spain) – GNSS comparison

The Guadalentín basin, SE Spain, is one of the driest regions of Europe (Figure 82). This basin is a tectonic depression located in the eastern part of the Betic Cordillera, an alpine orogenic belt resulting from the collision of the African and Iberian plates. The Alto Guadalentín aquifer is located between the cities of Lorca and Puerto Lumbreras. The continuous pumping of groundwater in the aquifer, mainly for agricultural use, led to a decrease in the piezometric levels of more than 200m since 1975, resulting in the overexploitation of the aquifer and the land subsidence. Lorca, affected by subsidence triggered by water overexploitation, has been studied using different techniques such as GNSS and InSAR. The accumulated vertical deformation close to Lorca is around 24 cm but larger in the centre of the basin, ranging up to 12 cm/year. Of all the validation sites, Lorca shows the highest rate of displacements for which a GNSS comparison is valuable due to the challenging performance for the EGMS. This strong subsidence area is represented by stations **LRCA**, **ORCA** and **LORC** (Figure 82).

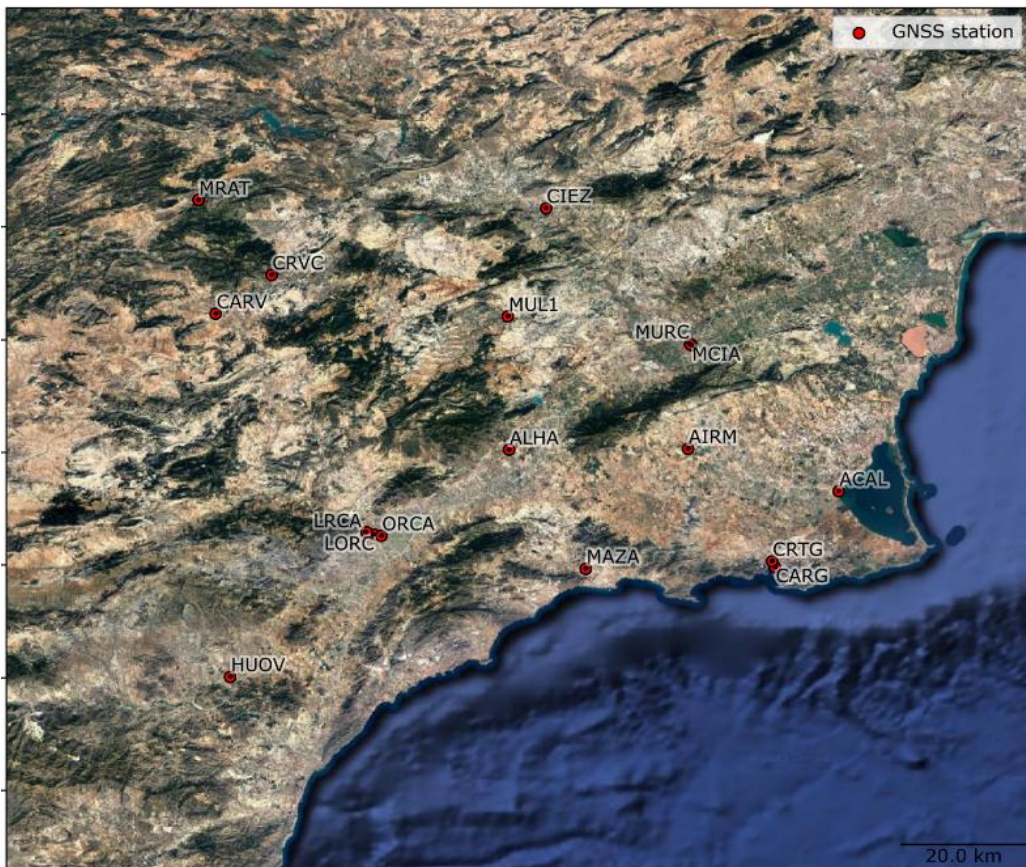


Figure 82: The GNSS station locations used for Lorca test site. (basemap: Google)

For the Basic/L2a products on the ascending track 103 shown in Figure 83, results vary slightly from station to station. In this figure, some of stations with the highest and the lowest displacements are illustrated. The second row illustrates very well how EGMS is able to capture the strongest deformations in the area of interest.

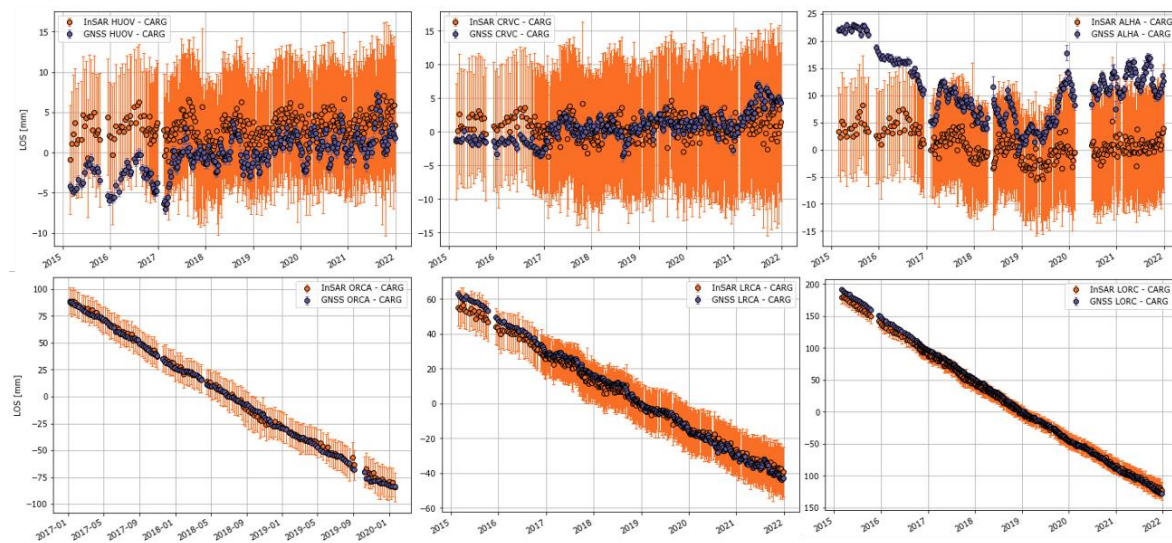


Figure 83: Example of double differences between pairs of stations of Basic/L2a products track 008/DESC. Reference station CARG.

All 30 stations pass the time series test for the Basic/L2a products (including all tracks) demonstrating that EGMS is able to reasonably capture different kind of ground deformation in the validation site.

Figure 83 (second row) illustrates how EGMS is able to capture the strongest deformation in the area of highest groundwater extraction rates with very high accuracy.

Figure 84 presents single differences between EGMS and GNSS for Calibrated/L2b products on the ascending track 103. Stations such as CRVC, MUL1, AIRM, MAZA, ACAL, and MCIA show consistent velocity differences below 0.5 mm/year across most EGMS products, indicating a near-perfect fit between GNSS and EGMS. These stations are outside the boundaries of the subsidence area of Lorca.

Calibrated/L2b products exhibit similar patterns to Basic/L2a regarding the fit between EGMS and GNSS products. For Calibrated/L2b, LORC station records a velocity difference of 3.2 mm/year for descending track (008). Nevertheless, for ascending track (001) the estimated velocity difference for LORC is 0.1 mm/year, in correspondence of the area where the highest displacement rates are recorded. The fit between the EGMS and GNSS time series at the stations of largest displacements is remarkable.

Thirty-five out of thirty-seven stations pass the time series test for Calibrated/L2b products (including all tracks) and the average velocity difference between EGMS and GNSS is significantly low, c.a. 1 mm/year (including all tracks and all stations). This includes all the stations within the subsidence area of Lorca.

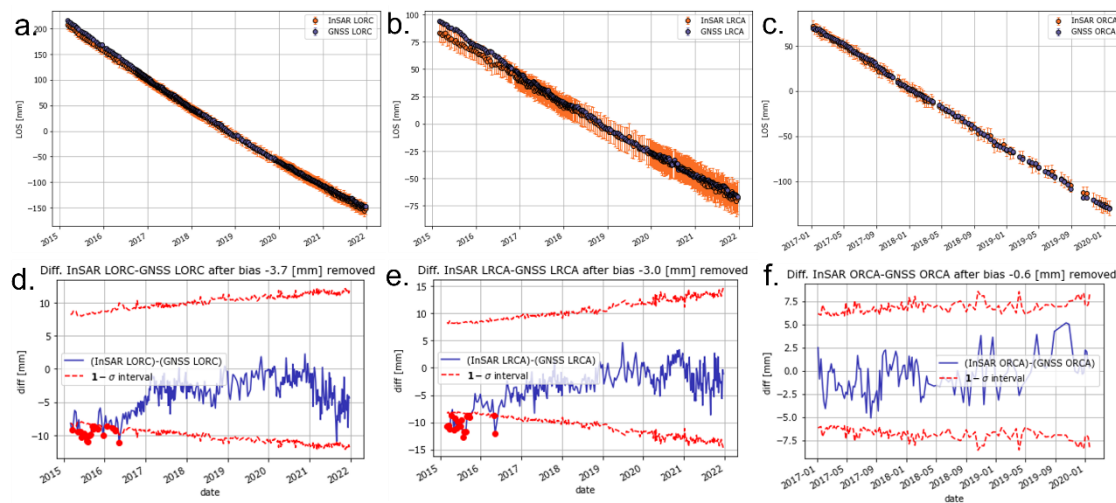


Figure 84: a) b) c) Single station time series comparison between EGMS and GNSS for Calibrated/L2b track 103/ASC.
d) e) f) corresponding differences between the EGMS and the GNSS time series.

Regarding Ortho/L3 products, the fit in up-down outperforms that in the east-west. Stations like MUL1 and MRAT exhibit the best time series fit in Up-Down and MAZA and MURC the Additionally, nine out of the 16 stations show velocity differences between EGMS and GNSS below 1 mm/year.

In Figure 85, the velocity correlation plots between EGMS and GNSS show which stations fit have similar and deviating velocities. Note that the x and y-axis of a) and d) the basic/L2a products have the smallest range, indicating that the velocity differences are the smallest for L2a products. The difference in the x and y-axis range for L2b products (figure 85-b and e) is significant, indicating that the ascending track generally shows lower velocity differences. As for the L3 products (figure 85-c and 85-f), the x and y-axis ranges show the highest velocity differences between EGMS and GNSS. As observed before, what is transversal to all the subplots is the general less good fit for AGUI and TERR stations.

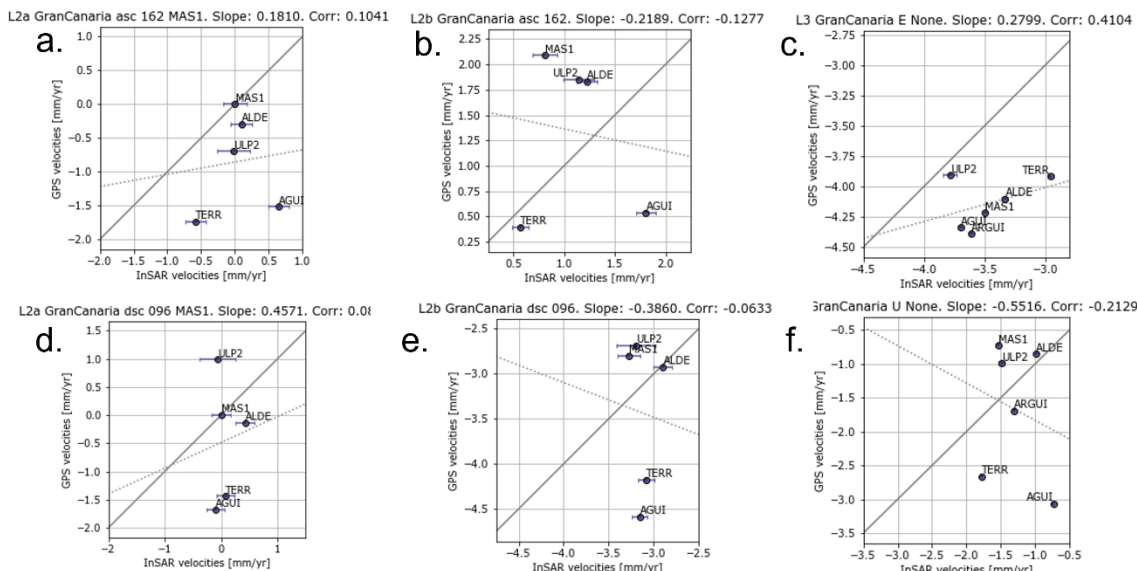


Figure 85: The best and worst station fit examples for Ortho/L3 products in both east-west and up-down directions.

Figure 86, containing bar charts, summarizes the IoA of all products per station.

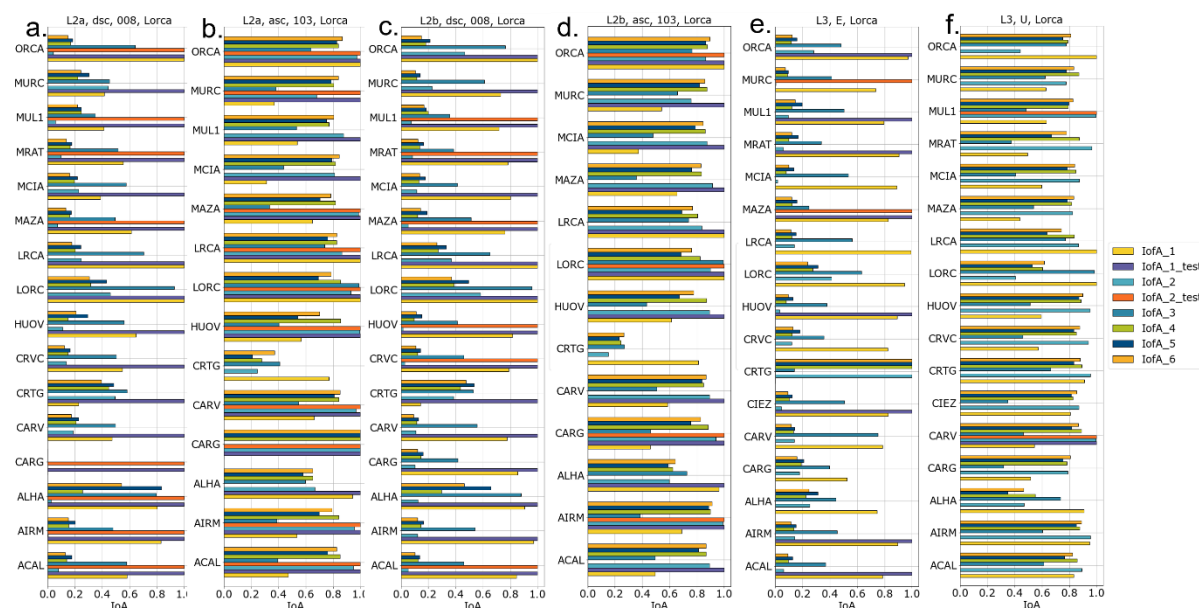


Figure 86: Indices of agreement for Basic/L2a, Calibrated/L2b with the corresponding ascending and descending tracks and Ortho/L3 products.

The overall performance at this test site indicates that ascending products align more closely with GNSS data than descending products for Basic/L2a and Calibrated/L2b.

Similarly, for Ortho/L3 products, the Vertical product show better results than the East/West products. Given the estimated velocity differences and time series fit, the EGMS seems functional to perform further assessment or even monitoring of the subsidence area and its surroundings.

Given the large displacements at Lorca and InSAR's problematic performance in large-magnitude displacement locations, the fit between EGMS and GNSS at this test site is excellent.

Lorca (Spain) – In situ comparison

The data used for the validation were three boreholes equipped with piezometers which four, five, and six times a year (irregularly) measure the ground water table fluctuation (Figure 87). The measurements are expressed in meters above sea level of the heads of the water table for each time step. In the Lorca case, the methodology presented by Ezquerro et al., 2020 was used:

$$\text{New water level change } (\Delta h) = \alpha \times \text{Water Change} \times \text{Compressible Thickness}$$

- with $\alpha = 0.05$.

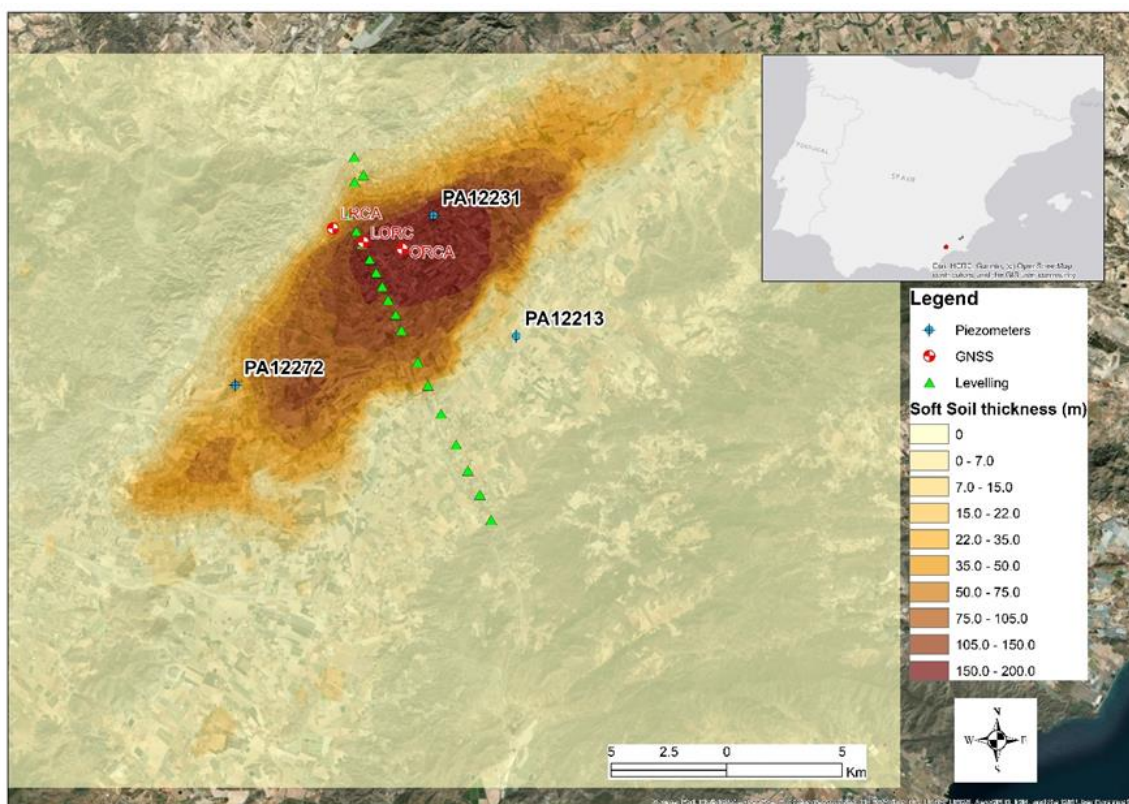


Figure 87: Lorca study case showing levelling, GNSS and piezometer positions.

The new piezometer velocity (in mm/y) based on the acquisitions per year in the study interval (2016-2021) were calculated by interpolating linearly the new water level changes.

In Lorca, the time series results show the lowest scores among all the in-situ case studies. In fact, a combined index ranging between 0.41 to 0.43 indicated intermediate consistency whereas only the agreement metric scored slightly better (0.55-0.61). One of the reasons of those low scores is that one piezometer, which is located in the thickest soil area (PA-12231) and experienced in the EGMS the highest rate of subsidence (a cumulated of 500 mm in five years), resulted in the lowest score in error possible, which leaded to lower the overall averaged scores.

Another reason is that, as can be seen in Figure 89, the nature of the piezometric time series is strongly non-linear, the opposite of the behavior of an EGMS time series in this area.

Last but not least, the non-agreement can be also justified by the lack of regularly spaced measurements, which led to a complex storage coefficient evaluation and soft soil compressible thickness data adjustment as previously described.

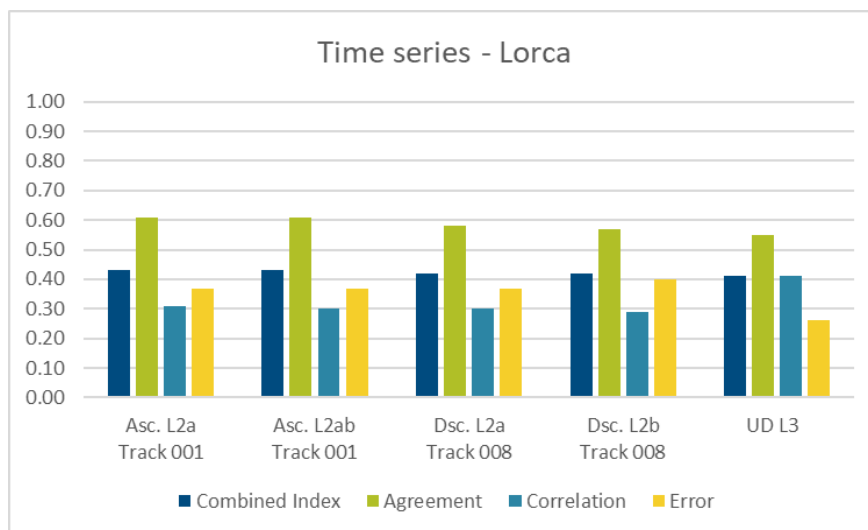


Figure 88: Time series results for the Lorca case study.

The Lorca comparison with insitu data is challenging due to strong non-linear deformation patterns difficult to capture with InSAR as shown in Figure 89. Despite that, EGMS is able to estimate velocities with decent accuracy.

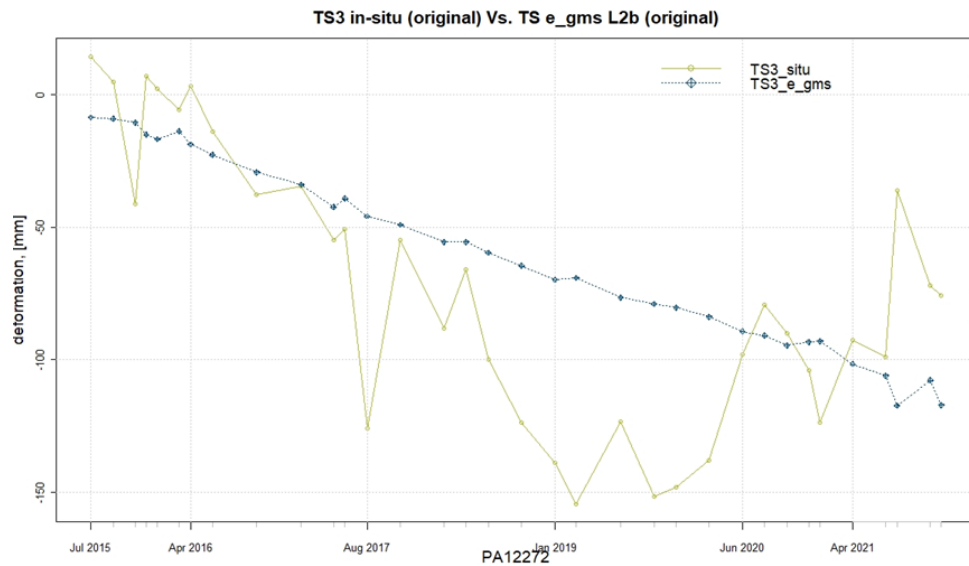


Figure 89: Time series plot of an in-situ data (station number PA12272) against the EGMS MP with the lowest MAE error.



REFERENCES

- Congalton, Russell. (2001). Accuracy assessment and validation of remotely sensed and other spatial information. *INTERNATIONAL JOURNAL OF WILDLAND FIRE*. 10. 321-328. 10.1071/WF01031.
- Vradi, A., Sala, J., Solari, L., & Balasis-Levinsen, J. (2023). VALIDATING THE EUROPEAN GROUND MOTION SERVICE: AN ASSESSMENT OF MEASUREMENT POINT DENSITY. *The International Archives of the Photogrammetry, Remote Sensing and Spatial Information Sciences*, 48, 247-252.
- European Environment Agency, 2021. European Ground Motion Service (EGMS) Quality Assurance & Control Report – Harmonisation Tests. land.copernicus.eu/user-corner/technical-library//quality-assurance-and-control-report-2013-harmonisation-test
- Fabris, M., Achilli, V., Menin, A., Estimation of Subsidence in Po Delta Area (Northern Italy) by Integration of GPS Data, High-Precision Leveling and Archival Orthometric Elevations. *International Journal of Geosciences*, 2014, 5, 571-585 <http://dx.doi.org/10.4236/ijg.2014.56052>
- Fabris, M., Battaglia, M., Chen, X., Menin, A., Monego, M., Floris, M., 2022. An Integrated InSAR and GNSS Approach to Monitor Land Subsidence in the Po River Delta (Italy). *Remote Sensing*. 14. 5578. <https://doi.org/10.3390/rs14215578>.
- Cenni, N., Fiaschi, S., Fabris, M. Monitoring of Land Subsidence in the Po River Delta (Northern Italy) Using Geodetic Networks. *Remote Sens*. 2021, 13, 1488. <https://doi.org/10.3390/rs13081488>
- Barra A, Solari L, Béjar-Pizarro M, Monserrat O, Bianchini S, Herrera G, Crosetto M, Sarro R, González-Alonso E, Mateos RM, Ligüerzana S, López C, Moretti S (2017) A methodology to detect and update active deformation areas based on Sentinel-1 SAR images. *Remote Sens* 9: 1002. <https://doi.org/10.3390/rs9101002>.
- Ezquerro, P., Tomás, R., Béjar-Pizarro, M., Fernández-Merodo, J.A., Guardiola-Albert, C., Staller, A., Sánchez-Sobrino, J.A. Herrera, G. Improving multi-technique monitoring using Sentinel-1 and Cosmo-SkyMed data and upgrading groundwater model capabilities. *Science of the Total Environment* 703 (2020) 134757 13
- Boni, R.; Pilla, G.; Meisina, C. Methodology for Detection and Interpretation of Ground Motion Areas with the A-DInSAR Time Series Analysis. *Remote Sens*. 2016, 8, 686. <https://doi.org/10.3390/rs8080686>
- Brewer, C.A.; Marlow, K. A. Color representation of aspect and slope simultaneously, Conference: Eleventh International Symposium on Computer-Assisted Cartography (Auto-Carto-11), Minneapolis, Minnesota, 1983.
- Pfeiffer, J., Zieher, T., Schmieder, J., Rutzinger, M. Strasser 2Hyndman, R., Newnham, G. & Culvenor, D. Spatio-temporal assessment of the Hydrological drivers of an active deep-seated gravitational slope deformation: The Voegelsberg landslide in Tyrol (Austria). *Earth Surf. Process. Landforms*. 2021;1–17.
- Hofmann, R.; Sausgruber, J.T. Creep behaviour and remediation concept for a deep-seated landslide, Navistal, Tyrol, Austria, *Geomechanics and Tunnelling* 10 (2017), No. 1. <https://onlinelibrary.wiley.com/doi/10.1002/geot.201600066>.
- Collilieux, X., Courde, C., Fruneau, B., Aimar, M., Schmidt, G., Delprat, I., Pesce, D., and Wöppelmann, G.: Radar corner reflector installation at the OCA Geodetic Observatory (France). In EGU General Assembly Conference Abstracts (p. 5201).
- Collilieux, X., Courde, C., Fruneau, B., Aimar, M., Schmidt, G., Delprat, I., Pesce, D., and Wöppelmann, G. (2022). Validation of a Corner Reflector installation at Côte d'Azur multi-technique geodetic Observatory. *Advances in Space Research*, 70(2), 360-370.
- Vick, L. M., Berg, J. N., Eggers, M., Hormes, A., Skrede, I., & Blikra, L. H. (2021). Keynote Lecture: The Jettan Rockslide—An Engineering Geological Overview. Understanding and Reducing Landslide Disaster Risk: Volume 6 Specific Topics in Landslide Science and Applications 5th, 289-315.
- Rouyet, L., Lilleøren, K. S., Böhme, M., Vick, L. M., Delaloye, R., Etzelmüller, B., ... & Blikra, L. H. (2021). Regional morpho-kinematic inventory of slope movements in northern Norway. *Frontiers in Earth Science*, 9, 681088.
- Hermanns, R. L., Oppikofer, T., Böhme, M., Dehls, J. F., Molina, F. Y., & Penna, I. M. (2018). Rock slope instabilities in Norway: First systematic hazard and risk classification of 22 unstable rock slopes from northern, western and southern Norway. In *Landslides and Engineered Slopes. Experience, Theory and Practice* (pp. 1107-1114). CRC Press.
- Aslan G., Foumelis M., Raucoules D., de Michele M., Bernardie S., Cakir Z., 2020, « Landslide Mapping and Monitoring Using Persistent Scatterer Interferometry (PSI) Technique in the French Alps », *Remote Sensing*, 12(8), 1305



- Teunissen, P. J. G. (2000a). Adjustment theory; an introduction (1 ed.). Delft: Delft University Press.,
- Teunissen, P. J. G. (2000b). Testing theory; an introduction (1 ed.). Delft: Delft University Press.
- Varnes, D.J., 1978. Slope movement types and processes. Special report, 176, pp.11-33.
- Hungr, O., Leroueil, S. and Picarelli, L., 2014. The Varnes classification of landslide types, an update. Landslides, 11, pp.167-194.
- Reyes-Carmona, C.; Barra, A.; Galve, J.P.; Monserrat, O.; Pérez-Peña, J.V.; Mateos, R.M.; Notti, D.; Ruano, P.; Millares, A.; López-Vinielles, J.; et al. Sentinel-1 DInSAR for Monitoring Active Landslides in Critical Infrastructures: The Case of the Rules Reservoir (Southern Spain). Remote Sens. 2020, 12, 809. <https://doi.org/10.3390/rs12050809>
- Carvalho, J., Pinto, C., Dias, R., Rabeh, T., Torres, L., Borges, J., Torres, R., Duarte, H., 2017. Tectonic Evolution of an Intraplate Basin: the Lower Tagus Cenozoic Basin, Portugal. Basin Research. 29. n/a-n/a. 10.1111/bre.12193.
- Heleno, S.I.N., Oliveira, L.G.S., Henriques, M.J., Falcão, A.P., Lima, J.N.P., Cooksley, G., Ferretti, A., Fonseca, A.M., Lobo-Ferreira, J.P., Fonseca, J.F.B.D., 2011. Persistent Scatterers Interferometry detects and measures ground subsidence in Lisbon. Remote Sensing of Environment, Volume 115, Issue 8, 2152-2167, ISSN 0034-4257, <https://doi.org/10.1016/j.rse.2011.04.021>.
- Pereira, N., Carneiro, J.F., Araújo, A., Bezzeghoud, M., Borges, J. 2013. Seismic and structural geology constraints to the selection of CO₂ storage sites—The case of the onshore Lusitanian basin, Portugal, Journal of Applied Geophysics, 102, pp. 21-38, <https://doi.org/10.1016/j.jappgeo.2013.12.001>.



GLOSSARY

ADA	Active Deformation Area
ASC	Ascending
ATS	Automatic Total Station
CLC	Corine Land Cover
CLMS	Copernicus Land Monitoring Service
CR	Corner Reflector
CRS	Coordinate Reference System
IoA	Index of agreement
DEM	Digital Elevation Model
DESC	Descending
DSGSD	Deep-Seated Gravitational Slope Deformation
EEA	European Environment Agency
GMS	Ground Motion Service
GNSS	Global Navigation Satellite System
InSAR	Interferometric Synthetic Aperture Radar
LOS	Line-of-Sight
MAE	Mean Absolute Error
MAE	Mean Absolute Error
MP	Measurement Point
PS / DS	Persistent Scatterer / Distributed Scatterer
R²	Coefficient of Determination
RMSE	Root Mean Square Error
S1	Sentinel-1
TS	Time Series

ANNEX: InSAR concepts summary

This section is intended as a summary for those unfamiliar with radar-based satellite data products and their geometric aspects.

SAR basics

A radar is a ranging technology, and the satellite with such an instrument onboard needs to look to one side to build a two-dimensional picture. Hence, images are acquired in the direction perpendicular to the flight direction, which is north-south. Therefore, we can only measure the projection of relative displacement along the vector between the satellite and the ground, which is named Line-of-Sight (LOS). Thus, the true direction of motion in the three-dimensional space is ambiguous, without some other form of information. Later in this section, it is explained how the EGMS 3D Ortho product is composed. Figure A1 illustrates the Sentinel-1 acquisition geometry:

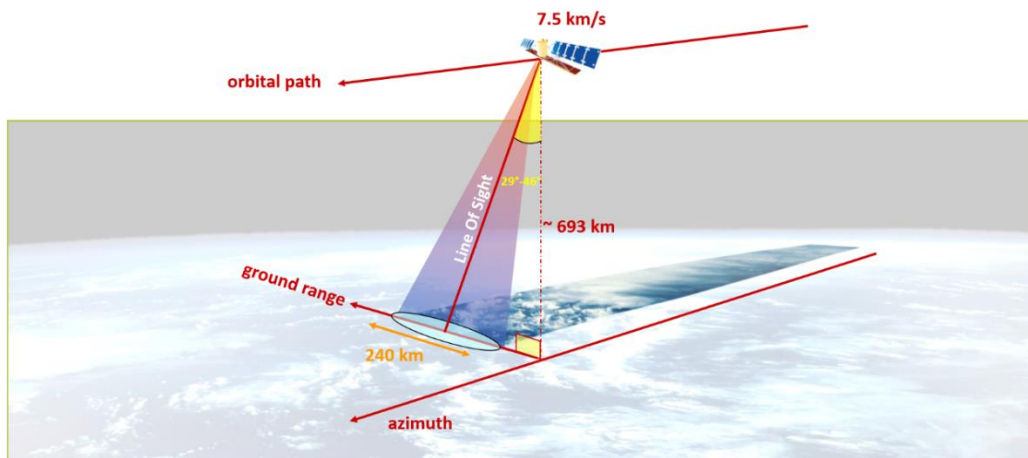


Figure A1: Data acquisition geometry (Sentinel-1)

Radar satellites are active systems that emit pulses of electromagnetic radiation. They are able to measure the strength of the return signal, the time-delay and the phase related to the angle of the signal's sinewave as it returns to the satellite. Unlike optical satellites, which are passive systems, radar satellites acquire images regardless of the time of day and level of cloud-cover; please see Figure A2 for an example of radar and optical images over the same area. EGMS products are made from hundreds of Sentinel-1 SAR image acquisitions over the same locations across the European territory.

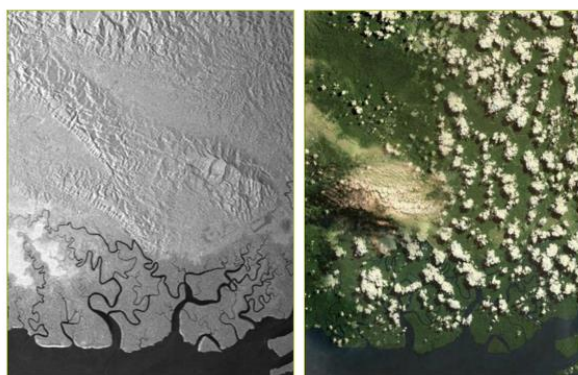


Figure A2: Radar (active system) versus Optical (passive system)

Acquisition geometry

Figure A3 below illustrates the sensitivity of L2 products to the direction of ground motion (Aslan et al., 2022). The geometry of ascending (a) and descending (b) satellite orbits showing flight and azimuth look directions. Colored arrows plotted in jet color map define the amount of deformation of the unit vector on different aspect angles that can be detected on the direction of LOS for ascending (c) and descending (d) viewing geometries. The grey arrows define the deformation of the unit vector. Negative values (hot colors) indicate an increase in the distance from the target to the satellite, and positive values (cold colors) show the motion towards the satellite (after Aslan et al., 2022).

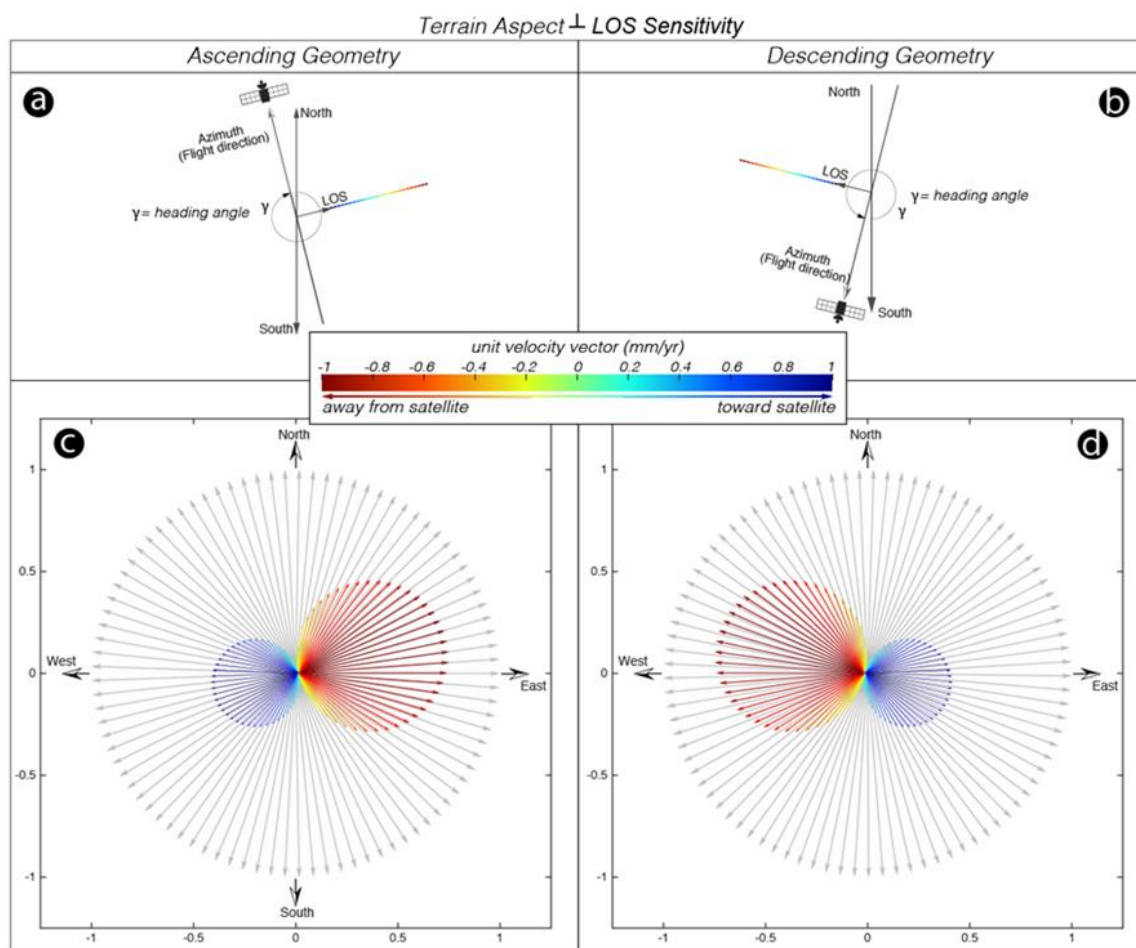


Figure A3: Effect of local terrain aspect on the sensitivity of LOS measurement along the downslope movements.

Ortho/L3 product

Ortho/L3 products are produced on a square grid with 100 metres spacing (Figure A4), with a six-days regular temporal sampling. For each grid cell, all available Calibrated/L2b is averaged, considering the different LOS, to produce separate ascending and descending displacement time series. Grid cells with non-existent or not enough data are excluded.

In the grid cells where sufficient ascending and descending orbits overlap, the vertical and eastward motion components are estimated. It is important to note that local north-south movements cannot be estimated due to the geometry of the satellite acquisitions. In the decomposition phase, then, the observed north-south displacement is neglected.

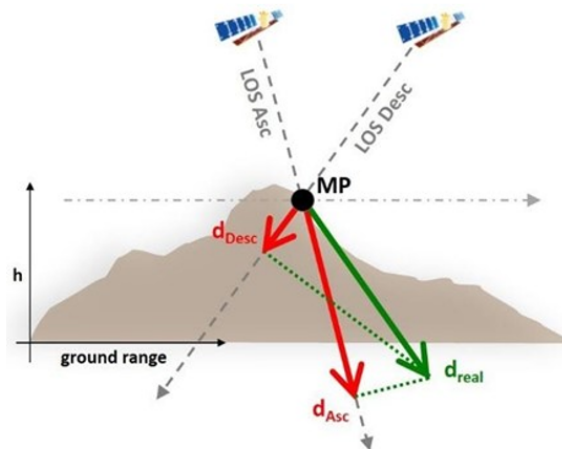
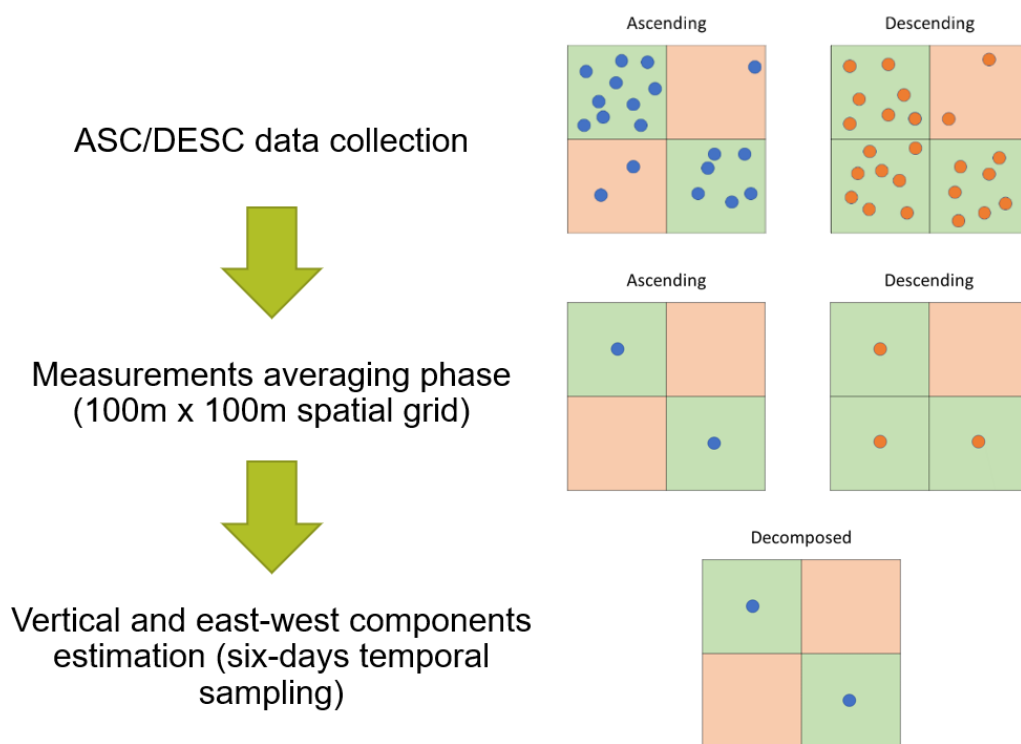


Figure A4: Otho/L3 product composition

Artificial corner reflectors

Corner reflectors (CRs) are designed to reflect radar signals back to the satellite antenna (Figure A5). They are normally deployed on locations that offer poor reflectivity (e.g. – densely vegetated or covered in snow). They are made of metal and oriented to the satellite to provide the strongest return possible.

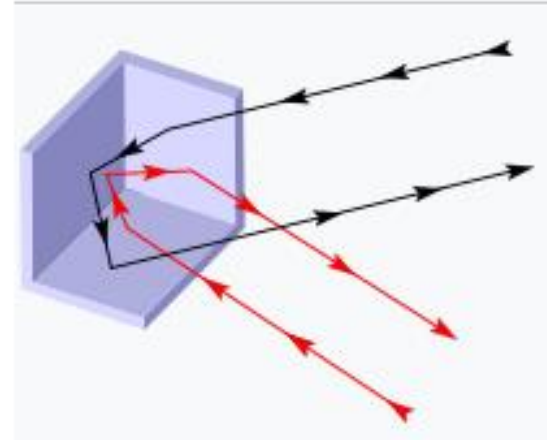


Figure A5: Left (Corner reflector), Right (working principle of CR) – source: Wikipedia